

# Berichte

zur Polar-  
und Meeresforschung

664  
2013

Reports  
on Polar and Marine Research



**Russian-German Cooperation SYSTEM LAPTEV SEA:**  
The Expeditions Laptev Sea -  
Mamontov Klyk 2011 & Buor Khaya 2012

---

**Edited by**  
**Frank Günther, Pier Paul Overduin, Aleksandr S. Makarov &**  
**Mikhail N. Grigoriev**  
with contributions of the participants



**Alfred-Wegener-Institut**  
Helmholtz-Zentrum für Polar-  
und Meeresforschung  
D-27570 BREMERHAVEN  
Bundesrepublik Deutschland

ISSN 1866-3192

## Hinweis

Die Berichte zur Polar- und Meeresforschung werden vom Alfred-Wegener-Institut Helmholtz-Zentrum für Polar- und Meeresforschung in Bremerhaven\* in unregelmäßiger Abfolge herausgegeben.

Sie enthalten Beschreibungen und Ergebnisse der vom Institut (AWI) oder mit seiner Unterstützung durchgeführten Forschungsarbeiten in den Polargebieten und in den Meeren.

Es werden veröffentlicht:

- Expeditionsberichte  
(inkl. Stationslisten und Routenkarten)
- Expeditions- und Forschungsergebnisse  
(inkl. Dissertationen)
- wissenschaftliche Berichte der  
Forschungsstationen des AWI
- Berichte wissenschaftlicher Tagungen

Die Beiträge geben nicht notwendigerweise die Auffassung des Instituts wieder.

## Notice

The Reports on Polar and Marine Research are issued by the Alfred-Wegener-Institut Helmholtz-Zentrum für Polar- und Meeresforschung in Bremerhaven\*, Federal Republic of Germany. They are published in irregular intervals.

They contain descriptions and results of investigations in polar regions and in the seas either conducted by the Institute (AWI) or with its support.

The following items are published:

- expedition reports  
(incl. station lists and route maps)
- expedition and research results  
(incl. Ph.D. theses)
- scientific reports of research stations  
operated by the AWI
- reports on scientific meetings

The papers contained in the Reports do not necessarily reflect the opinion of the Institute.

The „Berichte zur Polar- und Meeresforschung“  
continue the former „Berichte zur Polarforschung“

### \* Anschrift / Address

**Alfred-Wegener-Institut**  
Helmholtz-Zentrum für Polar-  
und Meeresforschung  
D-27570 Bremerhaven  
Germany  
[www.awi.de](http://www.awi.de)

Editor:  
Dr. Horst Bornemann

Assistant editor:  
Birgit Chiaventone

Die "Berichte zur Polar- und Meeresforschung" (ISSN 1866-3192) werden ab 2008 als Open-Access-Publikation herausgegeben (URL: <http://epic.awi.de>).

Since 2008 the "Reports on Polar and Marine Research" (ISSN 1866-3192) are available as open-access publications (URL: <http://epic.awi.de>)

**Russian-German Cooperation SYSTEM LAPTEV SEA:**  
The Expeditions Laptev Sea -  
Mamontov Klyk 2011 & Buor Khaya 2012

---

**Edited by**  
**Frank Günther, Pier Paul Overduin, Aleksandr S. Makarov &**  
**Mikhail N. Grigoriev**  
with contributions of the participants

Please cite or link this publication using the identifier  
hdl:10013/epic.41834 or <http://hdl.handle.net/10013/epic.41834>

ISSN 1866-3192



10<sup>th</sup> August – 2<sup>nd</sup> September 2011

**Russian expedition leader:**

Dr. Aleksandr Makarov

Arctic and Antarctic Research Institute

Beringa st. 38, 199397 St.Petersburg, Russia

**German expedition leader:**

Dr. Pier Paul Overduin

Alfred-Wegener-Institut

Helmholtz Zentrum für Polar und Meeresforschung

Department of Periglacial Research

Telegrafenberg A43, 14473 Potsdam, Germany

# Contents

1	Introduction	1
1.1	Itinerary	2
1.2	Acknowledgements	3
2	COAST Borehole (C1)	4
2.1	Borehole description and maintenance	4
2.2	Data recovery	6
2.3	Future needs	10
3	Polygon research at Cape Mamontov Klyk and on Muostakh Island (Laptev Sea)	11
3.1	Scientific background and objectives	11
3.2	Study sites	11
3.3	Material and methods	11
3.4	Field results	13
3.5	Outlook	15
4	Topographic survey of Ice Complex coasts	16
4.1	Introduction and motivation	16
4.2	Study sites	17
4.3	Field methods	17
4.4	Elements of remote sensing	19
4.5	Field results	20
5	Studies of Holocene ice wedges	55
5.1	Scientific background and objectives	55
5.2	Methods	55
5.3	Description of outcrops	56
5.3.1	General stratigraphic and geomorphologic situation	56
5.3.2	Ice wedge MUO11 IW1 (71°25'42.1" N, 129°59'41.5" E)	56
5.3.3	Ice wedge MUO11 IW2 (71°36'44.8" N, 129°56'26.4" E)	57
5.3.4	Ice wedge MUO11 IW3 (71°36'42.0" N, 129°56'46.3" E)	59
5.3.5	Ice wedge MUO11 IW4 (71°36'41.0" N, 129°56'51.5" E)	60
5.3.6	Ice wedge MUO11 IW5 (71°35'50.3" N, 129°59'26.7" E)	61
5.3.7	Ice wedge MUO11 IW6 (71°35'52.8" N, 129°59'22.2" E)	62
5.4	Preliminary results and outlook	63
6	Geophysical investigations of the coastal zone	64
6.1	Motivation and science goals	64
6.2	Geoelectrical DC resistivity	65
6.3	Seismic profiling	68

6.4	Preliminary results and outlook . . . . .	71
7	Distribution of organic carbon in bottom sediments on the underwater coastal slope	72
7.1	Scientific background and objectives . . . . .	72
7.2	Field results . . . . .	72
8	Scientific Permafrost Drilling Campaign	75
8.1	Scientific background . . . . .	75
8.2	Acknowledgements . . . . .	76
8.3	Itinerary . . . . .	76
8.4	Study Area and Methods . . . . .	78
8.5	Results . . . . .	80
8.5.1	Marine drilling . . . . .	80
8.5.2	Terrestrial drilling . . . . .	80
8.5.3	Sea ice bore holes . . . . .	80
	References	87
	List of figures	90
	List of tables	92
A	Appendix Ice Wedges	93
B	Appendix Core Logs	101
C	Appendix Drilling Campaign	106

# 1 Introduction

*Pier Paul Overduin & Aleksandr Makarov*

In 2003 (Schirrmester & Grigoriev, 2004) and 2005 (Overduin *et al.*, 2007), joint Russian-German expeditions to the Cape Mamontov Klyk region of the western Laptev Sea were launched with multiple scientific goals focussing on coastal permafrost and the paleoenvironment. The latter expedition resulted in a transect of boreholes, onshore and offshore, of which the 70 m deep onshore COAST C1 borehole (Overduin *et al.*, 2007) was retained and instrumented with a temperature datalogger. The last visit to this borehole took place in 2008. In 2011 it was necessary to revisit the site in order to collect the intervening three years of data, maintain the borehole, and replace the datalogger batteries.

Mamontov Klyk is remote and reaching the site requires considerable logistical effort. Seeing an opportunity in this challenge, a number of scientific goals were identified by the Russian and German partners and a team assembled. The region represents a stretch of coastline exposed more or less to the north and distant from mouths of major rivers, where the influence of coastal processes can be expected to predominate over processes arising from local geomorphological peculiarities. The inclination of the continental shelf is extremely shallow, so that most ships cannot approach the coast to make measurements. Coastal dynamics and the influence of marine transgressions on permafrost were therefore focal points of the expedition, in association with planned simultaneous acquisitions of remote sensing products. Mamontov Klyk also represents a westernmost study site for Laptev Sea regional studies of past climate variability. Two projects were aimed at current conditions in examining small polygonal ponds, ubiquitous throughout the arctic coastal plains, and at late Holocene polygon ice wedges. In this context, field goals were to:

- investigate landform development and marine transgressions at the mouth of the Urasalakh River, about 20 km west of Mamontov Klyk
- use shallow geoelectric and acoustic methods to investigate submarine permafrost distribution along and surrounding both 2003 and 2005 borehole transects
- investigate limnology of polygon water bodies to provide correlations of environmental conditions and bioindicators such as pollen, diatoms, chironomids, rhizopods and ostracods
- survey coastline positions and associated geomorphological features
- provide ground control points for georeferencing of satellite imagery
- sample surface sediments in the nearshore zone for the estimation of mass fluxes resulting from coastal erosion
- collect ice wedge samples for reconstructing late Holocene climate history through stable isotope composition
- recover data from and perform maintenance on the borehole datalogger

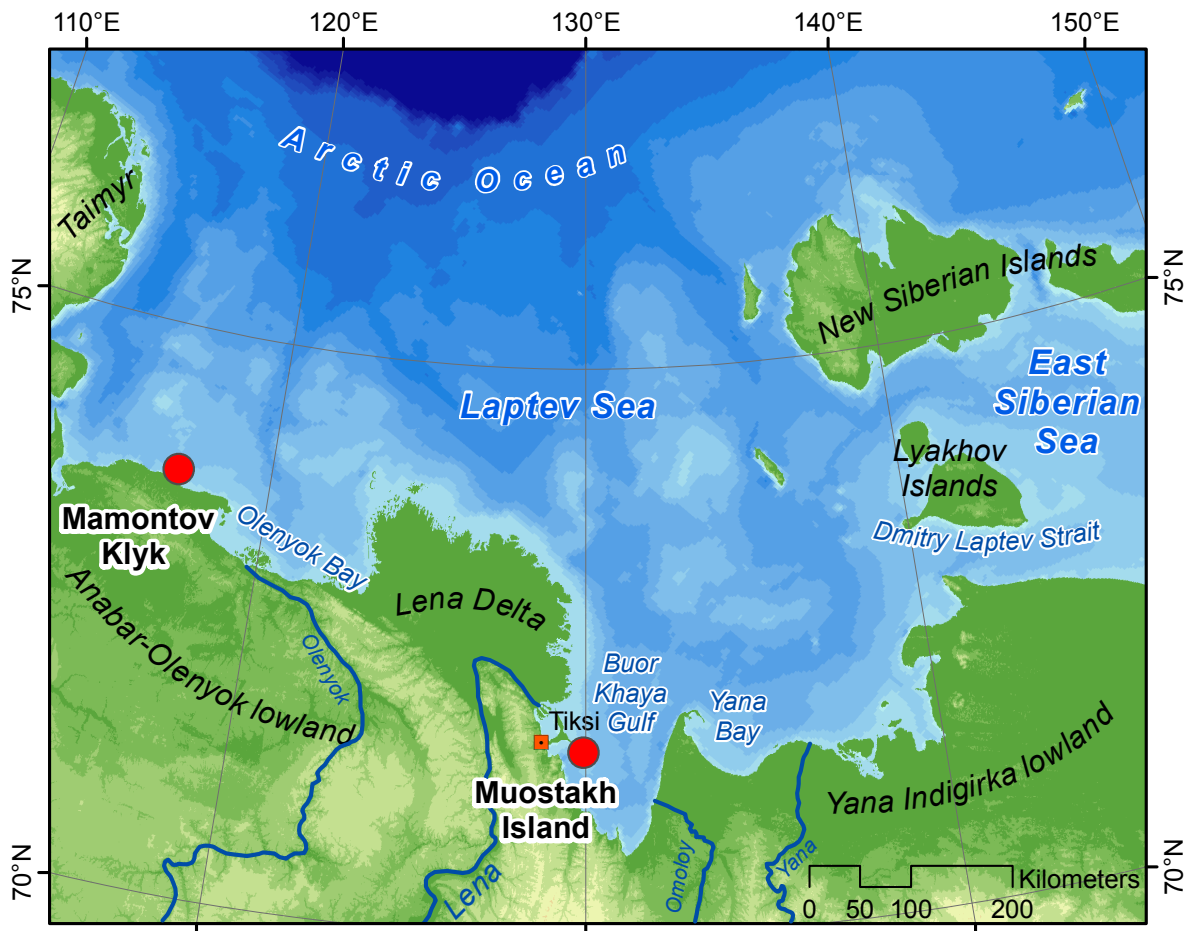


**Fig. 1.1:** The expedition began at Cape Mamontov Klyk in the western Laptev Sea and continued on Muostakh Island in the central Laptev Sea.

## 1.1 Itinerary

The helicopter was loaded on August 11<sup>th</sup>, and the 2-hour flight from Tiksi to Mamontov Klyk started at midday on August 12<sup>th</sup>, 2011. After establishing camp close to a derelict cabin a few hundred meters from the mouth of the Nuchchi Dzhielkh River, work commenced on August 14. Early on the morning of the 16<sup>th</sup>, the presence of a persistent polar bear in camp led to the difficult decision, made together with logistics in Tiksi and at the Samoylov Station in the Lena Delta, to relocate the camp as soon as possible. This represented an unavoidable disruption of the expedition's science goals. Due to restrictions for expeditions operating along the coastal border, the team was not equipped to safely carry out the original plan, which foresaw independent teams of 2 to 3 people working simultaneously. A second location was sought that would allow some of the goals to be met within the constraints of the Lena-Laptev 2011 expedition permit. On August 17<sup>th</sup>, a helicopter picked up the expedition and transferred it about 500 km eastward to Muostakh Island, which lies about 40 km eastward of Tiksi. Establishing a camp on Muostakh Island occupied August 18<sup>th</sup> and 19<sup>th</sup>; on the 20<sup>th</sup>, field work continued. Work ended on August 28<sup>th</sup> and the team was transferred to Tiksi by helicopter on August 29<sup>th</sup> (Fig. 1.1).



The group consisted of seven members from three organisations (Fig. 1.2), the Alfred Wegener Institute Helmholtz Centre for Polar and Marine Research in Potsdam, Germany (AWI), the Melnikov Permafrost Institute in Yakutsk, Siberian Branch of the Russian Academy of Sciences, Russia (PIY), the Arctic and Antarctic Research Institute in St. Petersburg, Russia (AARI), and the St. Petersburg State University (SPBU).



**Fig. 1.2:** Expedition participants on August 13<sup>th</sup>, 2011 at Mamontov Klyk from left to right: Aleksandr Makarov (AARI, russian expedition leader), Paul Overduin (AWI, german expedition leader), Sebastian Wetterich (AWI), Frank Günther (AWI), Aleksandr Sandakov (PIY), Alisa Baranskaya (SPBU), and Thomas Opel (AWI).

## 1.2 Acknowledgements

This project (Chapters 1-7: Mamontov Klyk 2011) was carried out as a part of the Helmholtz Association of Research Centers Joint Russian German Research Group on the Sensitivity of the Arctic Coast to Change at AWI, and is a direct contribution to the Helmholtz Association's Research Program „Marine, Coastal and Polar Systems: Polar Regions and Coasts in a changing Earth System (PACES)“ as an activity of Topic 1 - Work Package 5: The role of degrading permafrost and carbon turnover in the coastal, shelf and deep sea environment. The Potsdam Research Cluster for Georisk Analysis, Environmental Change and Sustainability (PROGRESS) contributed personnel and remote sensing data to support this expedition. The logistic services required for such an expedition are considerable and were provided by the Hydrobase (state hydrographic service) of Tiksi. We are grateful for Samuel Stettner's help in preparing this report.

## 2 COAST Borehole (C1)

*Pier Paul Overduin*

### 2.1 Borehole description and maintenance

The COAST Project C1 borehole was established during the COAST drilling campaign in the spring of 2005 (Overduin *et al.*, 2007), when it was also instrumented. Details on the recovered sediment record are described in Winterfeld *et al.* (2011). The borehole has a casing that extends below ground surface a few meters. The thermistor cable is suspended from a metal hook bolted to the borehole casing, just below the top. The first sensor is located at a borehole casing depth of 0.9 m, i.e. at -0.1 m relative to the ground surface. Sustained searching has produced no record of temperature sensor depths from members of the original establishing expedition. Table 2.1 uses thermistor position along the cable from the manufacturer (RBR) to compute depth below the ground surface.

However, it was necessary during installation to coil the datalogger cable since it was too long for the borehole. This is not obvious from the manufacturer's specifications, since the total borehole depth (70 m) exceeds the position of the furthest temperature sensor (68 m). At what depth a coiling or doubling of the cable was not recorded during installation. One of our goals was to evaluate the possibility of removing the datalogger cable, measuring temperature sensor positions and re-installing the cable during our visit on August 14, 2011.

The rusty steel pipe extended above the ground surface between 0.79 and 0.83 m (after lid was removed). To open the borehole, a pipe clamp is required (from Yakutsk, for example). A length of steel pipe has been left lying next to the borehole, which can be used to extend the clamp handle and apply additional torque to the lid. Active layer depth was about 56 cm adjacent to the casing. Ice from frozen condensate from the borehole had plugged the hole and frozen the cable into place. This ice began at a depth of 136 cm from the top of the borehole (Fig. 2.1), corresponding with the base of the active layer. Since excess cable between the logger and its attachment point to the borehole casing had been left hanging about 1.5 m into the hole, the logger was effectively frozen into place and could not be lifted out for maintenance and data recovery. The same situation had been encountered in 2008, during the last visit to the site, but there had not been sufficient time to find a solution.

**Tab. 2.1:** Datalogger channels, sensor distance along thermistor string and sensor depth relative to ground surface. See text for restrictions on sensor depth values.

Channel	Distance along cable from datalogger [m]	Depth relative to ground surface [m]
1	68	-65.1
2	63	-60.1
3	58	-55.1
4	53	-50.1
5	48	-45.1
6	43	-40.1
7	38	-35.1
8	33	-30.1
9	28	-25.1
10	25	-22.1
11	23	-20.1
12	21	-18.1
13	19	-16.1
14	17	-14.1
15	15	-12.1
16	13	-10.1
17	11	-8.1
18	9	-6.1
19	8	-5.1
20	7	-4.1
21	6	-3.1
22	5	-2.1
23	4	-1.1
24	3	-0.1

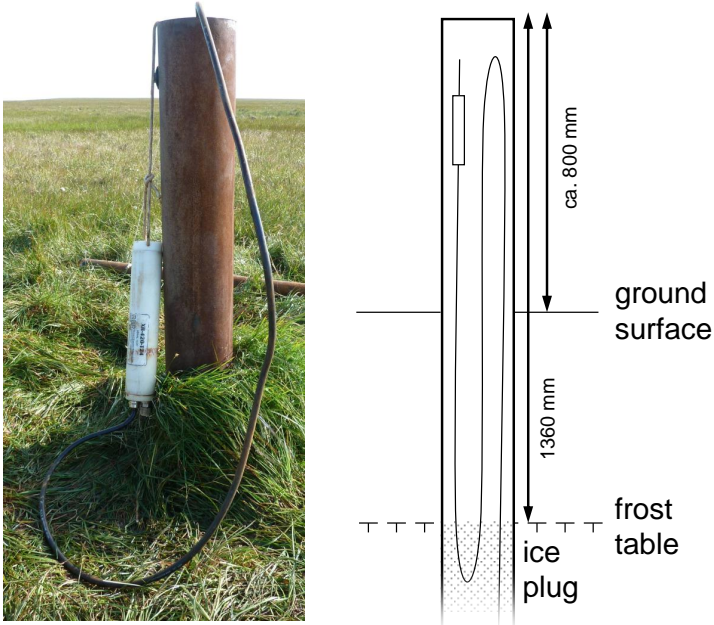


**Fig. 2.1:** Photograph of the borehole casing (August 14, 2011) and a schematic of the ground surface, frost table positions, and the upper portion of the cable within the borehole.

To free the cable from the ice plug, a metal pipe was used to break a hole through the center of the plug, with care taken not to damage the three lengths of cable disappearing into the ice plug. This was not sufficient to free the cable from the ice, and hot water was lowered in plastic bags to melt the ice. The L-bracket supporting the thermistor string juts out into the borehole casing (Fig. 2.2), so that larger containers of water could not be used (aluminium bottle, rubber hot water bottle and others were tried). After reading out data and changing batteries, the excess cable was looped, secured with cable ties, and now hangs in the upper portion of the casing. As long as the site is visited in mid to late summer, it is expected that the cable should hang well above the ice plug. Not all ice could be removed in this fashion, nor could we ascertain to what depth the ice plug extends. The thermistor string itself therefore remained frozen into the ice, and could not be removed from the borehole.

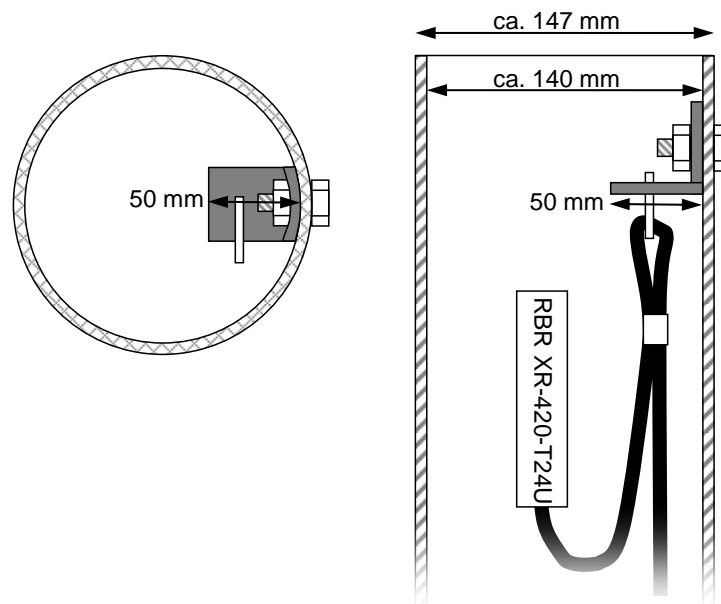


**Fig. 2.2:** Schematic of the borehole casing gives dimensions in plan view (left) and from the side (right). The casing, the bolt and L-bracket for suspending the thermistor string and basic dimensions are shown (not to scale).

## 2.2 Data recovery

The borehole datalogger is an RBR XR-420-T24U (serial number 4.60.010307). It was programmed and read out using RBR software. This software has since been replaced by RUSKIN software, which has not, however, been tested with the COAST C1 borehole logger. Two types of cable can be used to interface with the datalogger:

1. a watertight connection on the outside of the datalogger housing (at the writing of this report, such a cable was stored at the Hydrobase in Tiksi);
2. a smaller cable connection is accessible within the housing beside the batteries.

Three cables of the latter type have been purchased (responsible person: Conrad Kopsch, AWI Potsdam). Details on the cable, software and batteries can be taken from the manual for the logger. Battery voltage after 3 years of operation was 12.83 V, but is not logged. Temperature

data were recovered for 24 channels from August 13, 2011 until August 15, 2011, yielding 26304 hourly temperatures for each channel (Fig. 2.3). Temperatures varied between  $-31.3^{\circ}\text{C}$  and  $4.48^{\circ}\text{C}$  close to the ground surface. Seasonal variations in temperature are visible for all sensors, but at a depth of 20 m mean seasonal temperature amplitude is about  $0.09^{\circ}\text{C}$ . At this depth, temperatures warmed over the 3-year period by about  $0.1^{\circ}\text{C}$  per year, a value typical for the warming of cold permafrost at such latitudes (A. Kholodov, personal communication). This warming is visible throughout the borehole record and seems to be chiefly due to warming during the winter.

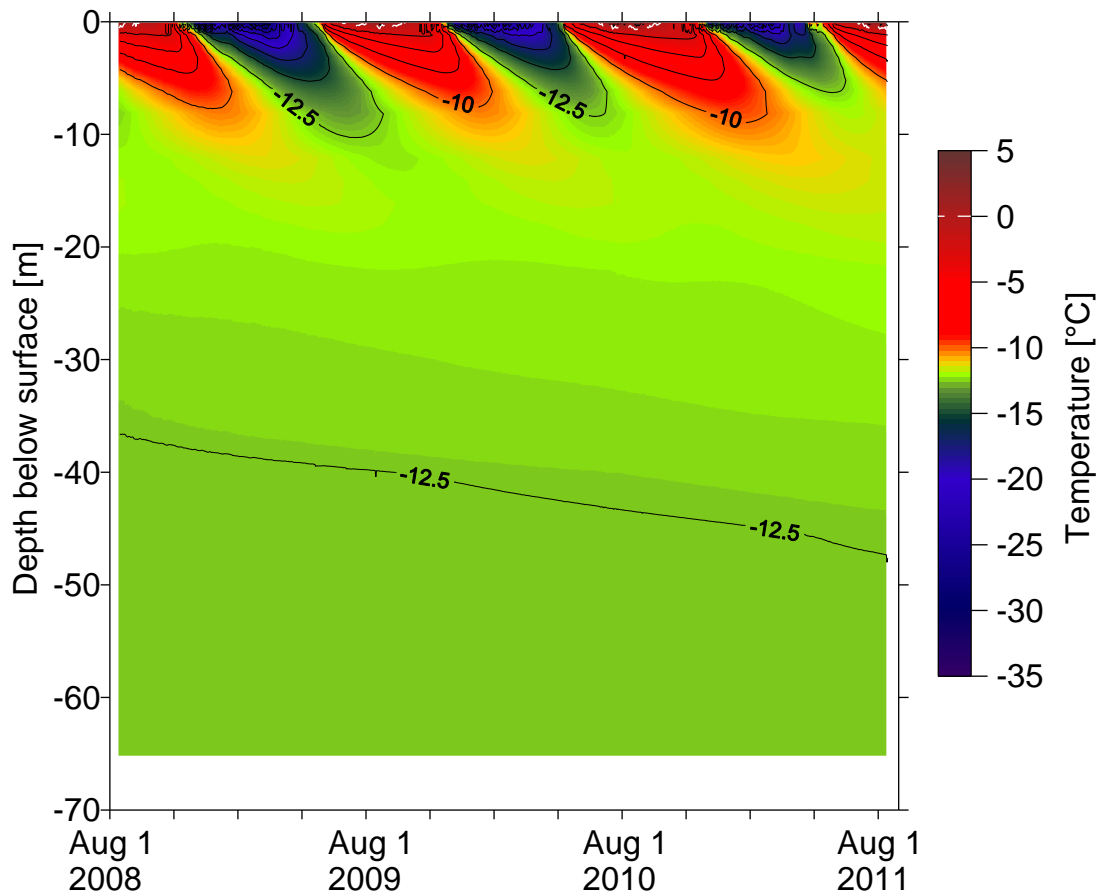


**Fig. 2.3:** Subsurface temperatures (unfiltered data) at the C1 borehole for the period from August 13, 2008 until August 15, 2011 using the sensor depths given in Table 1. Contour intervals are  $2.5^{\circ}\text{C}$ . The  $0^{\circ}\text{C}$  contour line is white and dashed.

There were two types of data errors in the temperature record:

1. errors due to sensors which no longer function correctly and
2. errors due to borehole processes which affected the readings of one or more sensors.

Channels 9 and 16 did not function properly for the entire period and yielded very noisy data, with a seasonal cycle in values between  $-124$  and  $-118^{\circ}\text{C}$ . All other sensors performed reliably but had outliers in the positive direction of up to  $10^{\circ}\text{C}$ , especially during the mid-summer of 2010 and in late summer 2011. Figures 2.4 and 2.5 give two examples of outlier events in the borehole.

Following such outliers, it took some hours for the temperature to re-assume pre-outlier levels. Outliers usually affected multiple sensors more or less simultaneously, but not the entire chain.

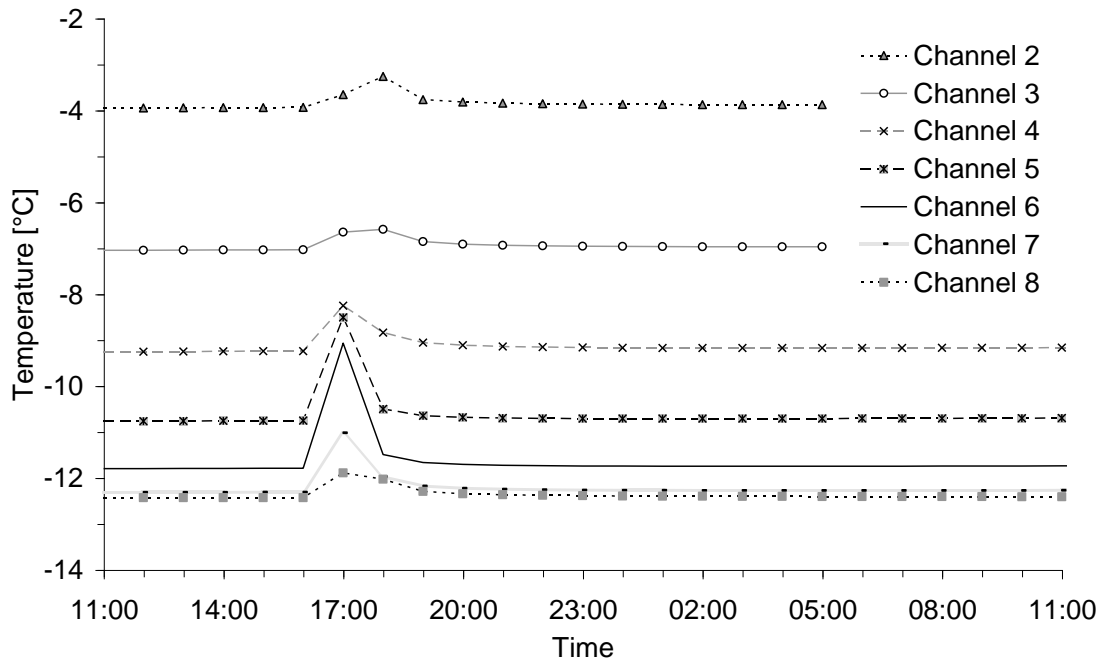


**Fig. 2.4:** An example of outlier temperature data. Temperature data from channels 2 to 8 are shown for the 24-hour period beginning at 11:00 on July 15, 2010. Sensor 6 undergoes the greatest deviation, other sensors register a thermal perturbation, with amplitude decreasing with increasing distance from the maximally influenced sensor.

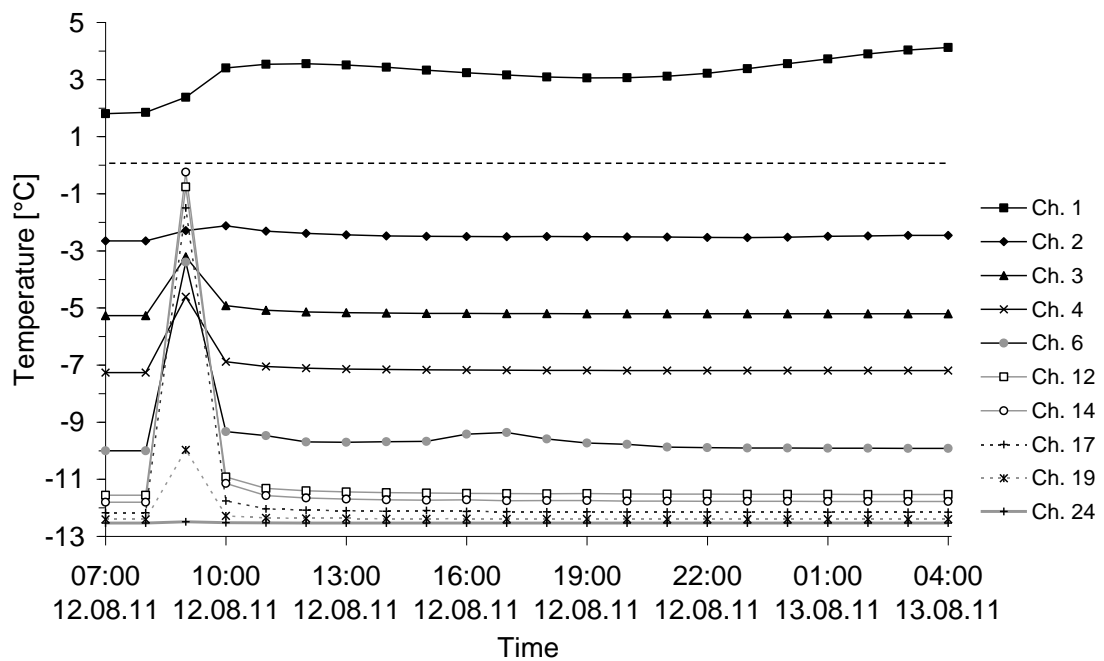


**Fig. 2.5:** Two days before reading out the station in 2011, a warming event affected channels 12-17 with smaller effects observed above and below these sensors. Relaxation back to pre-event temperatures took at least a few hours.

The possibility that these outliers reflect a measurement of something occurring in the borehole is real, for example, the release of latent heat energy through the refreezing of water that has infiltrated into the borehole. Supporting this interpretation is the fact that such events occur primarily in summer, and that no ice was present in the borehole between its upper end and the base of the active layer. Any ice that had accumulated above the base of the active layer from water vapour derived from ice sublimated from the borehole walls had melted. Outlier events are probably associated with infiltration of this meltwater into the borehole (through the ice plug) and refreezing at or close to sensors. In particular Fig. 2.5 shows warming of the most strongly affected sensors almost to 0 °C, and dissipation of warmth over a period of some hours.

To provide a trumpet curve (Fig. 2.6), reflecting long term temperature trends, the data were cleaned by:

1. truncating the record by removing the data from August 13 to August 31, 2008, during which work on the borehole presumably affected measurements.
2. removing outlier events by visual inspection of the data. A liberal approach was taken to removing tailing post-event data, but such visual inspection does not provide a consistent basis for rejecting data. A filter, based on high frequency changes in data, would be more objective, and can still be implemented on the raw data.

In addition, there was a step-like increase in temperature by less than 0.2 °C at the coldest part of the record of winter 2008 and 2009 for one sensor only (№13 in Table 2.1, at -16.1 m).

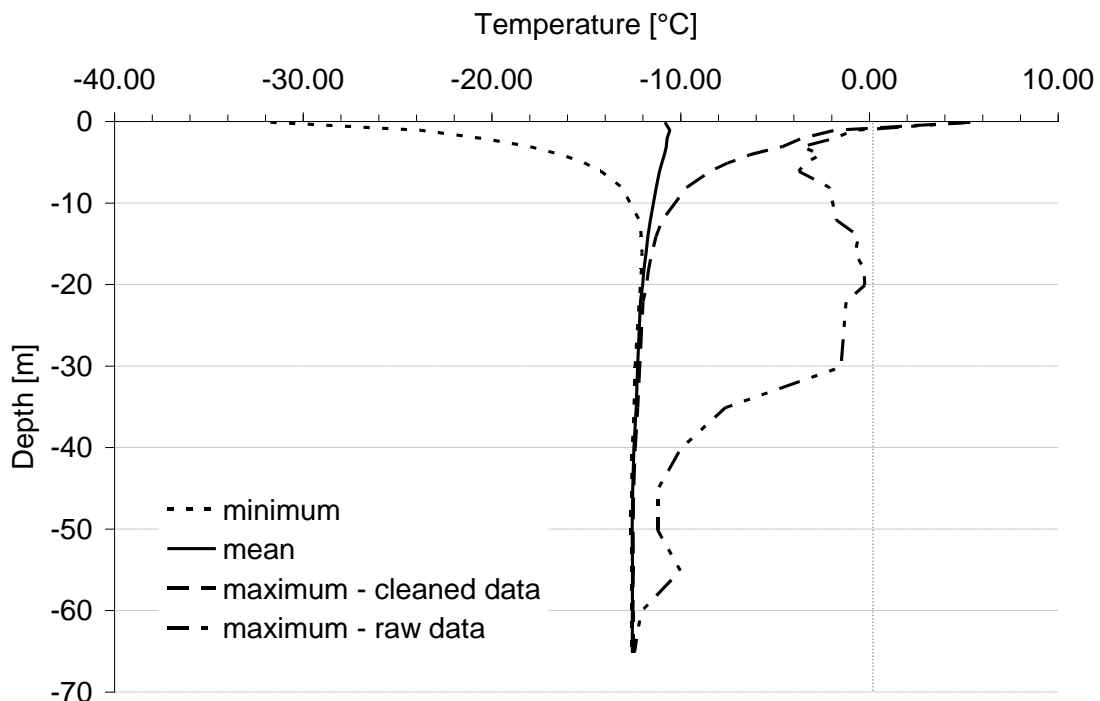


**Fig. 2.6:** Trumpet curve, for collected data compared to measurements made at time of borehole establishment, compared to 2005-2006.

### 2.3 Future needs

The COAST C1 borehole is currently located about 90 m from the upper edge of the coastal bluff. The coastal bluff is being eroded at a rate of just under 5 m per year. This borehole may thus provide a unique opportunity to observe the effects of coastal processes on the permafrost temperature regime and it should therefore be maintained. There are a number of issues with the borehole that ought, however, to be resolved.

As mentioned, the depths assigned to temperature sensors are not corroborated by field notes. Presentation of the data assuming a straight-hanging chain presents no obvious problems, such as gradient inversion, so that we have adopted the manufacturers distances along the string as depths, despite field reports that the thermistor string was looped. Even if the thermistor string can be removed from the borehole in order to measure depths, it is not clear whether it could be successfully re-inserted. In any case this would involve thawing of any ice surrounding the main cable. This ice might extend lower than can be effectively reached or be present at the base of the borehole.

The issue of sublimation and refreezing of borehole water vapour can be treated by inserting conduit into the borehole, which then houses a thermistor string. This is standard practice for boreholes belonging to the Thermal State of Permafrost (TSP) of Global Thermal Network - Permafrost (GTN-P), although neither network has an officially adopted borehole design or even set of best practices. A further improvement to the longevity and comparativeness of the data produced would be achieved if the borehole were filled with mineral oil or anti-freeze in order to facilitate exchange or replacement of thermistor strings.

The borehole has been programmed to log until **September 30, 2017**, measuring all channels at hourly intervals and filling the memory completely. The RBR software estimates battery usage of 1942 mAh by the end of logging, a value not exceeded by the nominal rating of the replacement batteries installed, which can, however, be adversely affected by shelf-life and temperature. We recommend replacing batteries after 3 years at the latest.



# 3 Polygon research at Cape Mamontov Klyk and on Muostakh Island (Laptev Sea)

*Sebastian Wetterich*

## 3.1 Scientific background and objectives

The intention of our limnological fieldwork on polygonal waters in summer 2011 at Cape Mamontov Klyk and on Muostakh Island was the record and the monitoring of abiotic parameters such as climate conditions, temperature fluctuations, ionic and stable isotope composition in polygon waters in relation to bioindicators such as pollen, diatoms, chironomids, rhizopods and ostracods. The investigation of the present-day conditions in the waters allows the quantification of influencing parameters, which control the modern occurrence of these indicator organisms. In future, results of the study can be useful for interpretation of fossil data from sediment cores and outcrops and also for quantitative palaeo-environmental reconstructions of the region using several palaeo-bioindicators.

## 3.2 Study sites

Limnological studies were undertaken in different landscape units around the camp (71°56'66.7" N, 132°19'63.1" E) in August 2010 (Fig. 3.1), i.e. on the floodplain of the Nuchchi-Dzhielekh River where polygons were represented as high-center type with interpolygonal ponds (Fig. 3.1a) and on the top of Yedoma hills (Fig. 3.1b).

## 3.3 Material and methods

Investigations on properties of water chemistry and physics in the waters were undertaken in order to describe the recent life conditions for organisms. Our investigations included the estimation of water and size. We quantified pH, electrical conductivity (EC) and temperature using a WTW pocket meter. Still in the field, the determination of total hardness, alkalinity and acidity was performed by means of titrimetric test kits (Viscolor).

For hydrochemical analyses in the lab the pond water was sampled above the sediment surface from each site. Samples for cation analyses (15 ml) were acidified with 200  $\mu$ l HNO<sub>3</sub>, whereas samples for anion analysis and residue samples were cool stored. Before conservation, samples for cation and anion analyses were filtered by a cellulose-acetate filtration set (pore size 0.45  $\mu$ m).



**Fig. 3.1:** Studied polygon types (a) at Cape Mamontov Klyk on the floodplain of the Nuchchi-Dzhielekh River and (b) on a Yedoma top at the northern edge of Muostakh Island.

Additionally, precipitation and pond water samples for  $\delta^{18}\text{O}$  and  $\delta\text{D}$  isotope analyses (30 ml) were preserved without any conservation.

Surface sediments of the ponds were sampled for sedimentological and botanical and zoological analyses. For these purposes studies on pollen, diatoms, chironomids, rhizopods and ostracods are planned. Living ostracods were caught in surface sediment samples from different pond zones using an exhaustor system (Viehberg, 2002) and preserved in 70 % alcohol. Further taxonomical work using soft body characteristics will provide the first description of modern ostracod assemblages from the study area.

A similar approach has already been applied on periglacial waters in the Lena Delta (Wetterich *et al.*, 2008), at the coastal area of the Dmitry Laptev Strait (Wetterich & Schirrmeister, 2008), in the Kolyma lowland (Wetterich & Schirrmeister, 2011b) and Buor Khaya Peninsula (Wetterich & Schirrmeister, 2011a).

One interpolygon pond in the floodplain (MKlyk-01, Fig. 3.1a) was selected as monitoring site. Here, we started continuous temperature measurements at four levels using temperature logging (HOBO Data Logger, H21-002; 12-Bit Temp Smart Sensor, S-TMB-M002) on August 14, 2011. The loggers were placed in two different water depths (0.25 m below the water line and at the waterline) and in the air (1 m and 2 m above the water line). The monitoring site was closed due to the evacuation of the camp at Cape Mamontov Klyk on August 17, 2011, and re-established on August 19, 2011 on Muostakh Island working until August 28, 2011 (Muo-01, Fig. 3.1b). There every four days repeated hydrochemical measurements and sampling of water and ostracods were performed in order to obtain temporal dynamics of the studied parameters and proxy as well as their relationships among each other.

### 3.4 Field results

Both studied waters belong to interpolygon waters (Fig. 3.1; Table 3.1). The size of the ponds reaches from 2 x 18 m with very shallow water depth of 0.25 m (MKlyk-01), and 12 x 12.5 m with 0.7 m water depth (Muo-01) (Table 3.2); representing rather different stages of polygon development.

The ground substrates of polygons are built up by coarse to fine disperse organic mud and rich in more or less decomposed plant detritus. Results of the finger-print hydrochemistry during the fieldwork are presented in Table 3.3. The studied polygon ponds are characterised by slightly acidic pH (pH 6) and moderate EC. The acidity varies between 0.1 and 0.8 mmol/l. The alkalinity ranges from 0.2 up to 1.4 mmol/l. Decreasing EC in Muo-01 rather reflect precipitation input during rainy days.

**Tab. 3.1:** Geographical features of the studied waters

Sample №	Date yy/mm/dd	Time	Region	Locality	Lat	Long
MKlyk-01a	11/08/14	16:00	Mamontov Klyk	Floodplain	73°36'16"	117°6'29.8"
Muo-01a	11/08/19	16:00	Muostakh	Yedoma top	71°35'35.4"	129°58'59.8"
Muo-01b	11/08/23	17:00	Muostakh	Yedoma top	-	-
Muo-01c	11/08/27	12:00	Muostakh	Yedoma top	-	-

**Tab. 3.2:** Morphological and sedimentological features of the studied waters

Sample №	Water type	Substrate	Size [m x m]	Depth [m] maximal	Sample depth [m]	
					water	ostracods
MKlyk-01a	interpolygon	organic mud	2 x 18	0.25	0.25	0.25
Muo-01a	interpolygon	organic mud	12 x 12.5	0.7	0.3-0.5	0.3-0.5
Muo-01b	-	-	-	-	-	-
Muo-01c	-	-	-	-	-	-

**Tab. 3.3:** Physico-chemical features of the studied waters. EC - electrical conductivity; Alk: Alkalinity; Aci - Acidity; TH - Total hardness

Sample №	EC [ $\mu\text{S}/\text{cm}$ ]	pH Viscolor	Alk [mmol/l]	Aci [mmol/l]	TH [ $^{\circ}\text{dH}$ ]	TH [mmol/l]
MKlyk-01a	701	6.0	1.4	0.1	7.5	1.4
Muo-01a	395	6.0	0.2	0.8	failed	failed
Muo-01b	290	6.0	0.5	0.3	5	0.9
Muo-01c	305	6.0	0.4	0.4	4	0.7

The temperature monitoring was performed during the fieldwork from August 14 until August 17 in MKlyk-01 (Fig. 3.2a). Due to the very shallow depth, water temperatures are co-varying in lower amplitude with air temperature variations. In Muo-01 temperature were measured between August 19 until August 28. Bottom water temperature variations only slightly resemble daily air temperature amplitudes. Heavy wind however mixed the water column on August 23, and equalled surface and bottom water temperatures (Fig. 3.2b). High daily maximum values of air temperatures seem to be overestimated due to the direct sun radiation that occurred before August 22.

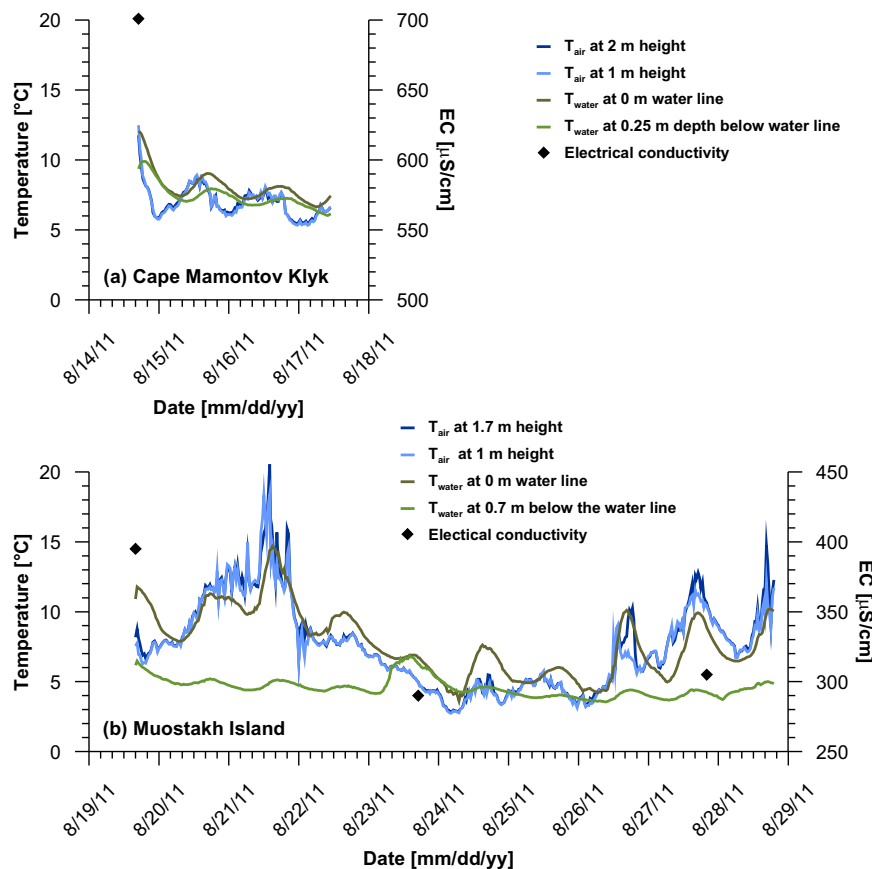


**Fig. 3.2:** Daily temperature variations at the monitored ponds: MKlyk-01 (a) and Muo-01 (b). Four levels are figured out:  $T_{air}$  in 2 (1.7) m and 1 m heights above the water surface;  $T_{water}$  at the water line and  $T_{water}$  above the sediments in 0.25 (0.7) m water depth. The right x-axes refer to electrical conductivity measurements which are shown as black diamonds. Note different scales for the diagrams.

### 3.5 Outlook

Pollen, diatoms, chironomids, rhizopods from sediments and live caught ostracods will be investigated to illuminate their relationship to environmental factors such as temperature, pH, and conductivity in polygon waters. Later, this information will be applied to fossil assemblages obtained from sediment cores and permafrost deposits in order to infer quantitative environmental changes via organism-environment transfer-functions. In the laboratory, water samples will be analysed for element content by means of an ICP-OES and anion content by Ion Chromatography. Furthermore, analyses of  $\delta^{18}\text{O}$  and  $\delta\text{D}$  isotopes on water and precipitation samples will be performed in order to compare these data with isotope values in calcareous ostracod valves. The understanding of the recent relationship between isotope ratios in waters and in ostracod valves will lead to an interpretation tool for palaeoenvironmental information preserved in fossil ostracods. For the same purpose element analyses (e.g. Ca, Mg, Sr) in waters and ostracod valves will be undertaken. Analyses of nitrogen organic and total carbon contents on surface sediment samples by CN-Analyzer as well as grain-size distribution by laser particle analyzer will be carried out in order to characterize the sedimentological setting of the investigated ponds. Such investigations on polygon waters will contribute to the joint Russian-German POLYGON project funded by the Russian Foundation for Basic Research (RFBR) and the Deutsche Forschungsgemeinschaft (DFG).

# 4 Topographic survey of Ice Complex coasts

*Frank Günther, Aleksandr Sandakov, Alisa Baranskaya & Paul Overduin*

## 4.1 Introduction and motivation

Coastal erosion along the mainland coast of the Laptev Sea is an agent of land-ocean interactions and the dominating process of transforming terrestrial permafrost into permafrost preserved under submarine conditions. Ice-rich unconsolidated Pleistocene permafrost deposits of Ice Complex type are cropping out along 25% of the Laptev Sea coastline. The geomorphology of the adjacent coastal lowlands is dominated by thermokarst processes, in particular within the spatial extent of the relief-forming Ice Complex. The mature thermokarst relief that advancing coastal erosion encounters on the mainland site leads to a variety of coastal slope types, differences in eroded volumes and subsequent carbon and clastic material fluxes from the coasts to the shallow shelf sea. The purpose of coastal erosion quantification requires consideration of the geomorphological heterogeneity, specifically accurate topographic information, in order to account for corresponding changes of the cryolithological composition in the near surface ground that is being eroded.

Within the framework of the Russian-German cooperation System Laptev Sea, geodetic measurements using a tacheometer were often conducted during previous expeditions (e.g., Are *et al.*, 2000; Grigoriev *et al.*, 2001, 2003; Grigoriev, 2004; Günther *et al.*, 2011). Cliff top line geodetic surveys provide the modern position of the upper edge of a coastline in a high level of detail, while annually repeated surveys give a better understanding of temporal variability of coastal erosion. In comparison with historical aerial photographs from the 1970's, which also exhibit a high level of detail, on site survey data were often used for determining mean annual coastline position changes over a certain period and coastal dynamics quantification (e.g., Günther *et al.*, 2011). In fact, this approach has traditionally not been applied by researchers because it is the best achievable or imaginable kind of time series dataset, but rather because of the lack of available remote sensing data, comparable to the spatial resolution and stereo capability of the almost 40 years old airphotographs of this region.

As part of continuing coastal thermo-erosion studies in the Laptev Sea region, during this expedition in 2011 topographic surveys were undertaken in the vicinity of Cape Mamontov Klyk along the Olenyok-Anabar coastal lowland and on Muostakh Island in the Buor Khaya Gulf. Beside the conventional use as described above, the data will be mainly used as topographic reference measurements. Our aim is to make use of the possibilities offered by modern very-high resolution optical remote sensing data. Georeferencing of satellite images plays an essential role in spatial calibration of multitemporal and multisensor data for change detection analyses. While georeferencing corrects for most distortions connected with the acquisition system, orthorectification accounts for relief-induced displacement effects and creates satellite image

products with the geometry of a map, allowing for distance and area measurements. Current high resolution sensors such as GeoEye are characterized by their high agility, resulting most often in non-vertical perspective images. Despite the almost flat terrain of the northeast Siberian tundra lowlands, sharp breaks in elevation along coastal cliffs may cause considerable positional errors within the image by a multiple of the initial spatial resolution of the dataset. Therefore, accurate terrain approximation is a prerequisite for coastal erosion monitoring. This is especially true when most recent changes over short time scales are of interest and should be compared to long-term developments.

## 4.2 Study sites

The studied coastline on Mamontov Klyk stretched along the WNW-ESE oriented 2.5 km long segment between the Nuchchi Dzhielekh River mouth and the navigation mark at Cape Mamontov Klyk. According to Schirrmeyer *et al.* (2008) the coastal cliff is composed of less ice-rich silts and sands of fluvial origin with peat layers that are covered with 20 - 30 m thick ice-supersaturated silty to sandy deposits of the Ice Complex formation. The hinterland of the studied coastline segment is dissected by thermo-erosional valleys, oriented parallel to the coast and draining into the Nuchchi Dzhielekh River. The terrain surface on yedoma interfluvies is flat, while it is dominated by high-centered polygons and vegetation covered thermokarst mounds on gentle slopes on both sides of thermo-erosional valleys. Most the coastal cliff itself is built of undisturbed yedoma. In places where Ice Complex extends down below sea level, coastal cliffs were considerably steeper than in places where sands are cropping out at sea level.

Muostakh Island is well known for its exceptional rapid coastal erosion rates of up to 25 m/yr. The island is elongated from NNW to SSE,  $\approx 7.5$  km long and  $\leq 500$  m wide and represents a remnant of the Late Pleistocene accumulation plain. Being entirely composed of Ice Complex deposits it is covered by moss-grass and dwarf shrub tundra. The east-facing coast is actively eroding and characterized by near vertical cliffs in the north and more gentle eroding coastal slopes in the south. The west-facing coast is characterized by an alternation of reactivated and dead erosional cliffs. The steep coastal slopes of the west coast are interrupted by a thermokarst depression that is cut along 600 m, forming a stable flat coast. South of the former polar station an almost 10 km long sand spit, which in places might be submerged during high tides, is extending the islands dimensions in this direction. On the northern edge of the island, a sand spit is currently developing (Fig.4.2) and served as one installation site of the tacheometer during the survey of Muostakh's northern cliff (Fig. 4.35 & 4.36).

## 4.3 Field methods

According to the tight expedition time schedule we had two measurement days on Mamontov Klyk on 14<sup>th</sup> and 15<sup>th</sup> August and six measurement days on Muostakh Island from 17<sup>th</sup> to 29<sup>th</sup> August 2011. We used a ZEISS ELTA C30 tacheometer (Fig. 4.1a) for distance and height measurements with a work setup similar to Günther *et al.* (2011). Measurements were taken in twos with the corresponding reflector mirror KTR-1N, mounted on a telescopic bar with an adjustable length of up to 4 m. Usually we operated the reflector with a length of 2 m (Fig. 4.1b).

To ensure repeated surveys and to be able to continue the survey on the next day with consistent positioning, we defined a local coordinate system. A network of well distributed anchor points, so called backside points, had to be set up, within which the “free-stationing” approach could be applied. For each backside point coordinates of an absolute coordinate system were collected using the waypoint averaging function of a positioning system device. All points of this network were marked with a measurement plastic plug in the ground and a numbered wooden stick (Fig. 4.2).



**Fig. 4.1:** Methodological setup of topographic surveys: (a) tacheometer operator on coastal cliff top near navigation sign Mamontov Klyk; (b) reflector mirror operator on a coastal slope.



**Fig. 4.2:** Fixed and marked backside point (№ 29) near the northern cape and adjacent sand spit of Muostakh. Backside points can be used for repeat surveys during following expeditions in order to support consistent instrument positioning.



## 4.4 Elements of remote sensing

A variety of earth observation satellites were tasked for synchronous to field work remote sensing data acquisition. A high degree of uncertainty about successful acquisitions affected our field work, since the large spectrum of spatial and spectral resolutions of the sensors require individual kinds of reference data and ground control points. We need to find the right balance of objects which are distinctive enough, having a high contrast but at the same time are observable from space. Very small water bodies or small islands within such are appropriate objects, but particularly run the risk of disappearing until the next successful acquisition. Only a quarter of collected ground control points later have proven their usefulness.

RapidEye is a constellation of five satellites identical in construction, providing high resolution multispectral imagery with a revisit time of one day. The combination of so far incompatible characteristics of high geometric resolution (6.5 m) and large areal coverage (70 x 140 km) offers the unique opportunity to set up a geometrically and seasonally consistent reference dataset not only for coastline change detection in remote areas of the East Siberian arctic lowlands. The RapidEye dataset is a prerequisite to integrate images of the CORONA mission from the 1960's with important information on old coastline positions. CORONA images have already been used at Mamontov Klyk for ground truthing of studies on periglacial geomorphology (Grosse, 2004). GeoEye provides very high geometric resolution of about half a meter in panchromatic mode and is capable for acquisition of stereo scenes, allowing the generation of high detail digital elevation models (DEM), which are then used for ortho-rectification. GeoEye and RapidEye data were acquired on 8<sup>th</sup> and 13<sup>th</sup> August 2011, respectively, over the Anabar-Olenyok coastal lowland, shortly before arrival of the expedition team. Figure 4.3 illustrates the high topographic detail available from a GeoEye DEM of the Mamontov Klyk area.

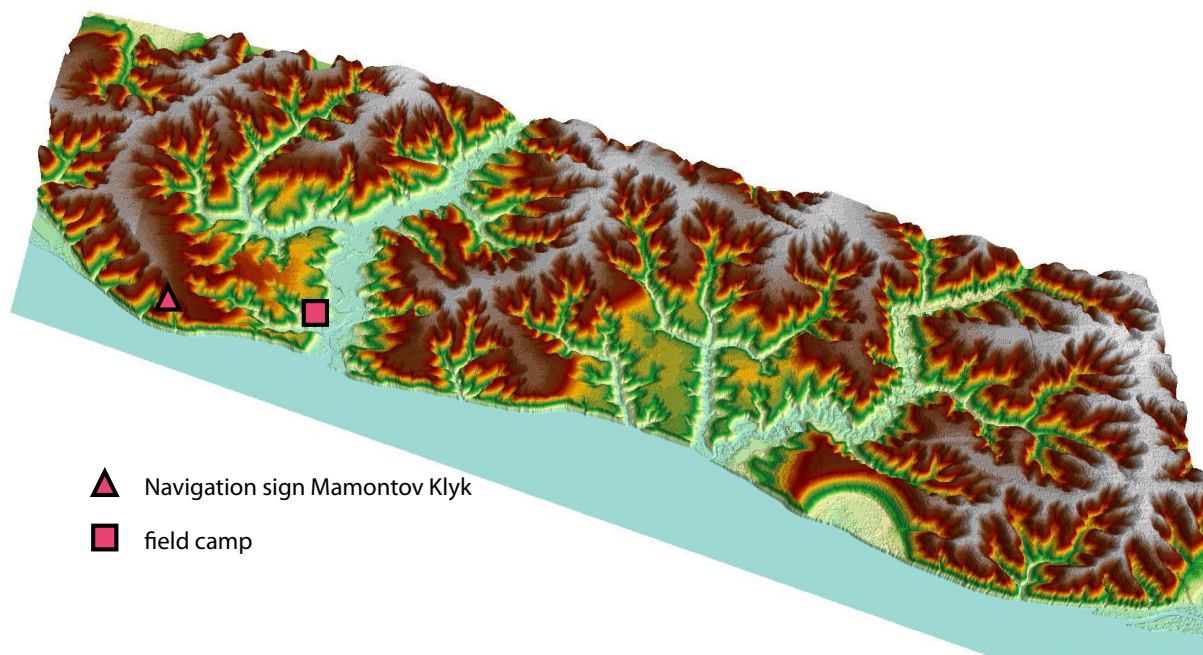


**Fig. 4.3:** Oblique view of a digital elevation model of the Mamontov Klyk area created from GeoEye stereo imagery, using on-site tacheometric measurements as topographic reference data; point indicates field camp location near Nuchchi Dzhielkh River mouth.

## 4.5 Field results

### Mamontov Klyk

Around Cape Mamontov Klyk 310 points were measured (Table 4.1). A tacheometric transect (Fig. 4.4), starting from the navigation sign and extending inland along a saddle separating two wide hollows, included small ponds and distinctive crosses between high centered polygons, which serve as input reference height points for subsequent photogrammetric DEM generation (Fig. 4.3). In this manner the height accuracy of the GeoEye DEM in the field work area could be determined as root mean square error (RMSE) of 0.8 m. Measurements along the cliff top serve as reference height points too and as a baseline for coastline change detection. The surface of a thermo-terrace next to the navigation sign was in part stabilized by fresh vegetation cover and in other parts the headwall was actively eroding. Thermokarst mounds (*baydzharakhs*) were levelled in the upper part and steep conical in the lower part, where the cliff bottom is eroding. This observation encouraged us to further study different space-time dynamics of thermo-abrasion along the cliff bottom and thermo-denudation along the cliff top. Approximately in the area of the C1 borehole the coastal cliff becomes less wide and steeper (Fig. 4.4).

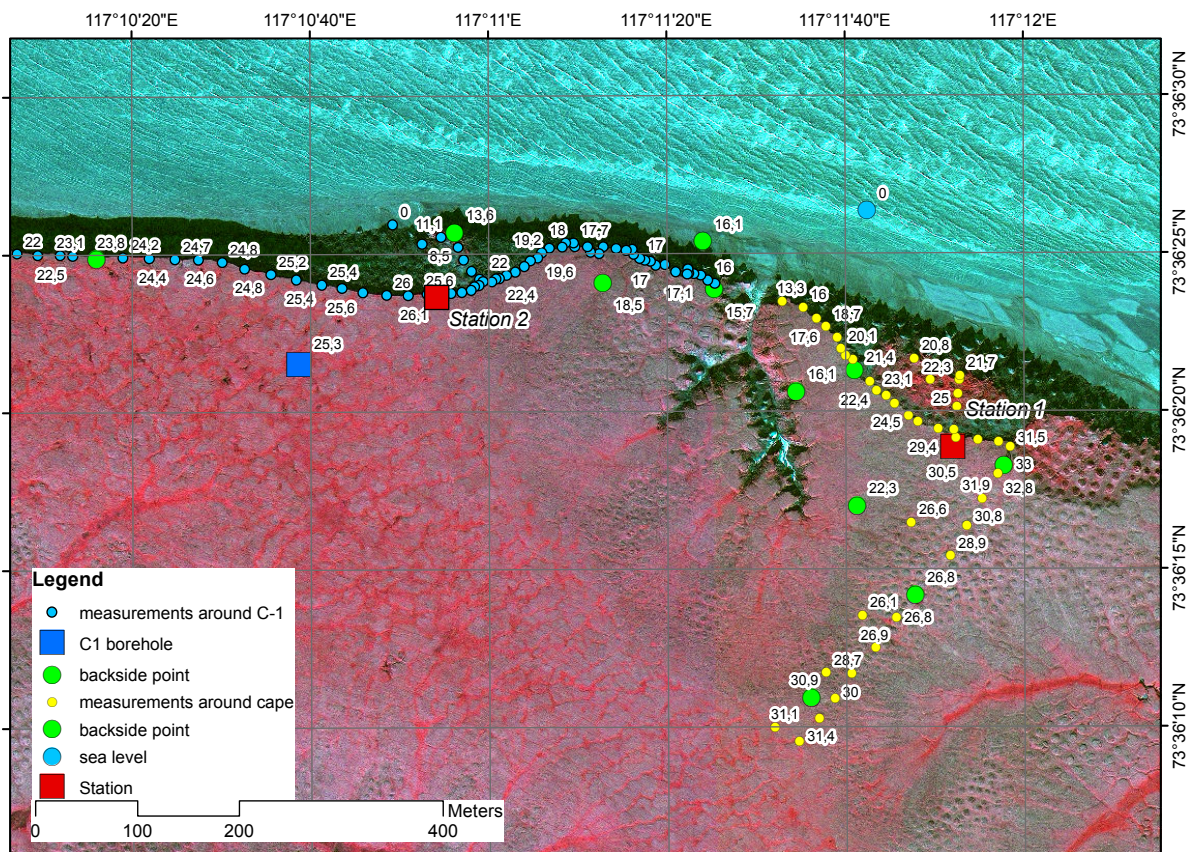


**Fig. 4.4:** Topographic survey on Cape Mamontov Klyk: point measurements were taken using a tacheometer from two different instrument positions (stations) on 14<sup>th</sup> and 15<sup>th</sup> August 2011 (background: 2011 GeoEye image).

## 4.5 Field results

Around the third tacheometer station we established a monitoring site for cliff top retreat observations. During the originally scheduled two weeks stay on Mamontov Klyk we planned repeat surveys along a coastline, where a cliff protrusion that is associated with compacted material of a former valley bottom alternate with undisturbed Ice Complex segments. For this purpose initial point measurements were made at short intervals (Fig. 4.5), but a repeat survey was not conducted later. A set of two ortho-rectified GeoEye images aligned to one another allows preliminary estimations of annual coastal erosion for the survey area of around  $4\text{m}/\text{yr}$  over the last two years.

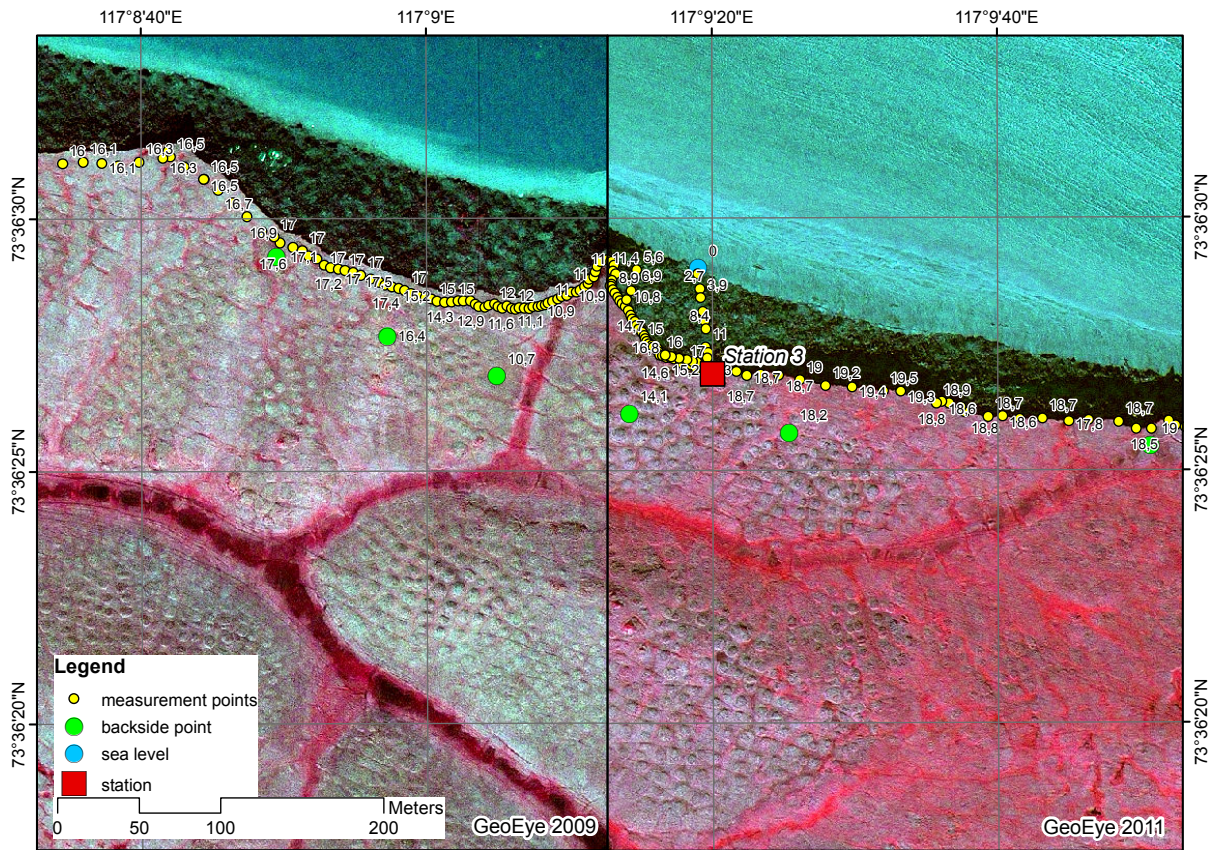


**Fig. 4.5:** Tacheometric survey on Cape Mamontov Klyk: point measurements were taken using a tacheometer from two different instrument positions (stations) on 14<sup>th</sup> and 15<sup>th</sup> August 2011 (background: 2009 and 2011 GeoEye image).

**Tab. 4.1:** Summary of topographic survey on Cape Mamontov Klyk divided into campaigns of different tacheometer stations.

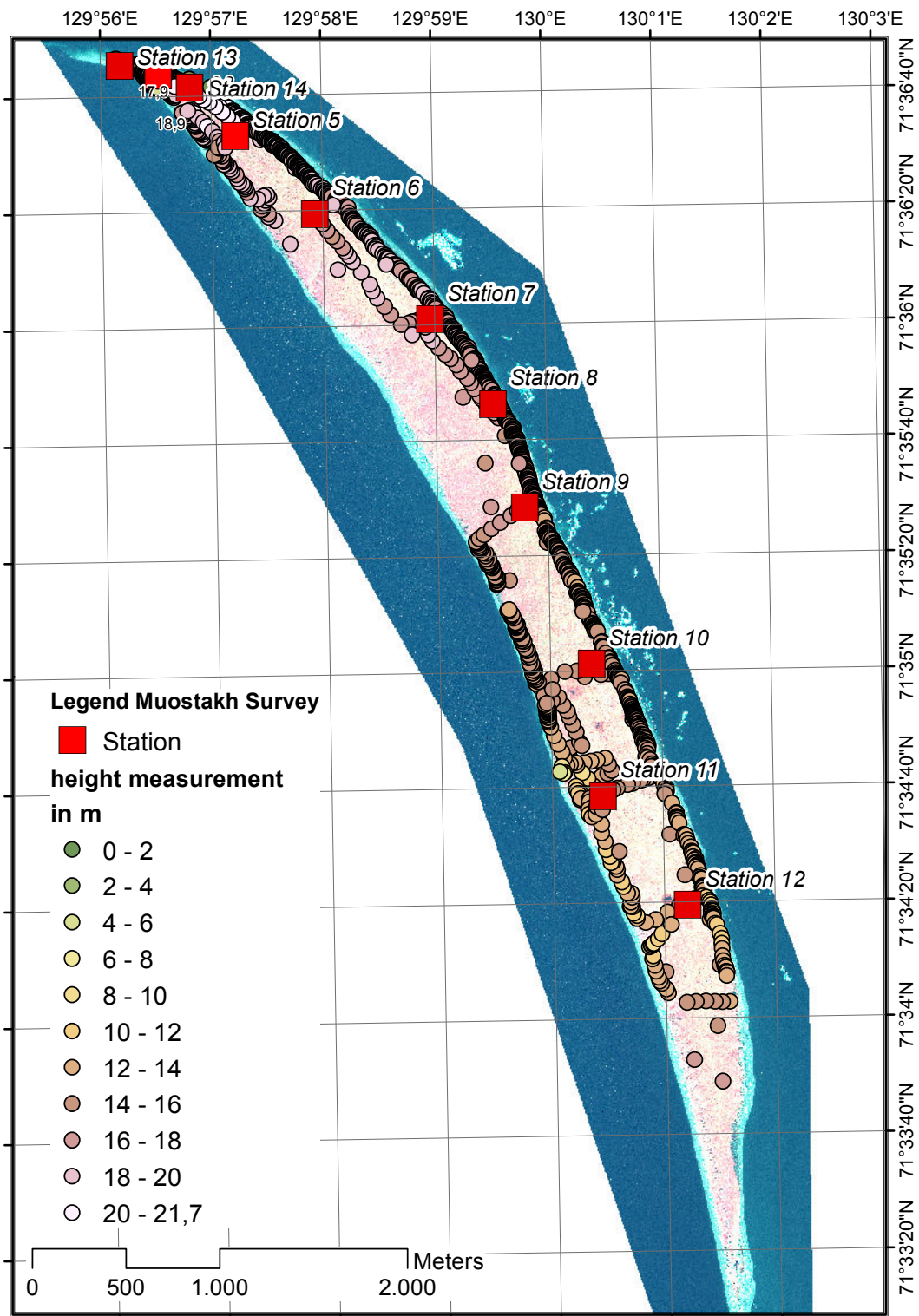
Station №	measurement points ( <i>n</i> )	cliff top height range [m]	backside points for geocoding ( <i>n</i> )	geocoding XY-RMSE [m]
1	49	13.3 - 31.5	6	0.57
2	74	15.4 - 26.3	5	0.27
3	187	10.8 - 21	8	0.85
<i>total</i>	310	0-33	22	0.68

### Muostakh

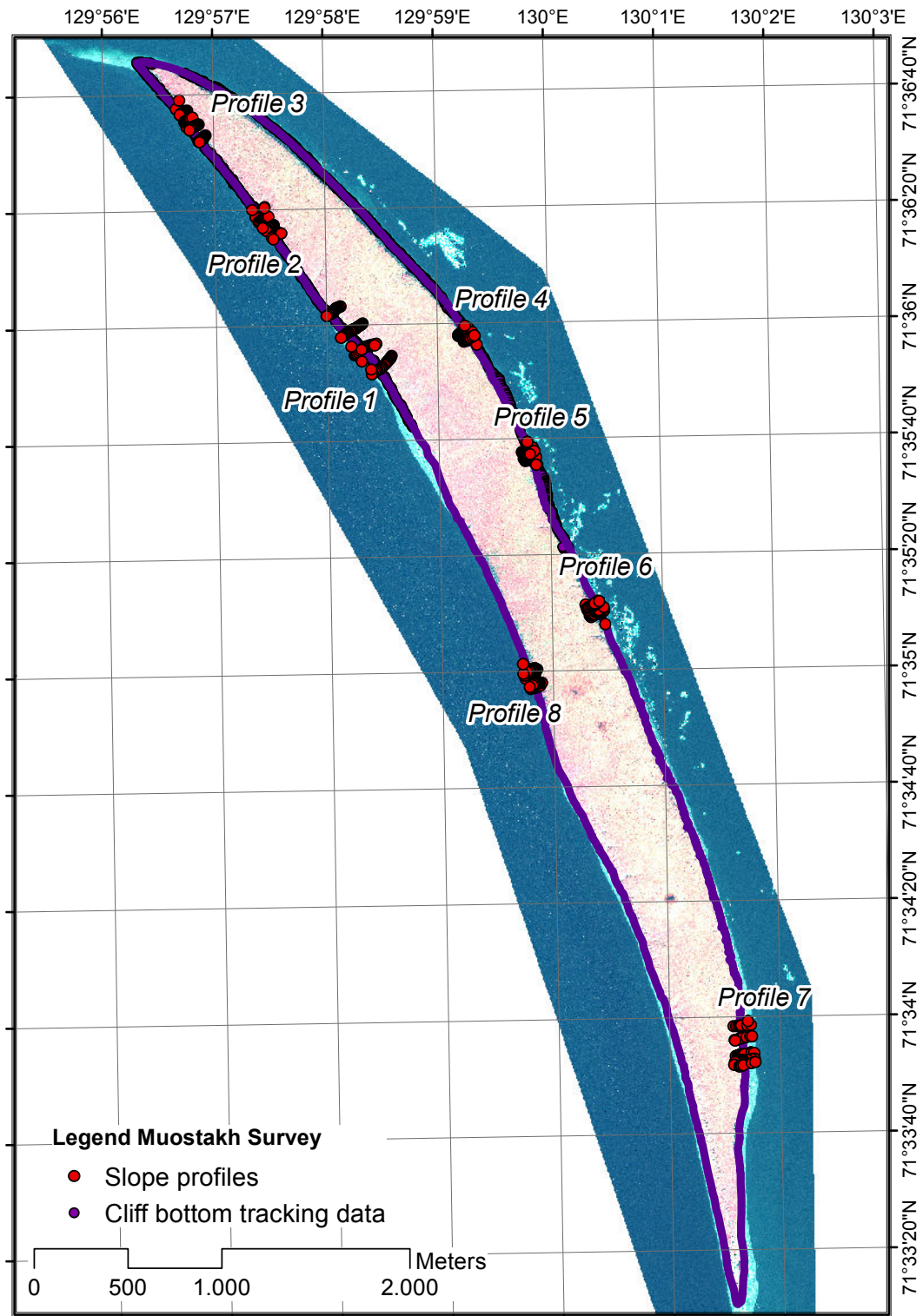
On Muostakh Island altogether 1350 points were measured (Table 4.2). The local coordinates had to be transformed into an absolute coordinate system using all backside points and stations with known absolute coordinates as control points. This was done in two steps. Since each station was equipped with a high redundancy of backside points, in a first step separate geocoding of each point cloud of a particular station was conducted and provided good results, often with sub-metre accuracies. In this way we improved the known coordinates of all control points and could identify local outliers using least squares adjustment. Mean stationing accuracies of 0.15 m within the project revealed the whole survey point cloud to be highly self-consistent. Consequently in a second step all control points with improved coordinates were included in an one-time affine transformation of the whole project from the local to an absolute system, to restore the initially correct point relations. with an overall absolute geocoding RMSE of 1.36 m. Uncertainties of the preparatory control point improvement and the final geocoding step were 1.01 and 1.36 m, respectively. The quadratic sum corresponds to a cumulative geocoding uncertainty of the whole survey of 1.7 m. Figure 4.6 shows the spatial distribution of tacheometric measurements. Figures 4.10 to 4.37 show the backside point environment for each of the 11 tacheometer stations and associated point measurements, which were mainly concentrated along the upper edge of actively eroding cliffs.

On the northern cape of Muostakh we found the long-term reference point near the geodetic landmark was eroded away. For maintainance of the long-term annual on-site visits of the colleagues from the Mel'nikov Permafrost Institute in Yakutsk, we established a transect of new reference points and included it into the survey project (Fig. 4.37). In order to provide a benchmark for the year of our expedition, we here report that, preliminary estimations indicate that coastal erosion of the northeastern cliff of Muostakh between 2010 and 2011 ranged from 14-16 m/yr, depending on the bearing angle from the previous reference point.

In addition to the tacheometric cliff top survey, a mapping campaign of the cliff bottom with automatic position tracking encircled the whole island (Fig 4.7). Moreover, we measured coastal profiles at four locations along the west and four locations along the east-facing coast. The wide distribution of coastal profile sites reflects different slope types and baidzharakh patterns that were identified on active and inactive slopes. At each location two profiles were made following the shortest path downslope between baidzharakhs and two across baidzharakhs. Figure 4.7 shows slope profile locations and figure 4.8 the data in an exemplary manner.



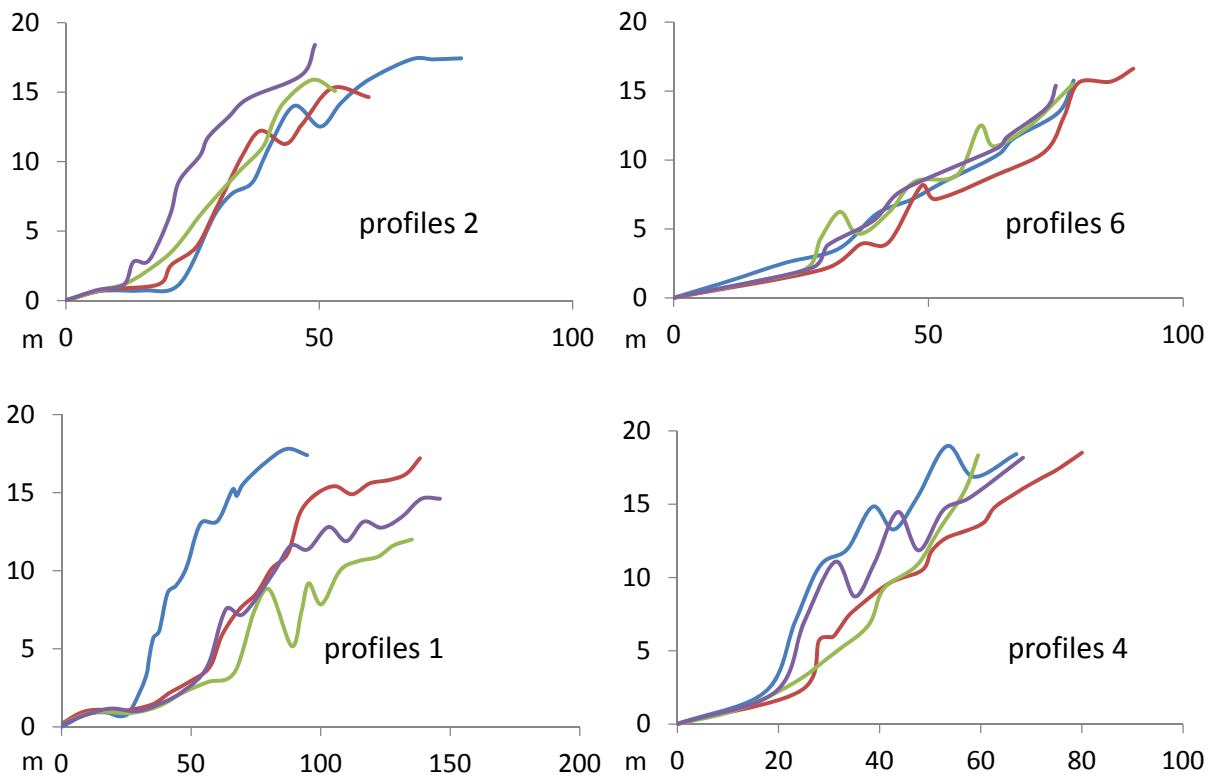
**Fig. 4.6:** Topographic survey of coastal cliffs on Muostakh Island: point measurements were taken using a tacheometer from a variety of instrument positions (stations) between 20<sup>th</sup> and 26<sup>th</sup> August 2011 (background: 2010 GeoEye image).



**Fig. 4.7:** Topographic survey on Muostakh: locations of slope profile measurements (background: 2010 GeoEye image).

**Tab. 4.2:** Summary of topographic survey on Muostakh Island divided into campaigns of different tachometer stations.

Station №	№ measurement points	xy stationing accuracy [m]	elevation range [m]	№ backside points for geocoding	geocoding XY- <i>RMSE</i> [m]
4	195	-	-0.2 - 21.4	9	1.35
5	159	0.09	14.1 - 20.6	8	1.08
6	122	0.17	15.8 - 20.2	8	0.84
7	117	0.06	15.9 - 18.5	7	0.97
8	92	0.06	14.6 - 18.3	8	0.97
9	222	0.06	12.1 - 16.9	8	0.73
10	126	0.16	12.5 - 16.5	8	1.04
11	132	0.31	5.5 - 16.2	6	1.08
12	66	0.3	8.9 - 16.7	11	1.33
13	92	0.03	0.8 - 20.7	8	0.9
14	27	0.03	0 - 20.7	7	0.67
<i>total</i>	1350	0.15	-0.2 - 20.7	43	1.01

**Fig. 4.8:** Examples of coastal slope profiles; at each location two profiles were made between baidzharakhs and two across them; different spacing of isolated baidzharakhs reflect varying ground ice conditions along the coastline.

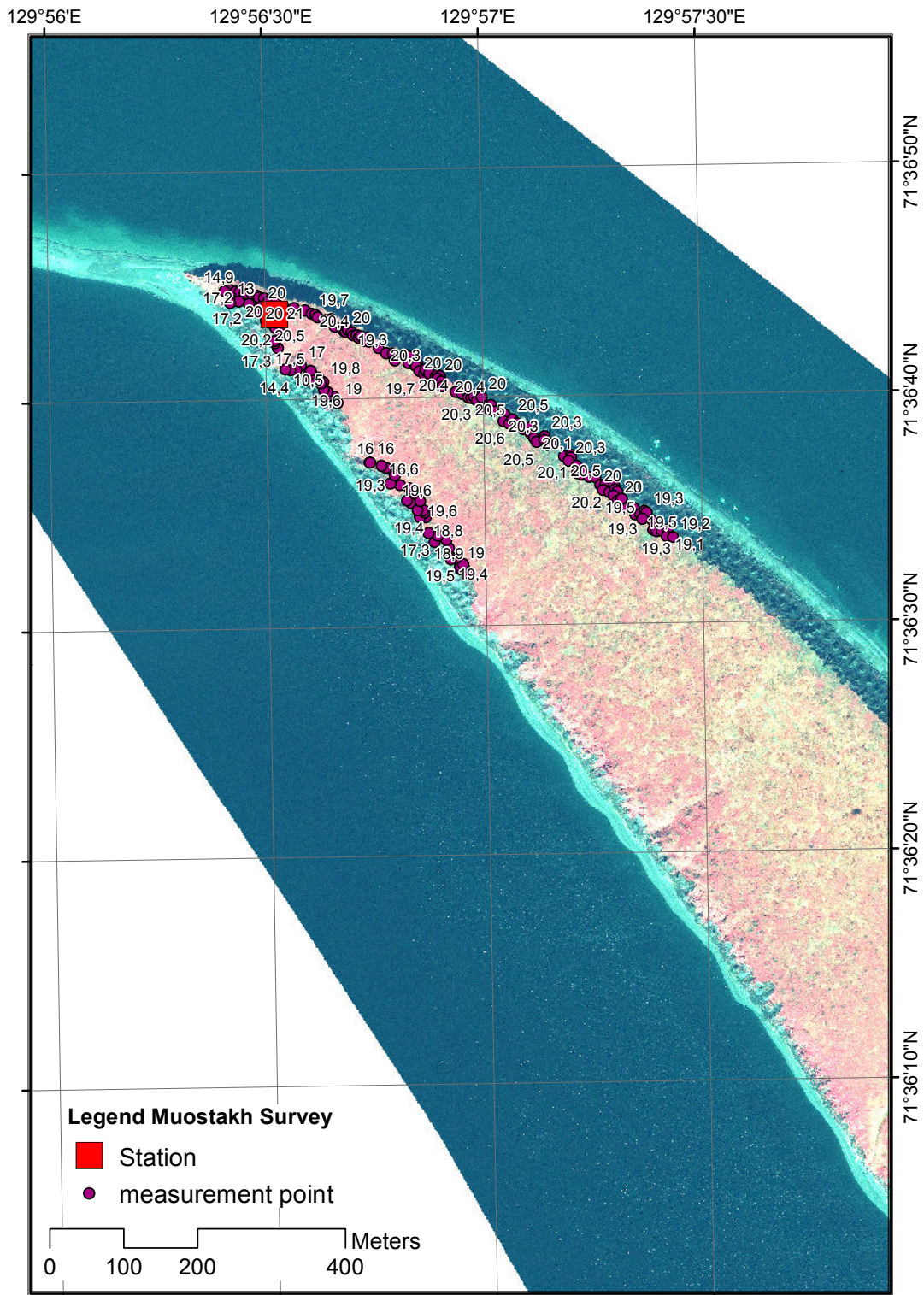


**Fig. 4.9:** Tacheometric survey on Muostakh: Point measurements labelled with elevation in m a.m.s.l. taken from tacheometer station 4 on 20<sup>th</sup> August 2011 (background: 2010 GeoEye image).



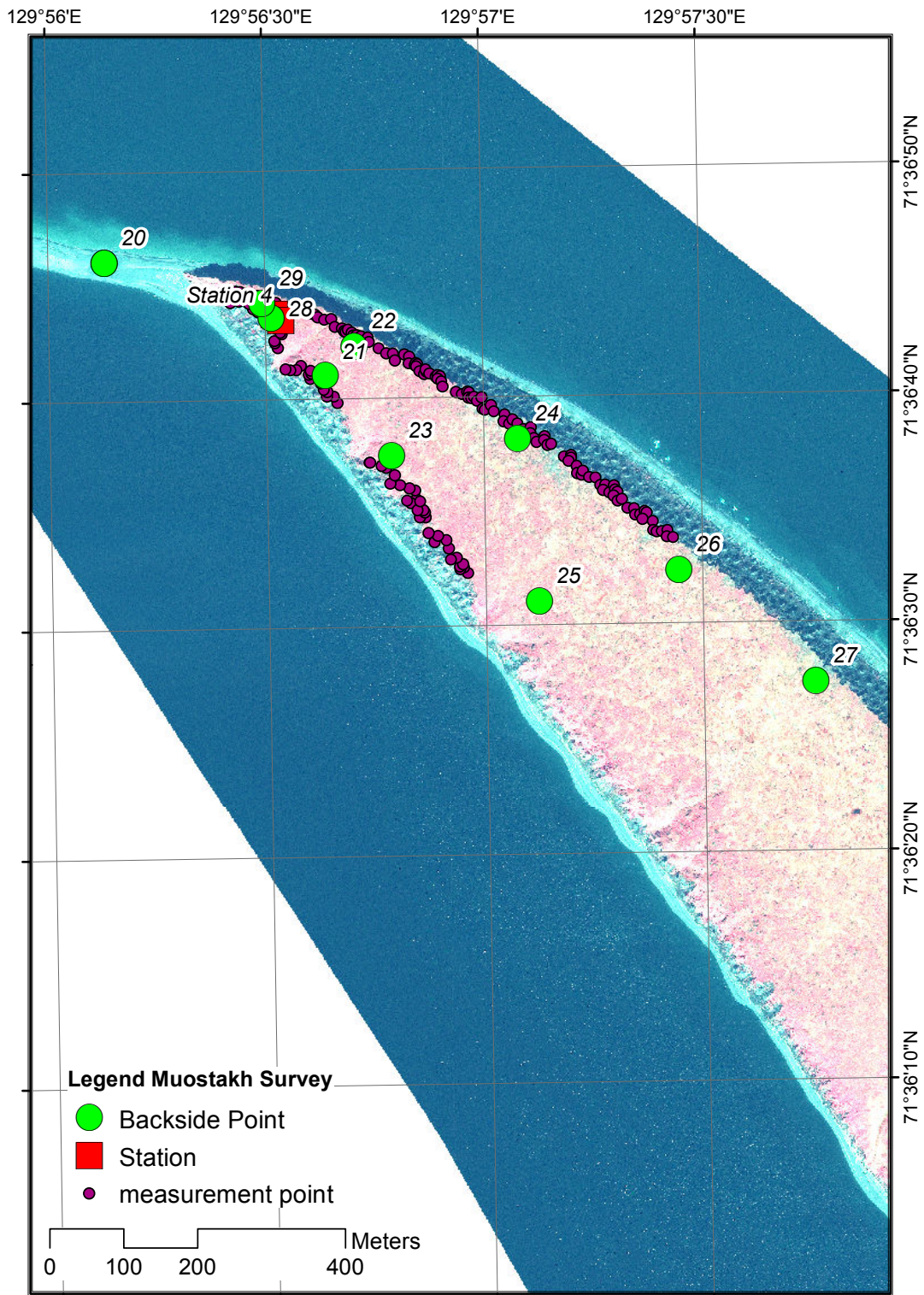


**Fig. 4.10:** Tacheometric survey on Muostakh: Calibration of new backside points taken from tacheometer station 4 (background: 2010 GeoEye image).

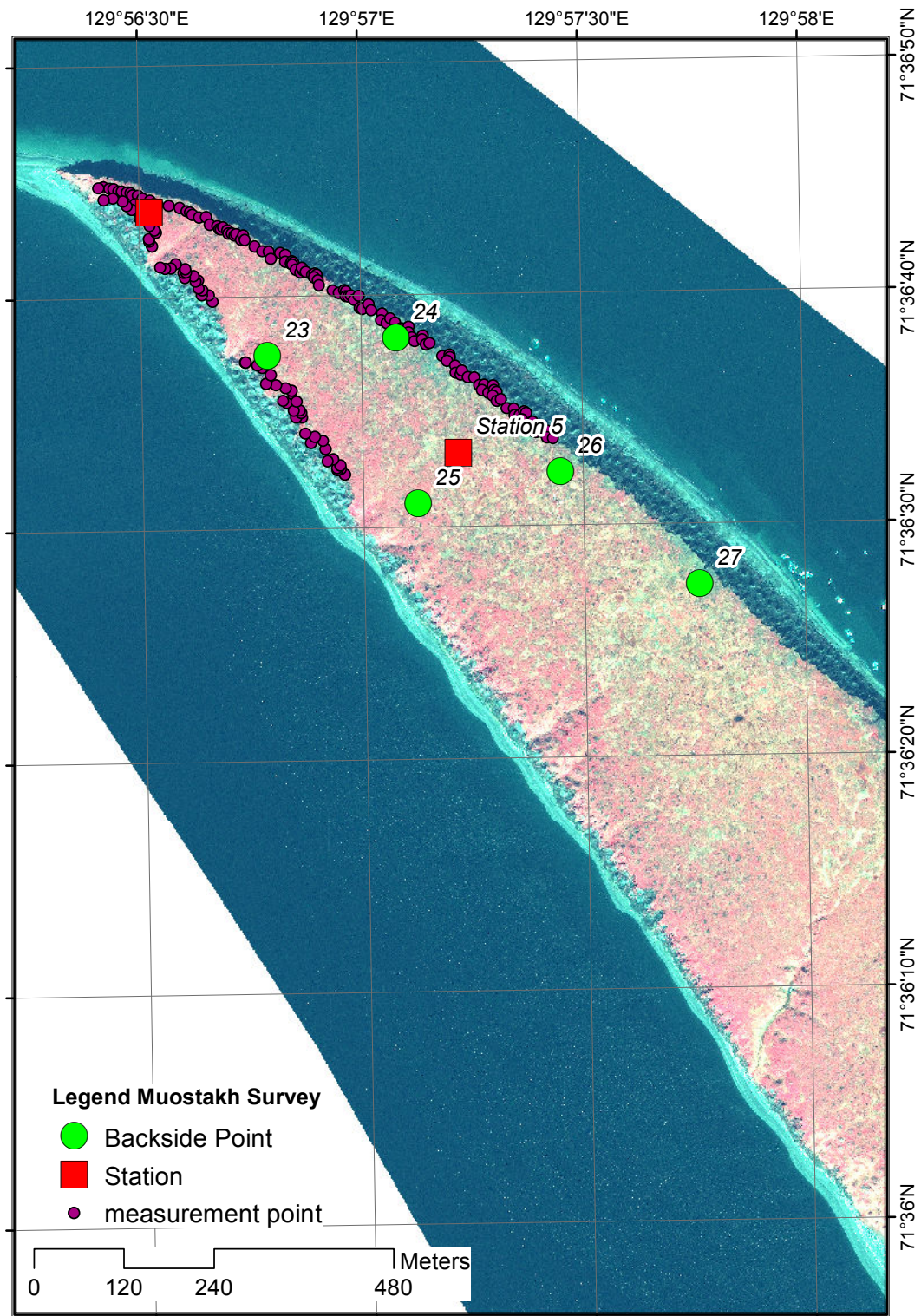


**Fig. 4.11:** Tacheometric survey on Muostakh: Free stationing of tacheometer station 5 based on a set of known backside points (background: 2010 GeoEye image).

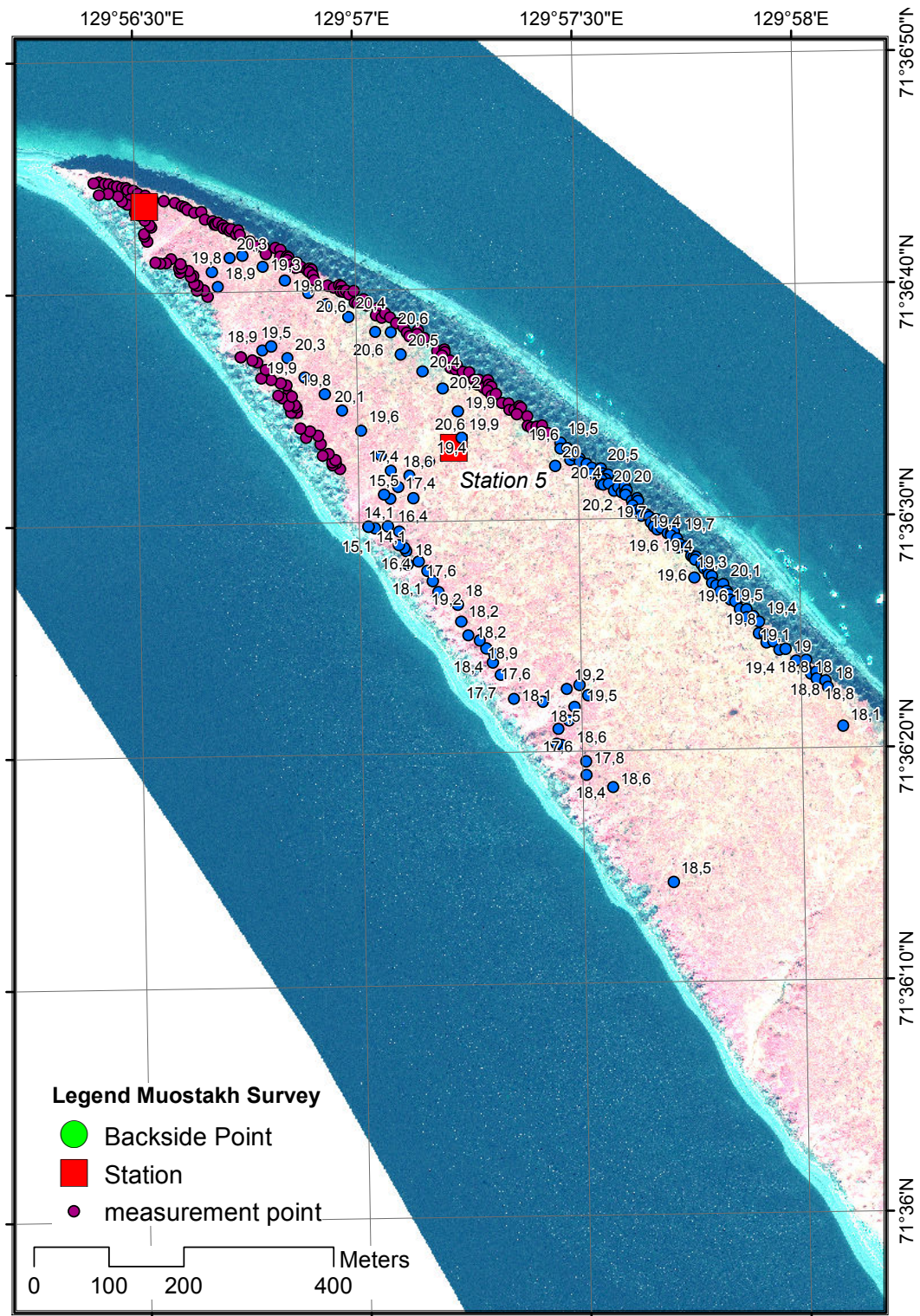


**Fig. 4.12:** Tacheometric survey on Muostakh: Point measurements labelled with elevation in m a.m.s.l. taken from tacheometer station 5 on 20<sup>th</sup> August 2011 (background: 2010 GeoEye image).

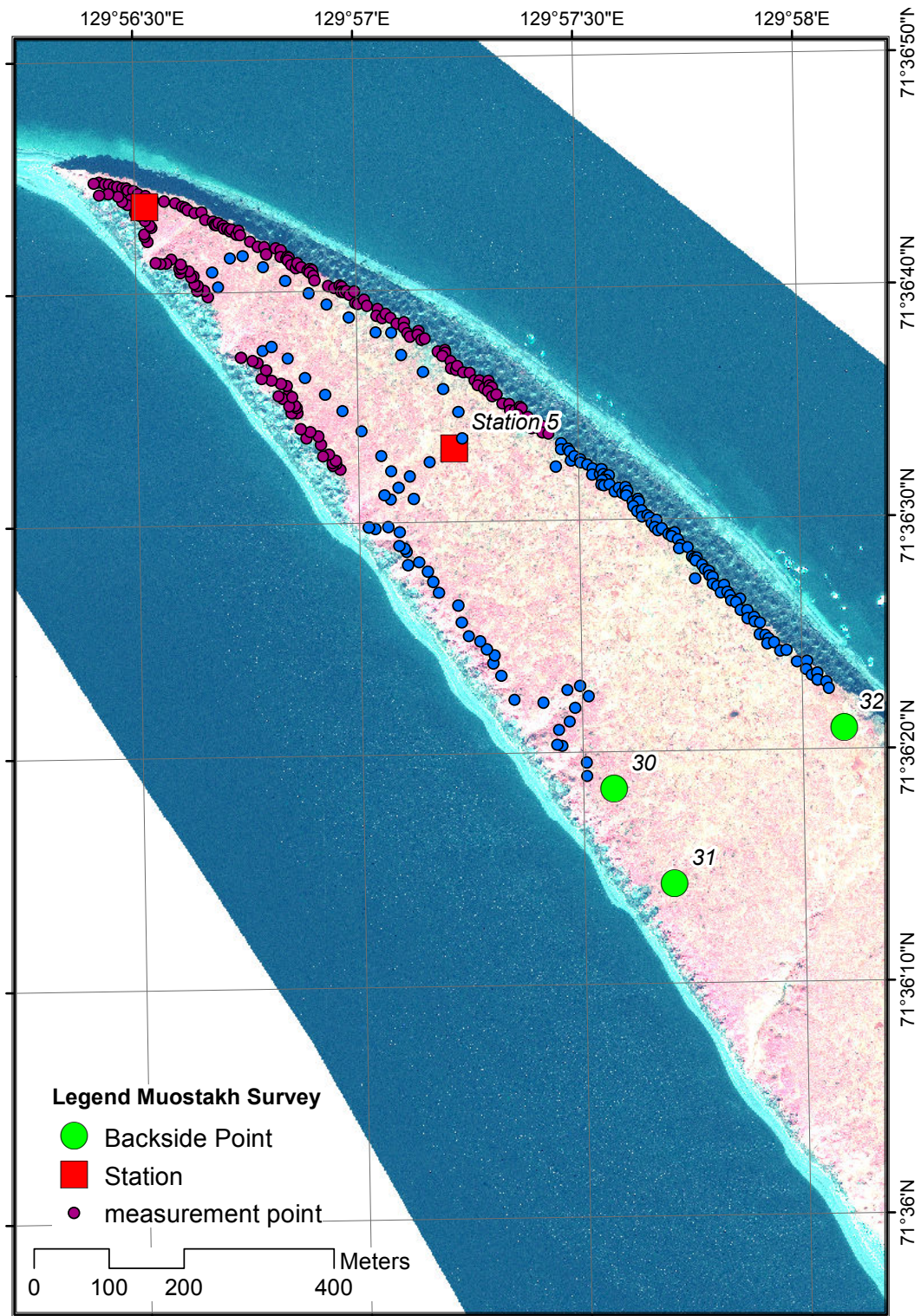


**Fig. 4.13:** Tacheometric survey on Muostakh: Calibration of new backside points taken from tacheometer station 5 (background: 2010 GeoEye image).

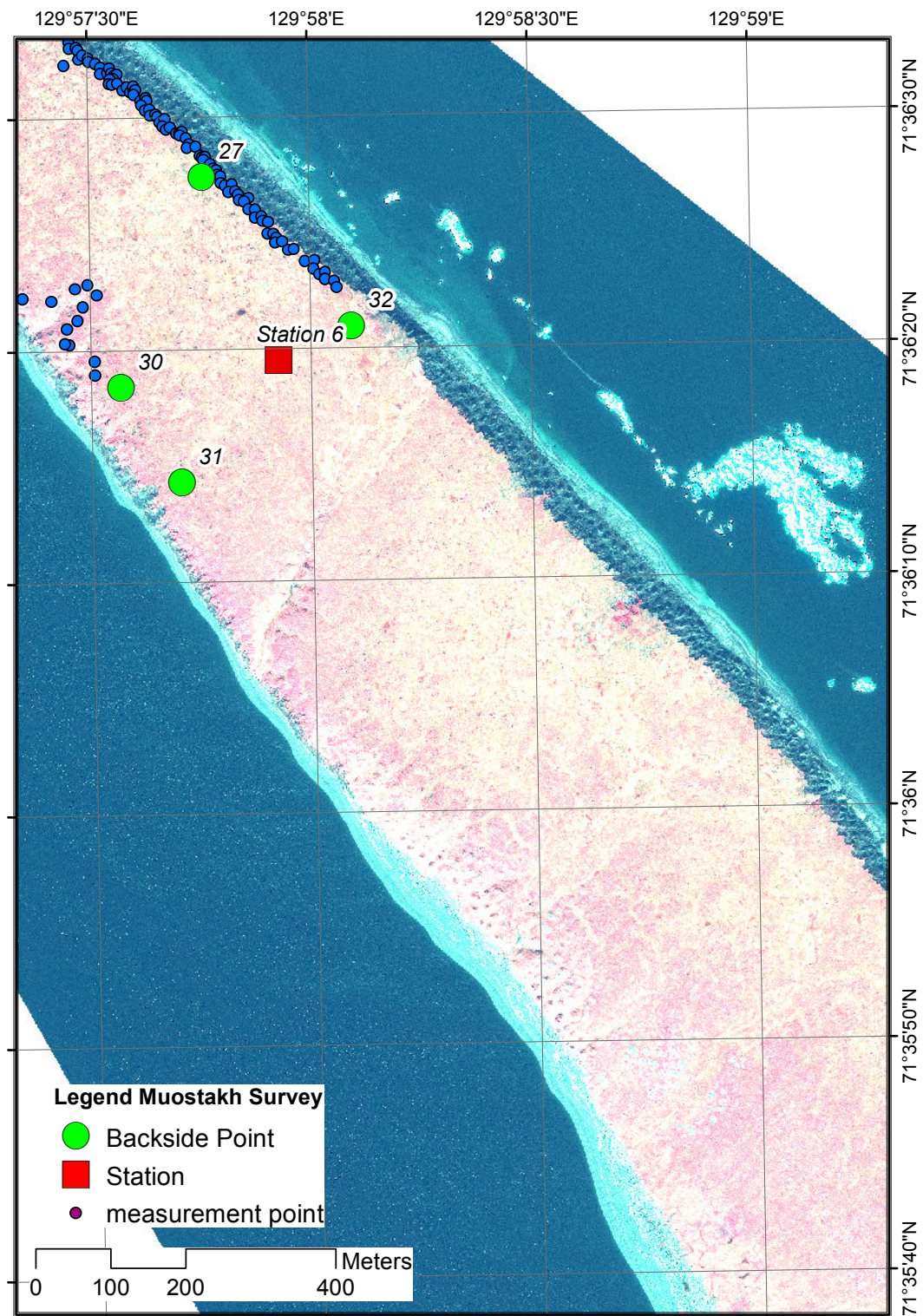


**Fig. 4.14:** Tacheometric survey on Muostakh: Free stationing of tacheometer station 6 based on a set of known backside points (background: 2010 GeoEye image).

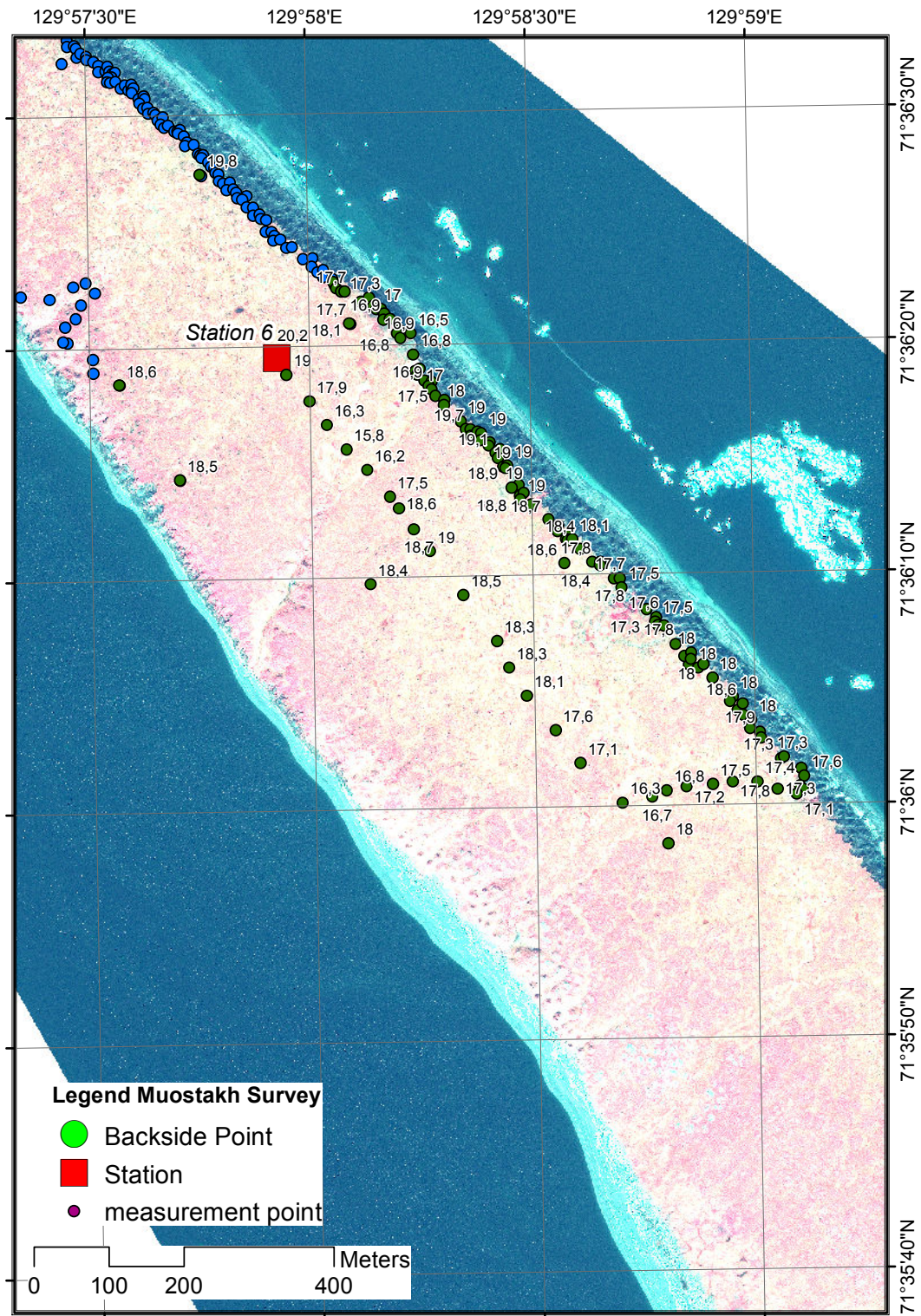


**Fig. 4.15:** Tacheometric survey on Muostakh: Point measurements labelled with elevation in m a.m.s.l. taken from tacheometer station 6 on 21<sup>st</sup> August 2011 (background: 2010 GeoEye image).

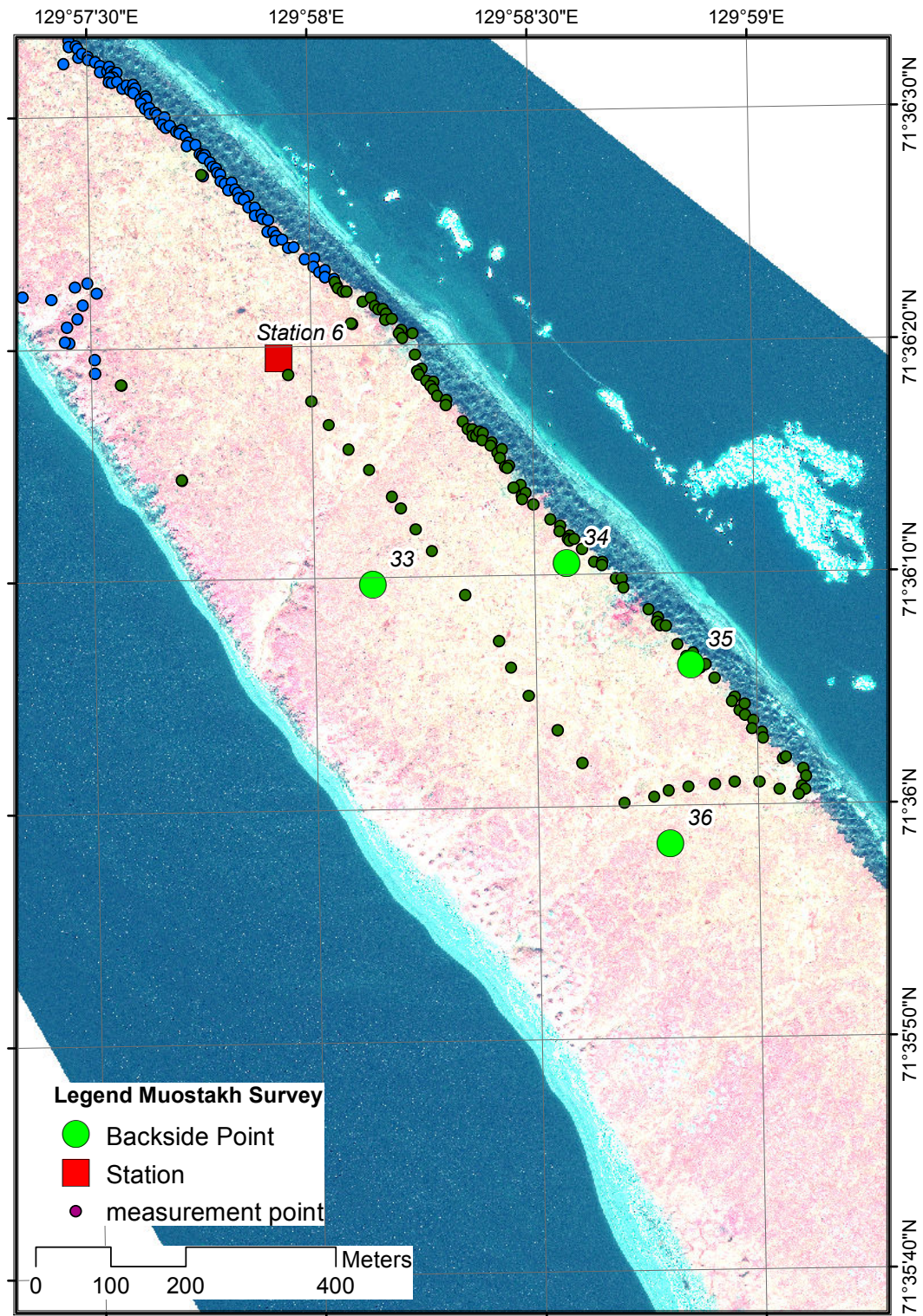


**Fig. 4.16:** Tacheometric survey on Muostakh: Calibration of new backside points taken from tacheometer station 6.

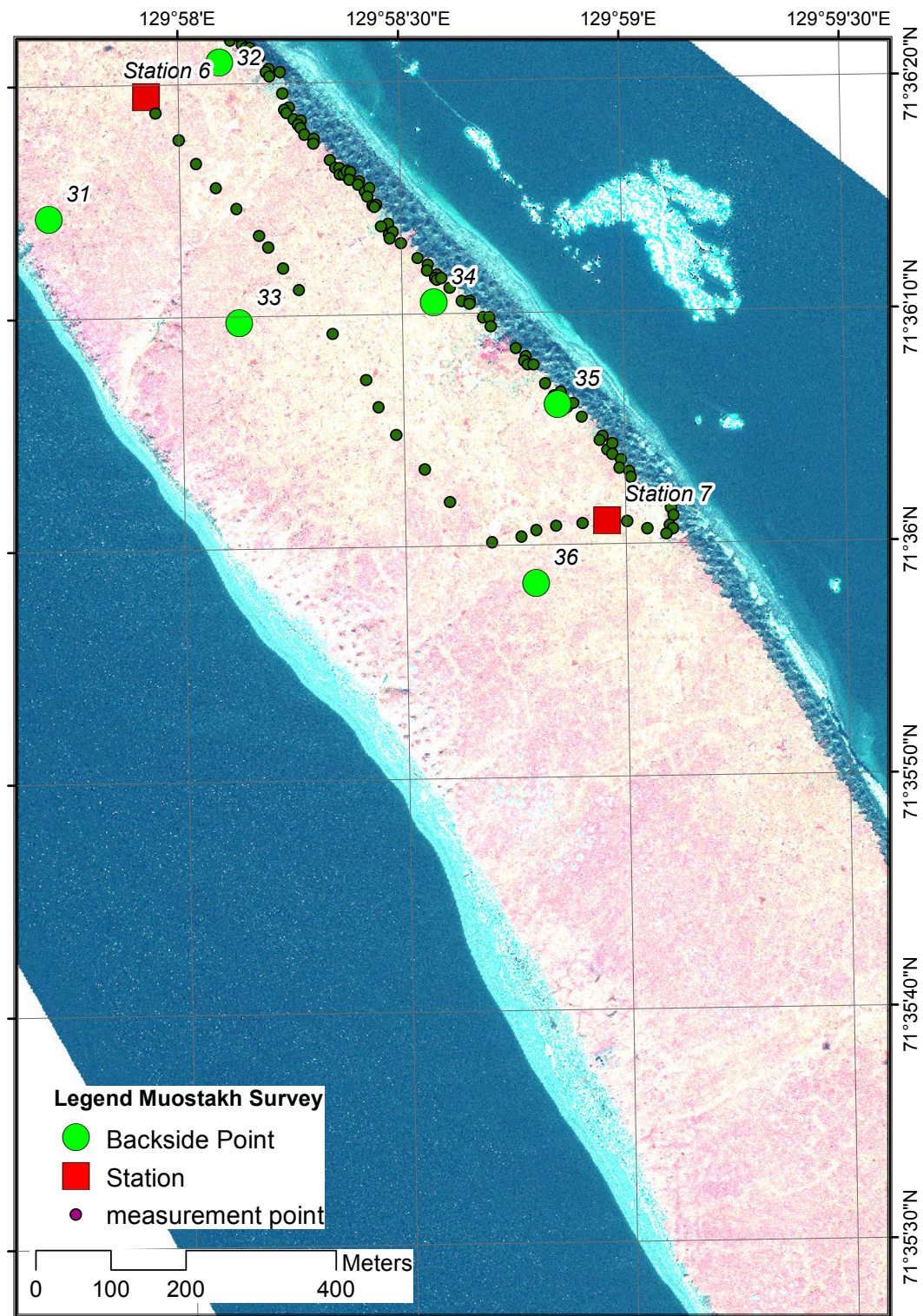


**Fig. 4.17:** Tacheometric survey on Muostakh: Free stationing of tacheometer station 7 based on a set of known backside points (background: 2010 GeoEye image).



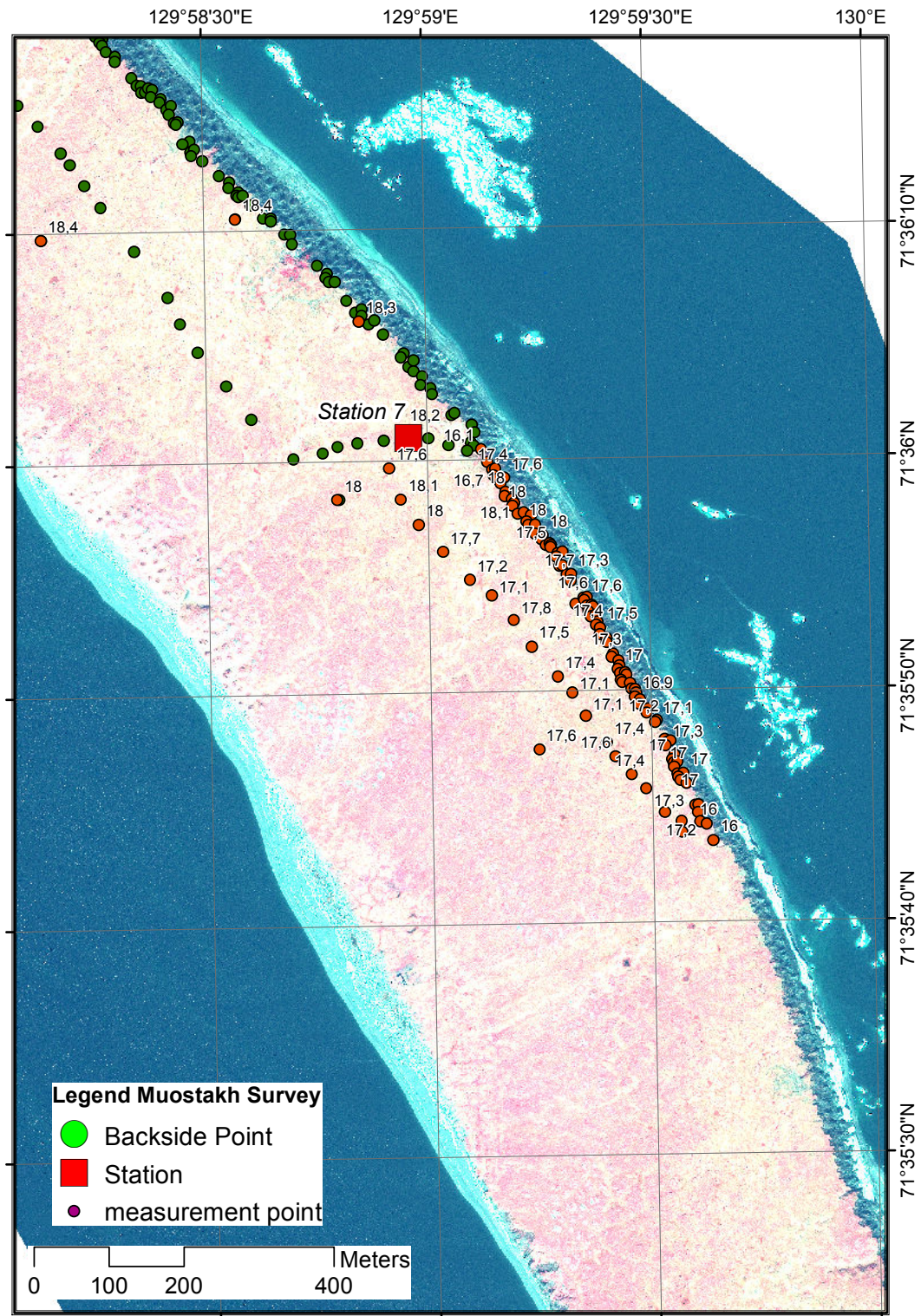


**Fig. 4.18:** Tacheometric survey on Muostakh: Point measurements labelled with elevation in m a.m.s.l. taken from tacheometer station 7 on 21<sup>st</sup> August 2011 (background: 2010 GeoEye image).

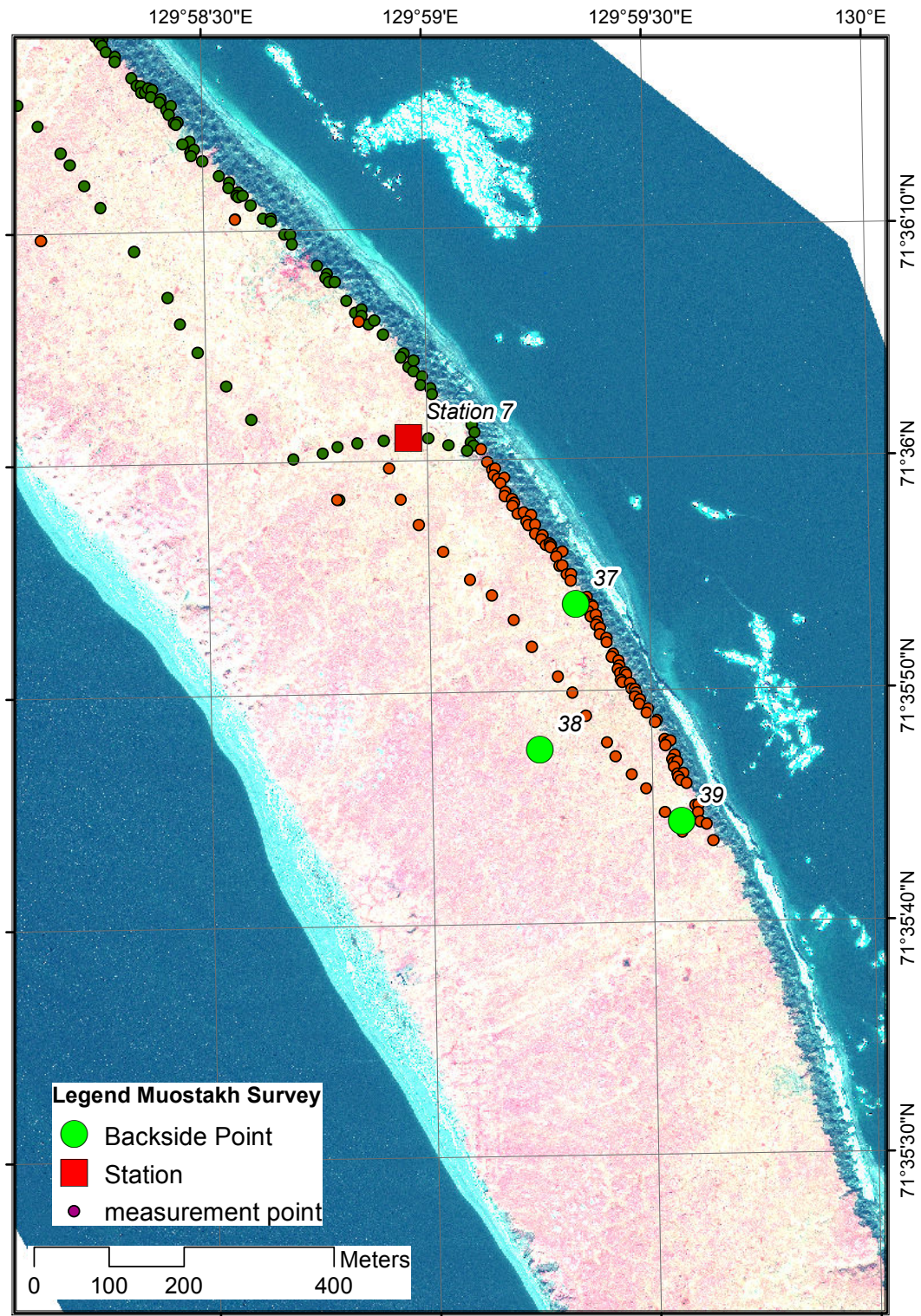


**Fig. 4.19:** Tacheometric survey on Muostakh: Calibration of new backside points taken from tacheometer station 7 (background: 2010 GeoEye image).

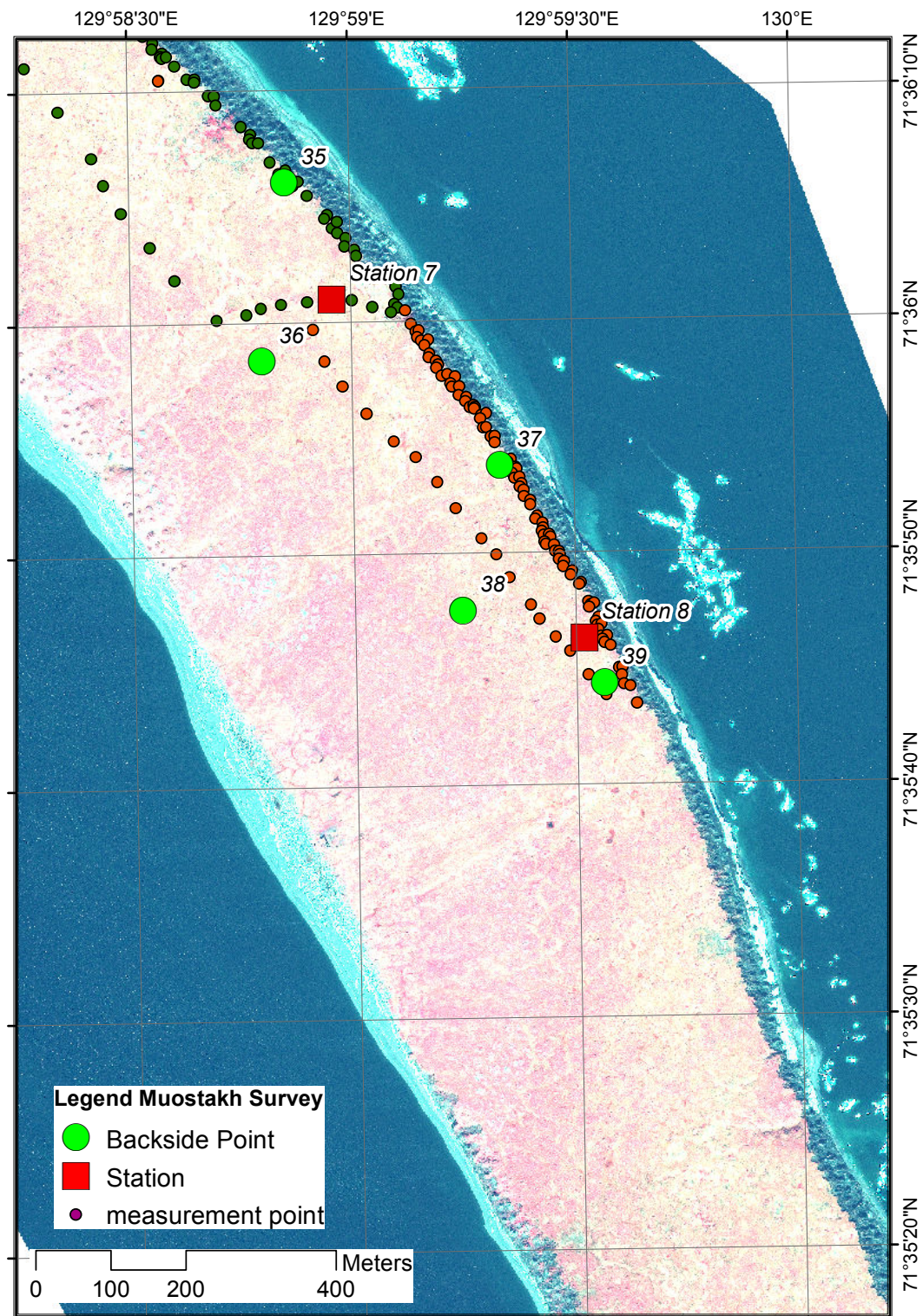


**Fig. 4.20:** Tacheometric survey on Muostakh: Free stationing of tacheometer station 8 based on a set of known backside points (background: 2010 GeoEye image).

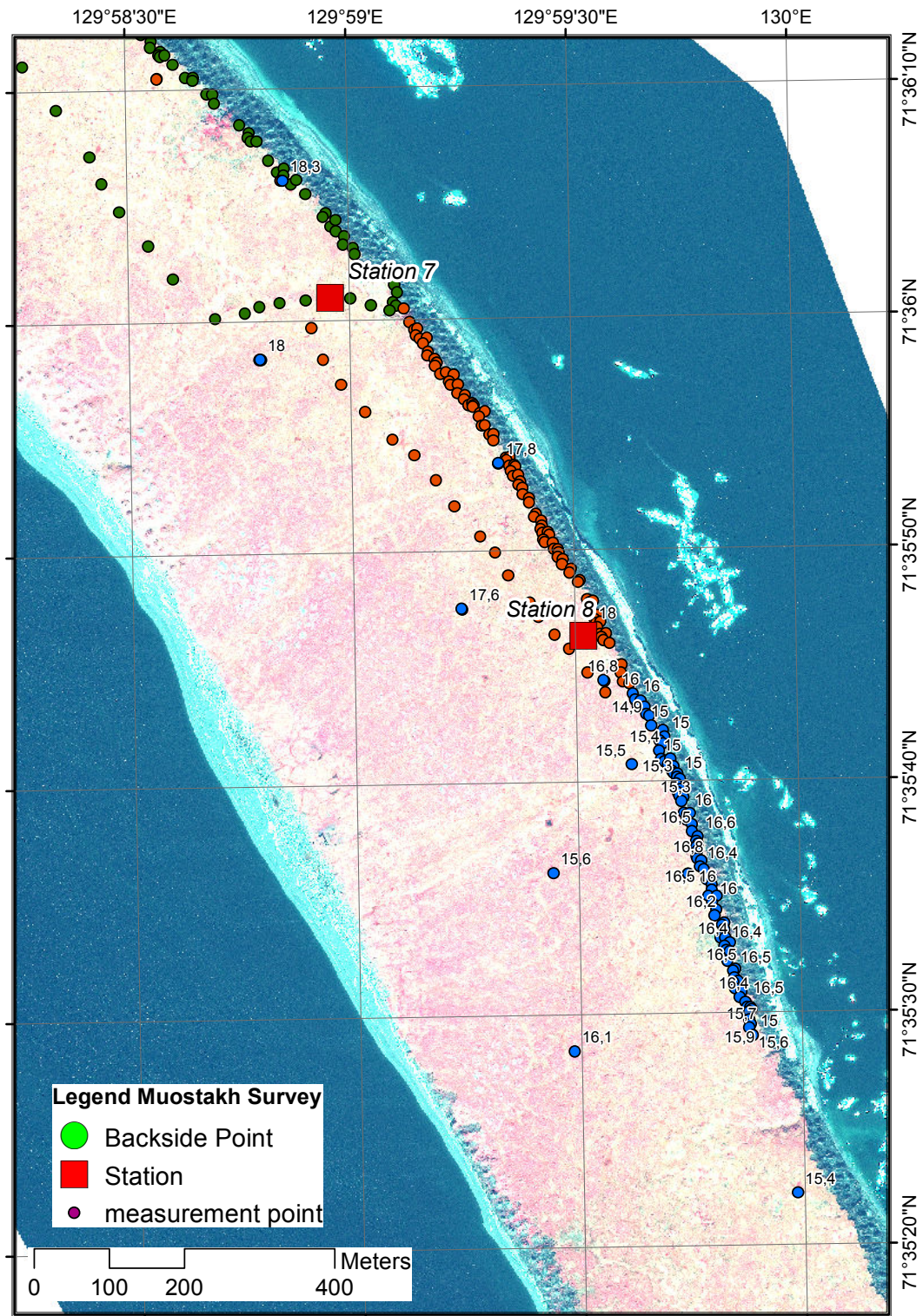


**Fig. 4.21:** Tacheometric survey on Muostakh: Point measurements labelled with elevation in m a.m.s.l. taken from tacheometer station 8 on 21<sup>st</sup> August 2011 (background: 2010 GeoEye image).

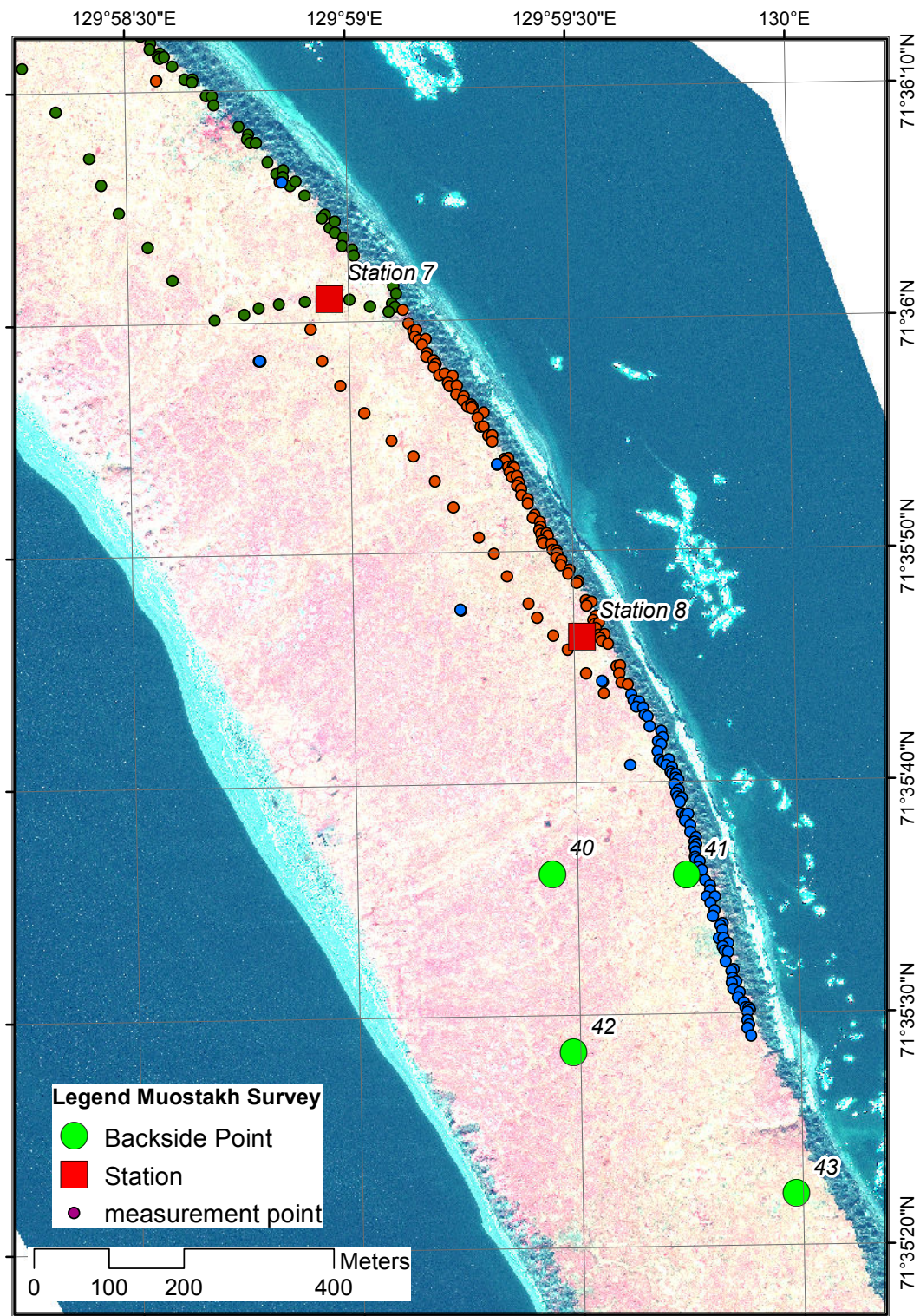


**Fig. 4.22:** Tacheometric survey on Muostakh: Calibration of new backside points taken from tacheometer station 8 (background: 2010 GeoEye image).

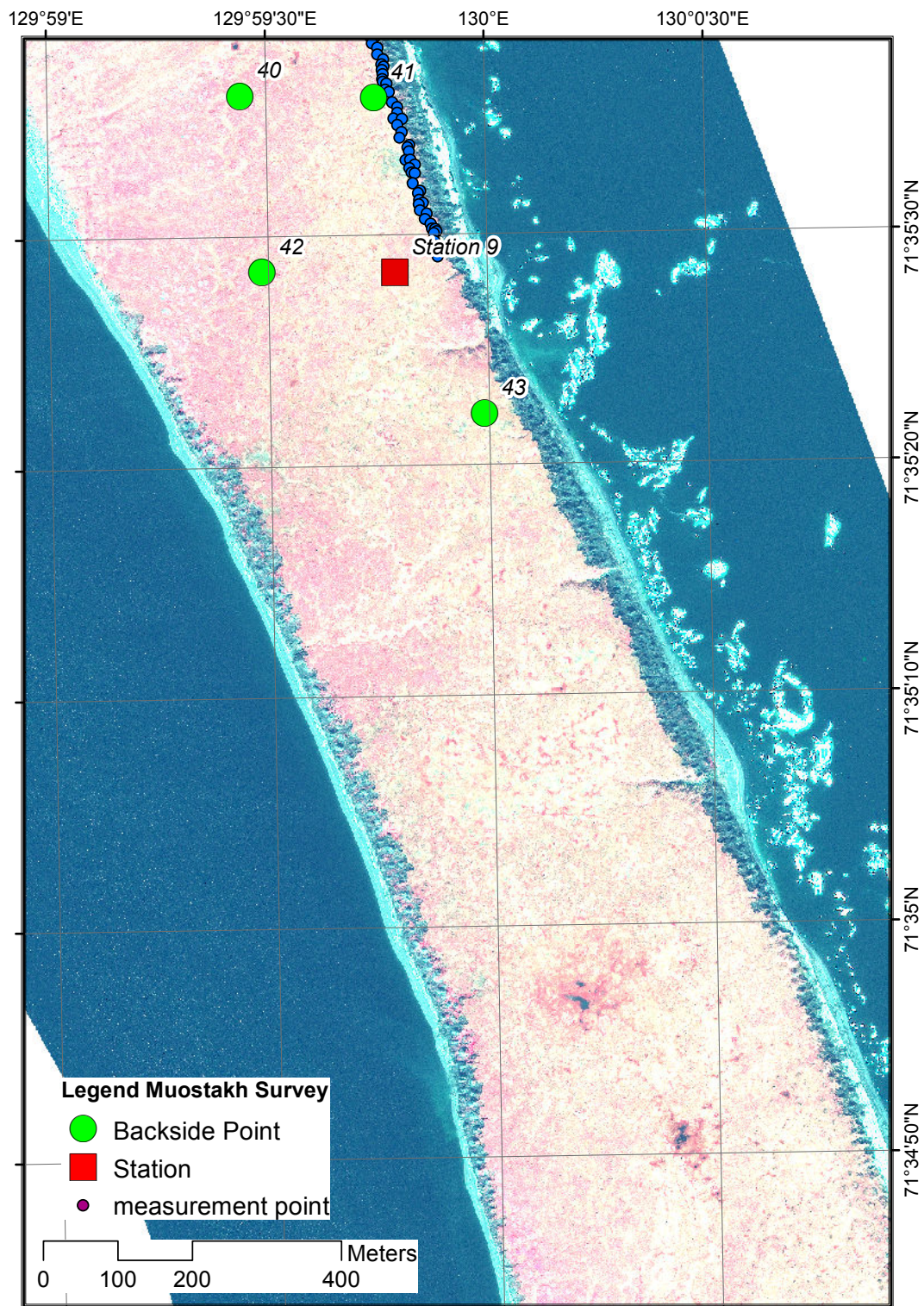


**Fig. 4.23:** Tacheometric survey on Muostakh: Free stationing of tacheometer station 9 based on a set of known backside points (background: 2010 GeoEye image).

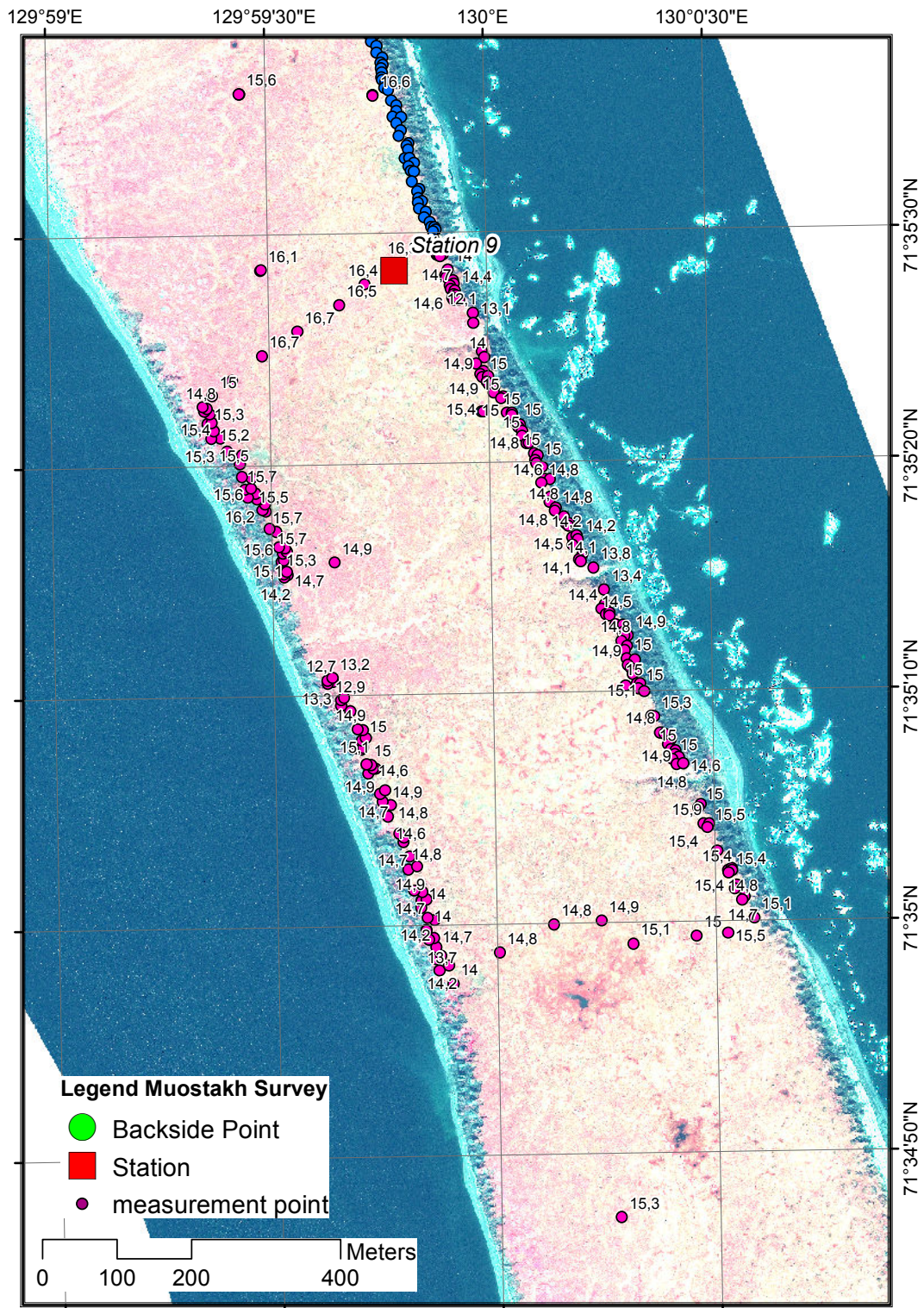


**Fig. 4.24:** Tacheometric survey on Muostakh: Point measurements labelled with elevation in m a.m.s.l. taken from tacheometer station 9 on 24<sup>th</sup> August 2011 (background: 2010 GeoEye image).

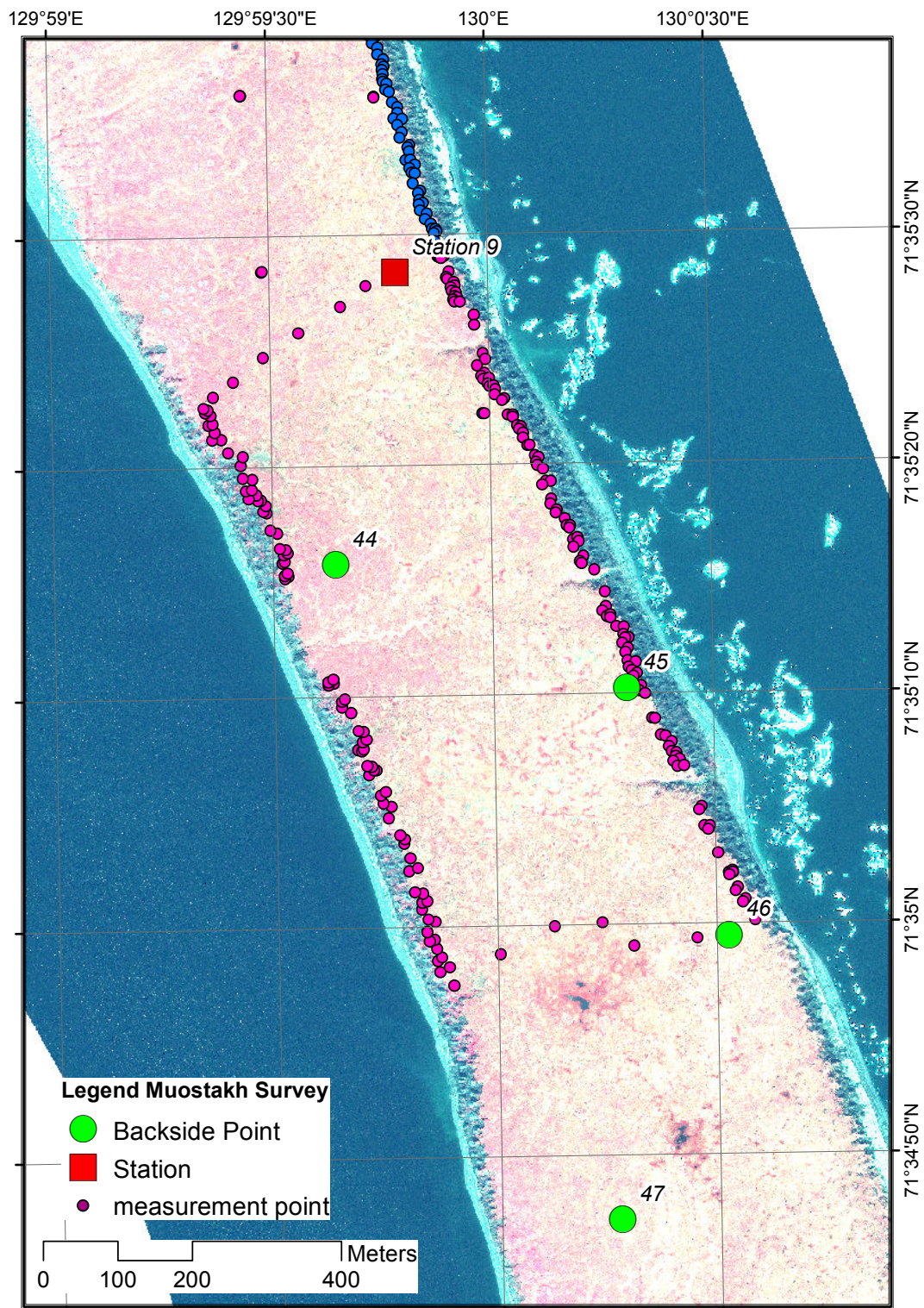


**Fig. 4.25:** Tacheometric survey on Muostakh: Calibration of new backside points taken from tacheometer station 9 (background: 2010 GeoEye image).



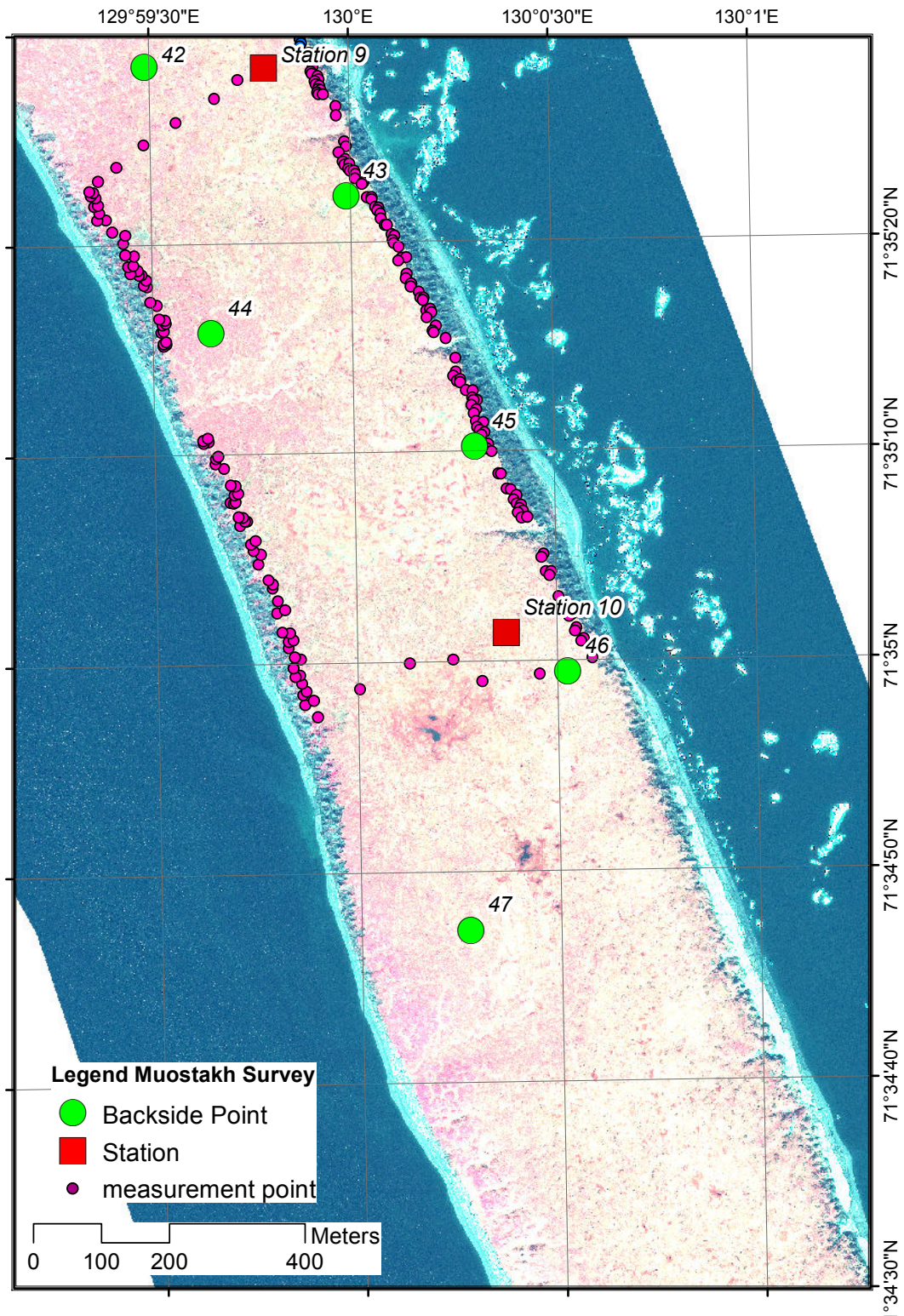


**Fig. 4.26:** Tacheometric survey on Muostakh: Free stationing of tacheometer station 10 based on a set of known backside points (background: 2010 GeoEye image).



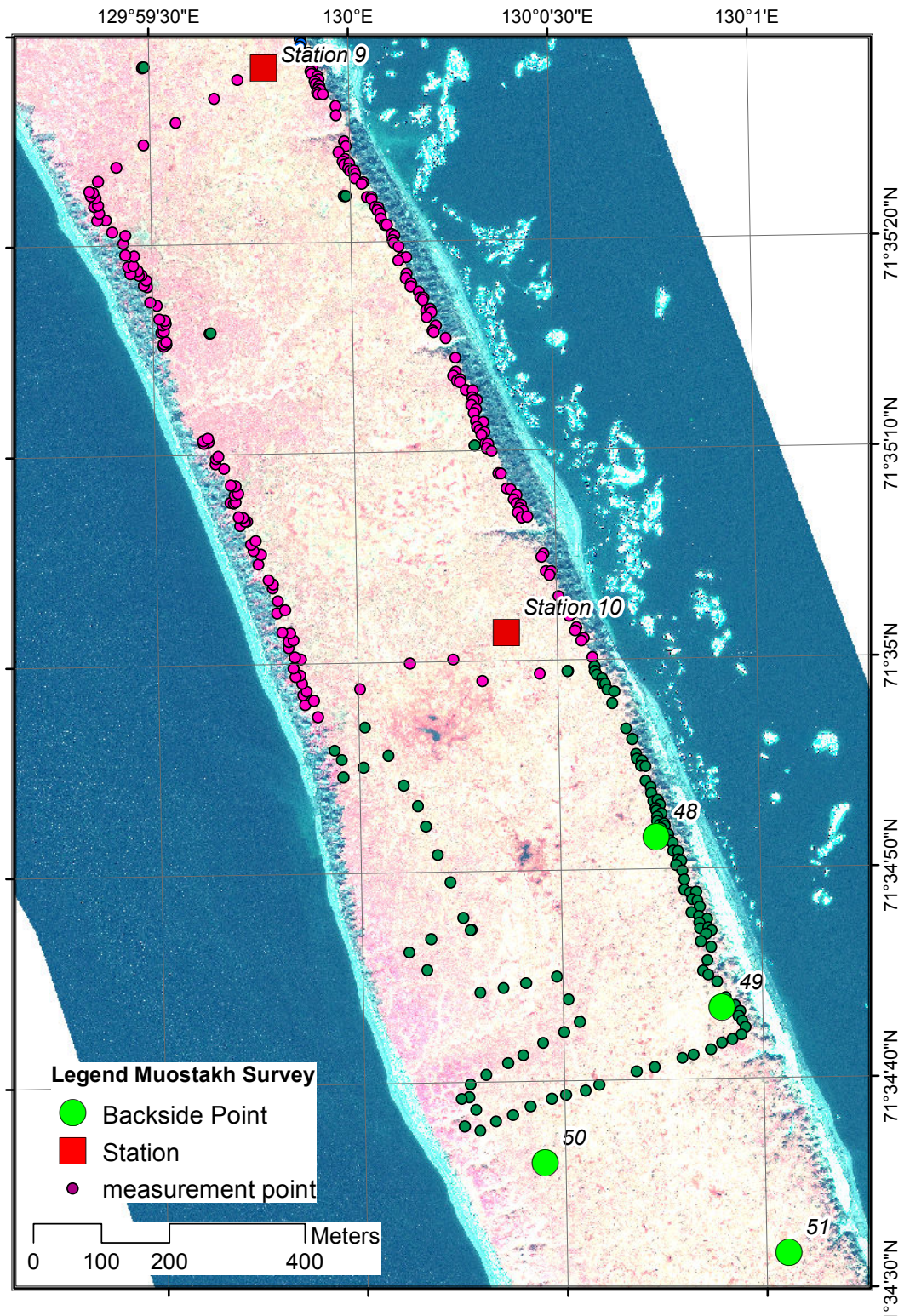


**Fig. 4.28:** Tacheometric survey on Muostakh: Calibration of new backside points taken from tacheometer station 10 (background: 2010 GeoEye image).

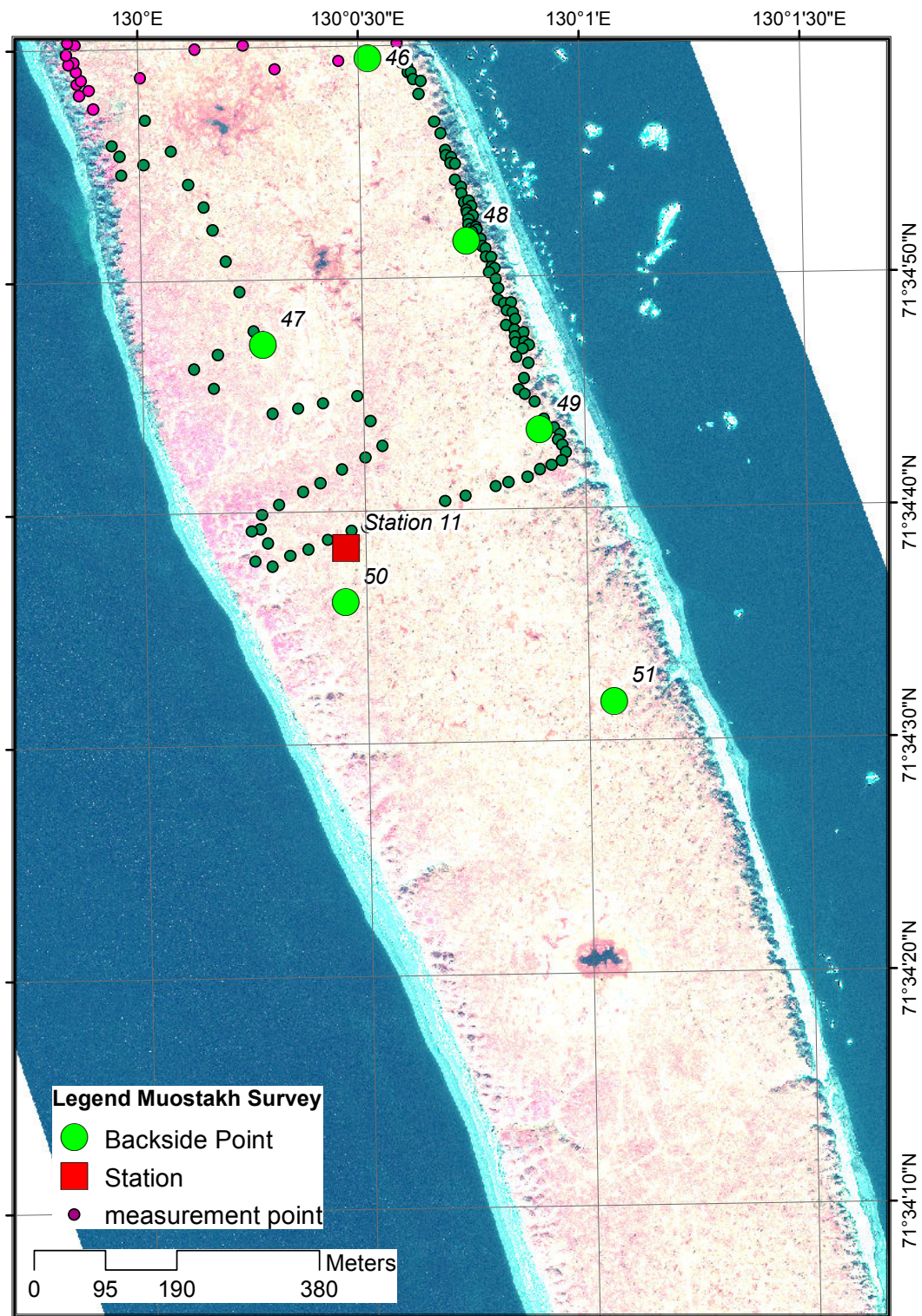


**Fig. 4.29:** Tacheometric survey on Muostakh: Free stationing of tacheometer station 11 based on a set of known backside points (background: 2010 GeoEye image).

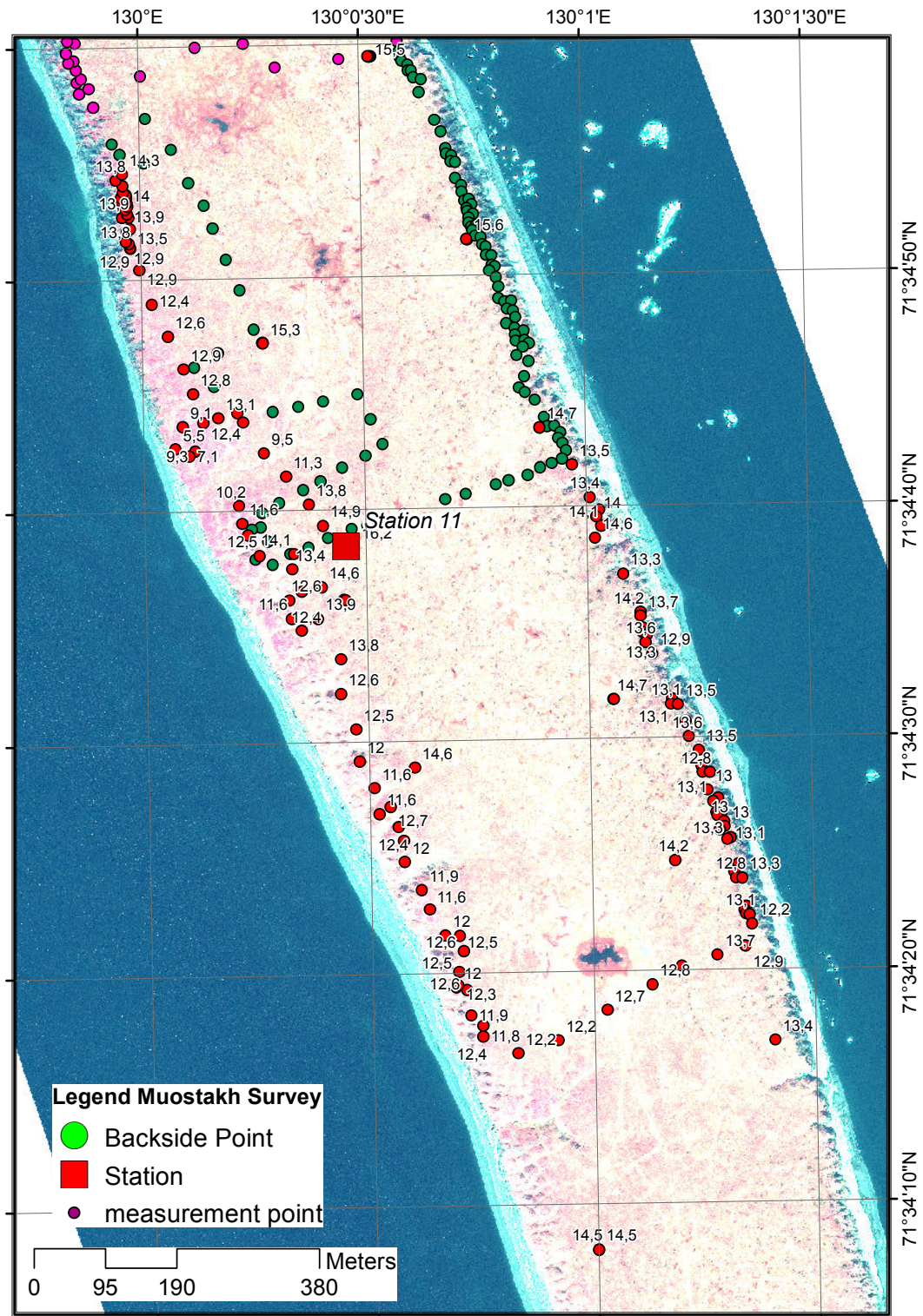


**Fig. 4.30:** Tacheometric survey on Muostakh: Point measurements labelled with elevation in m a.m.s.l. taken from tacheometer station 11 on 25<sup>th</sup> August 2011 (background: 2010 GeoEye image).

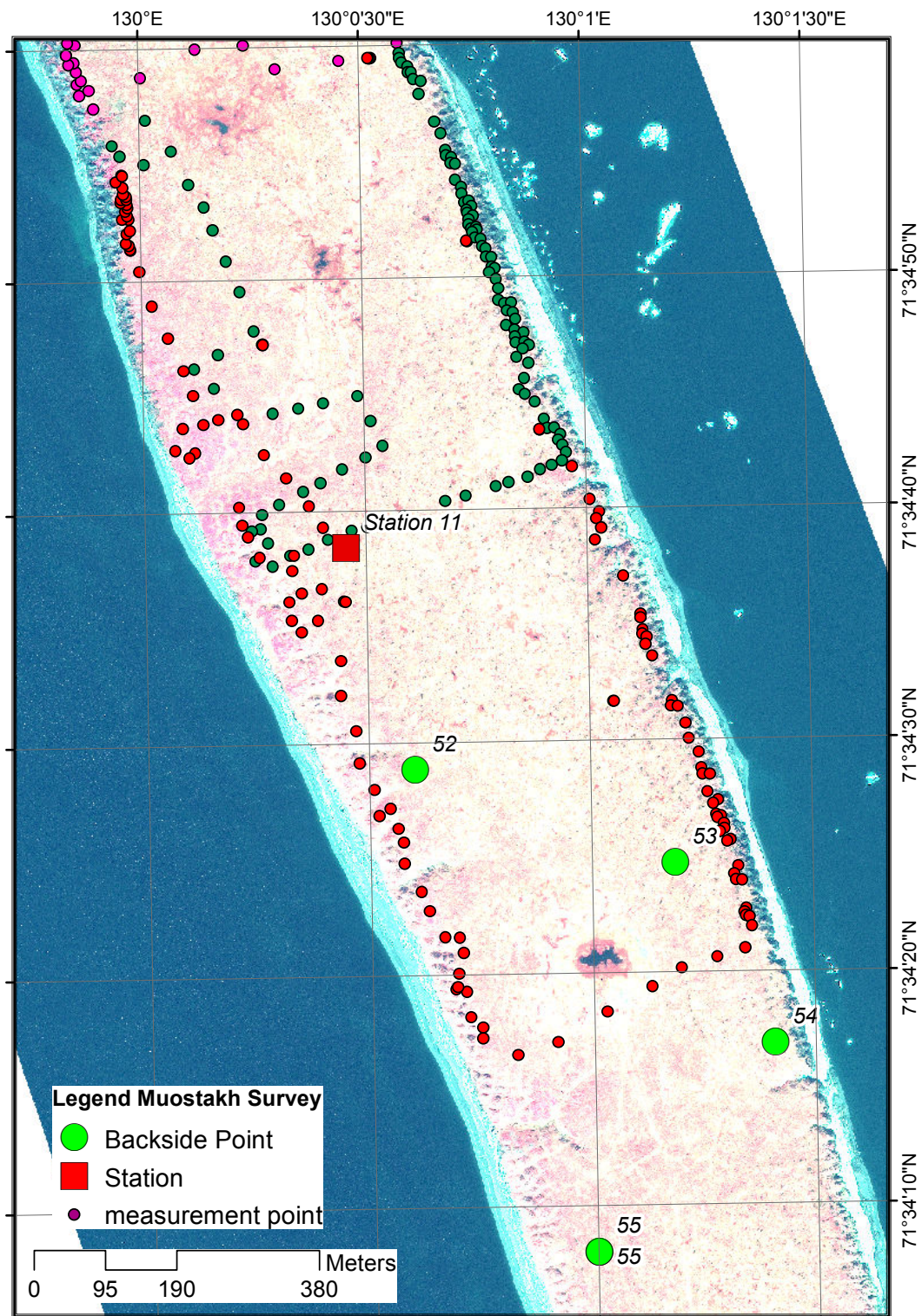


**Fig. 4.31:** Tacheometric survey on Muostakh: Calibration of new backside points taken from tacheometer station 11 (background: 2010 GeoEye image).

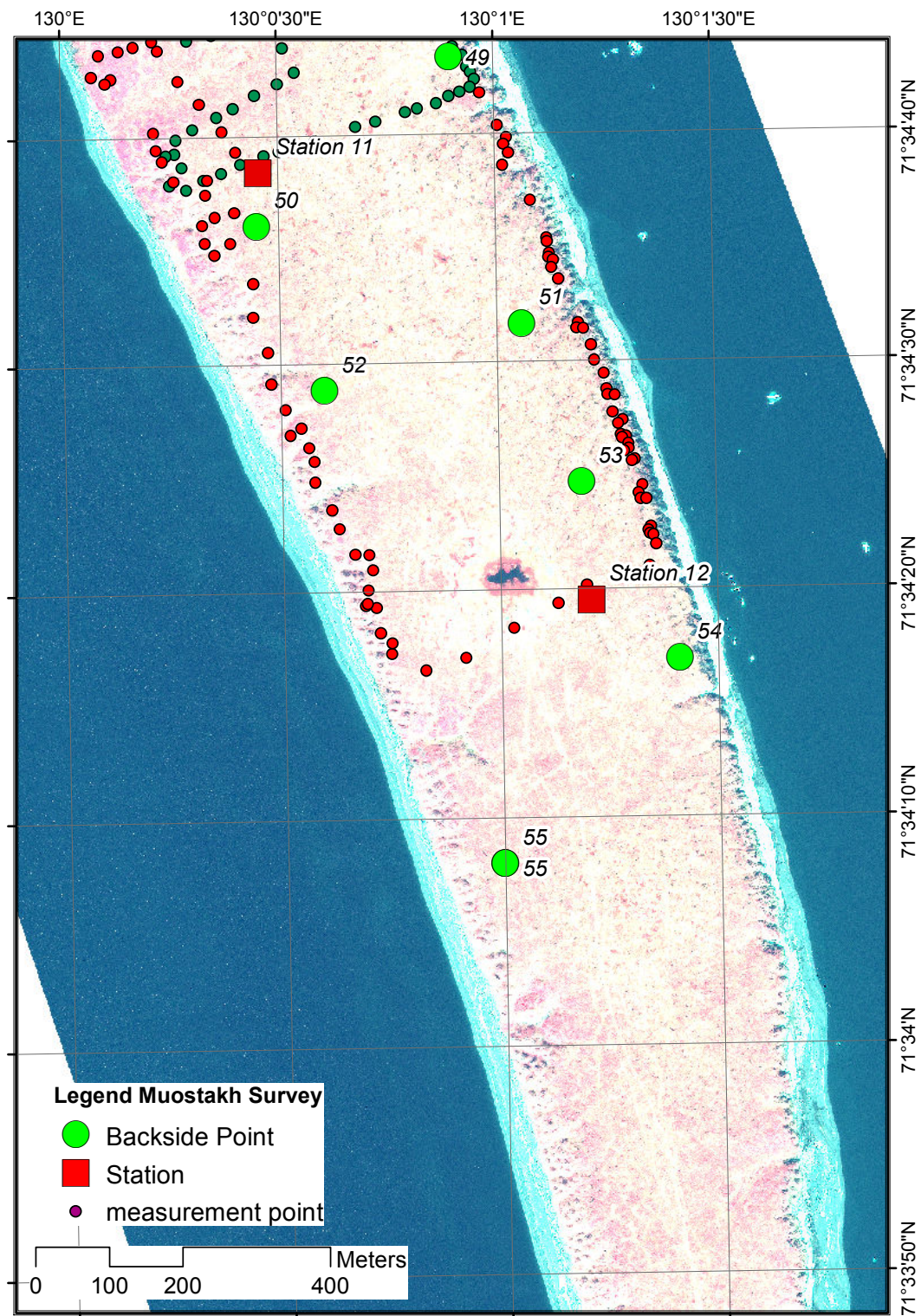


**Fig. 4.32:** Tacheometric survey on Muostakh: Free stationing of tacheometer station 12 based on a set of known backside points (background: 2010 GeoEye image).

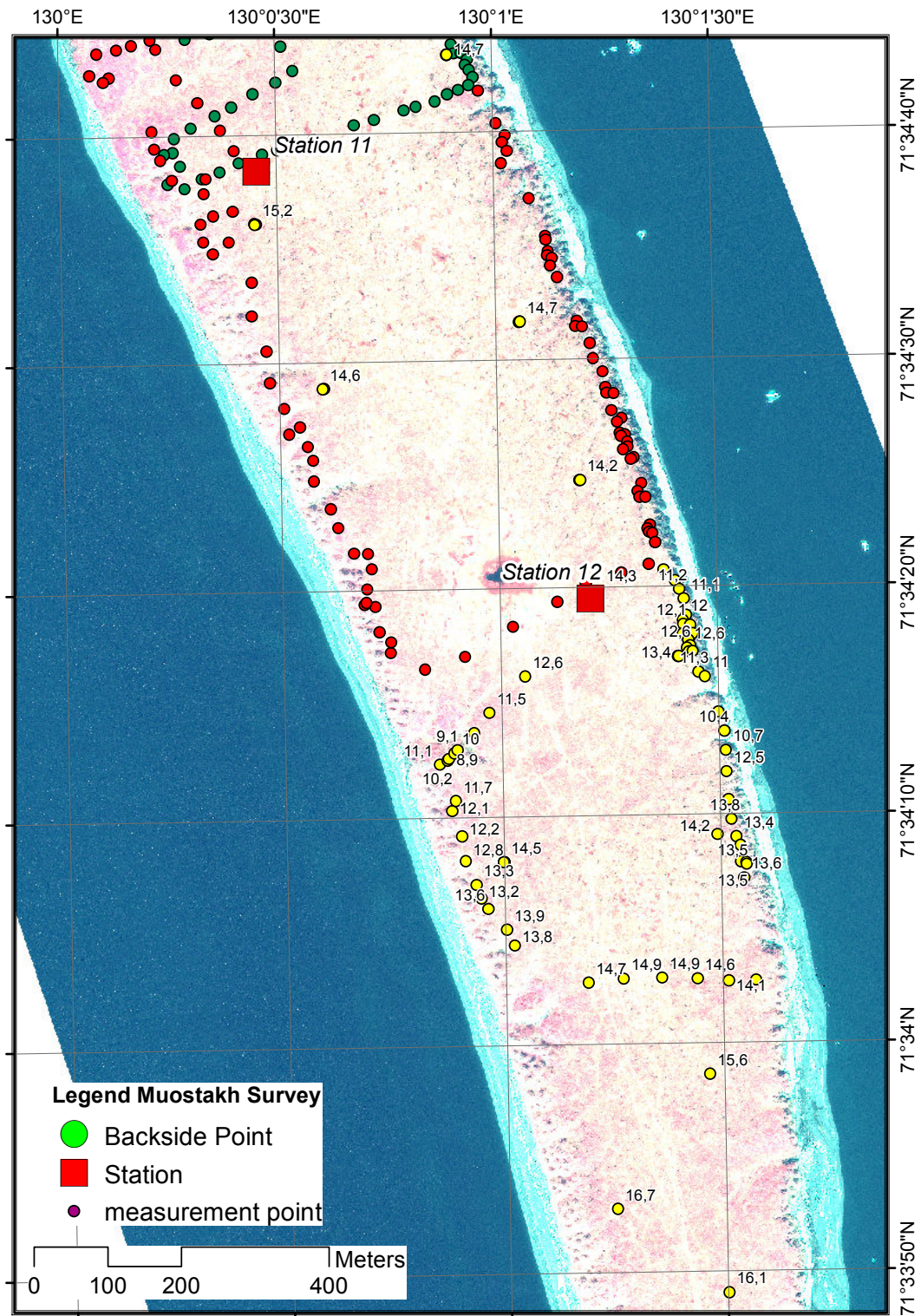


**Fig. 4.33:** Tacheometric survey on Muostakh: Point measurements labelled with elevation in m a.m.s.l. taken from tacheometer station 12 on 25<sup>th</sup> August 2011 (background: 2010 GeoEye image).



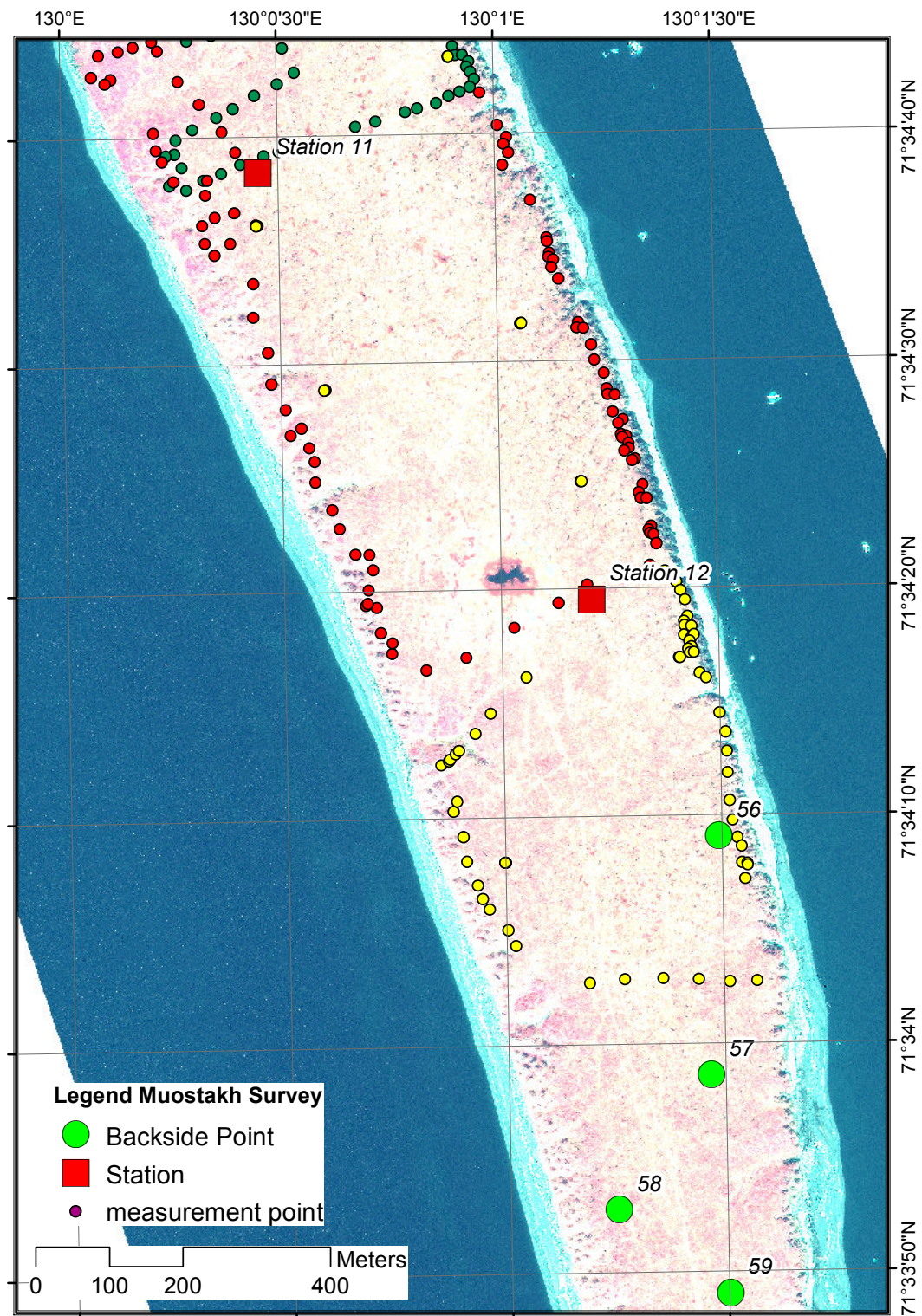


**Fig. 4.34:** Tacheometric survey on Muostakh: Calibration of new backside points taken from tacheometer station 12 (background: 2010 GeoEye image).

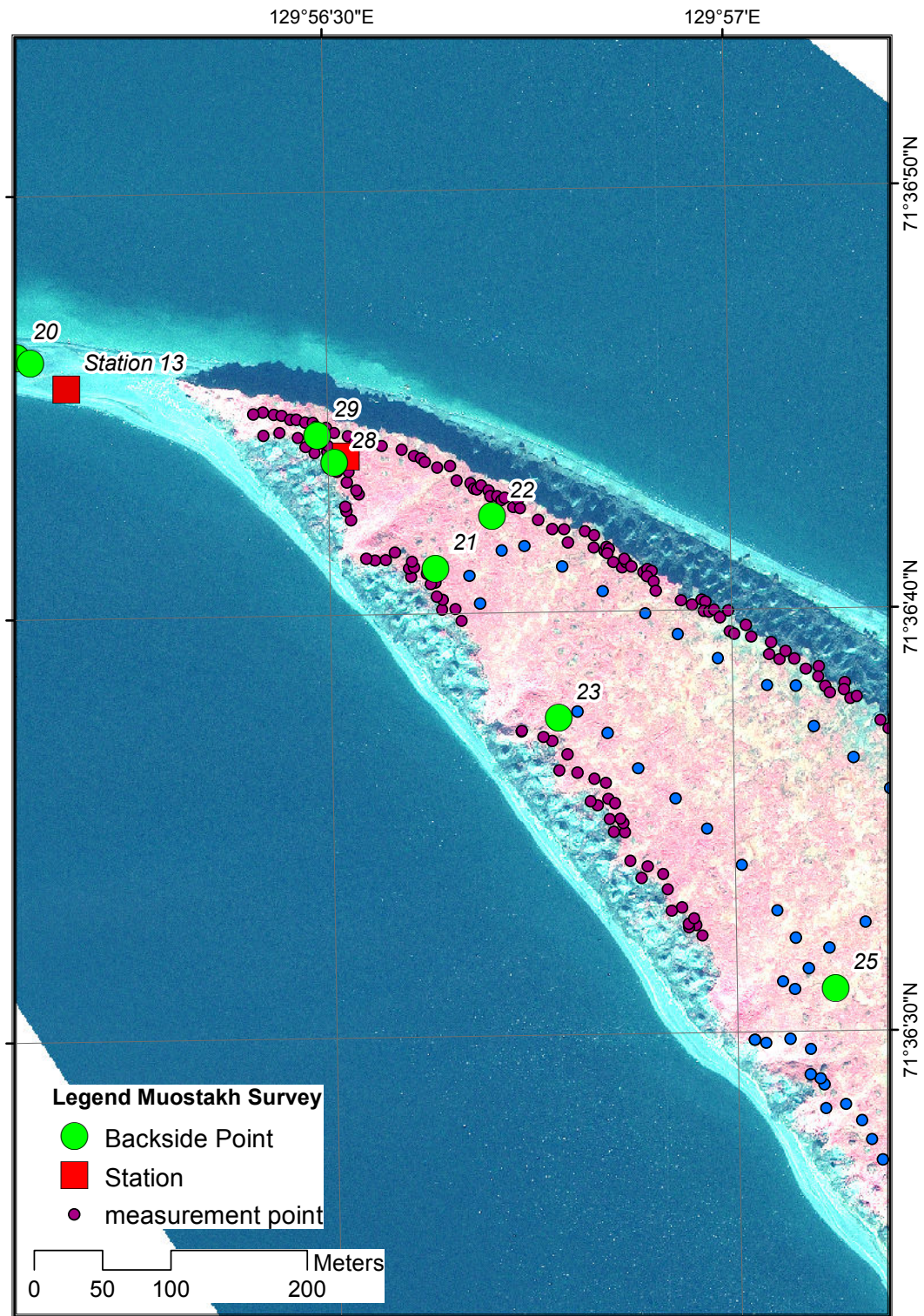


**Fig. 4.35:** Tacheometric survey on Muostakh: Free stationing of tacheometer station 13 based on a set of known backside points (background: 2010 GeoEye image).

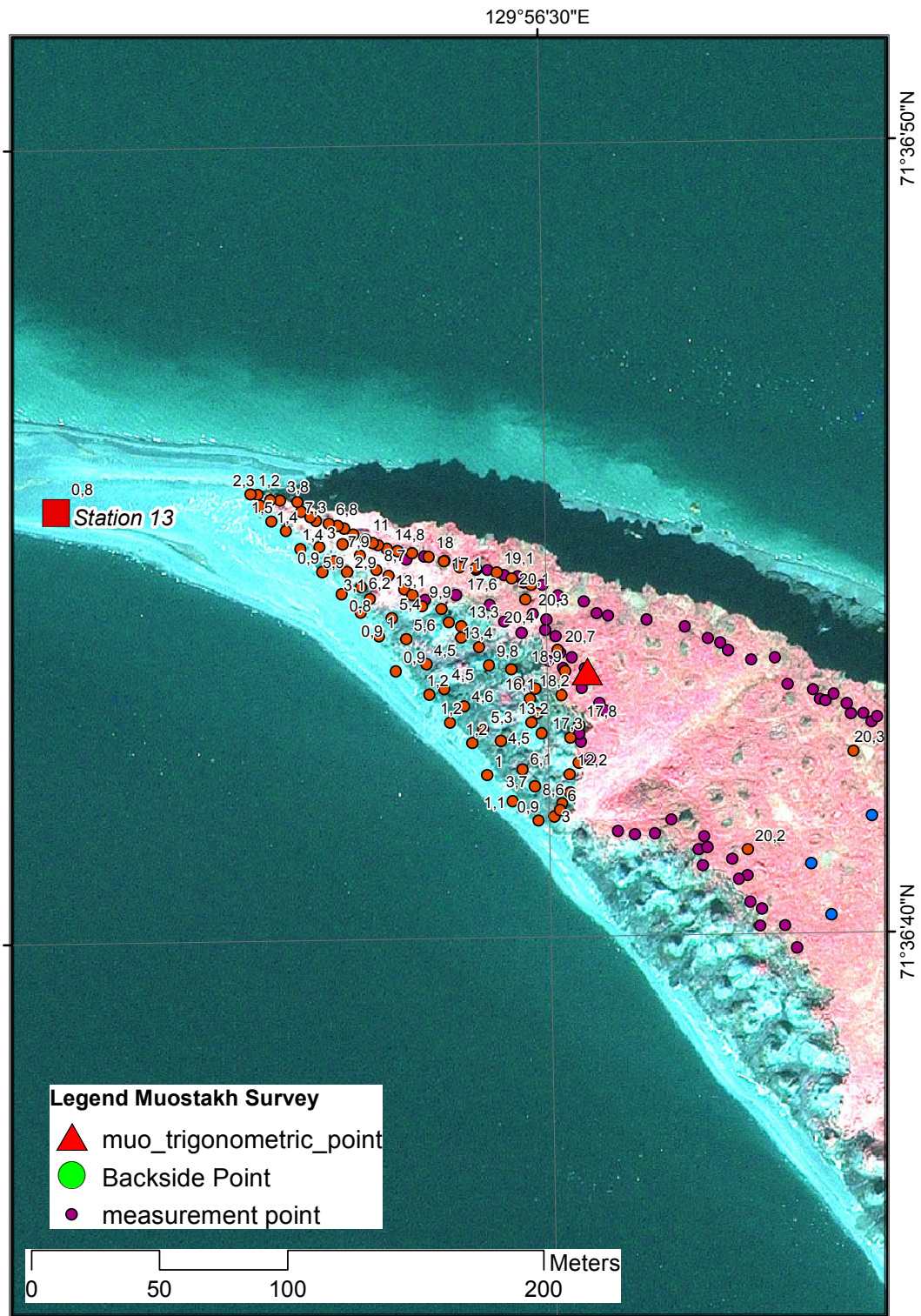


**Fig. 4.36:** Tacheometric survey on Muostakh: Point measurements labelled with elevation in m a.s.l. taken from tacheometer station 13 on 26<sup>th</sup> August 2011 (background: 2010 GeoEye image).

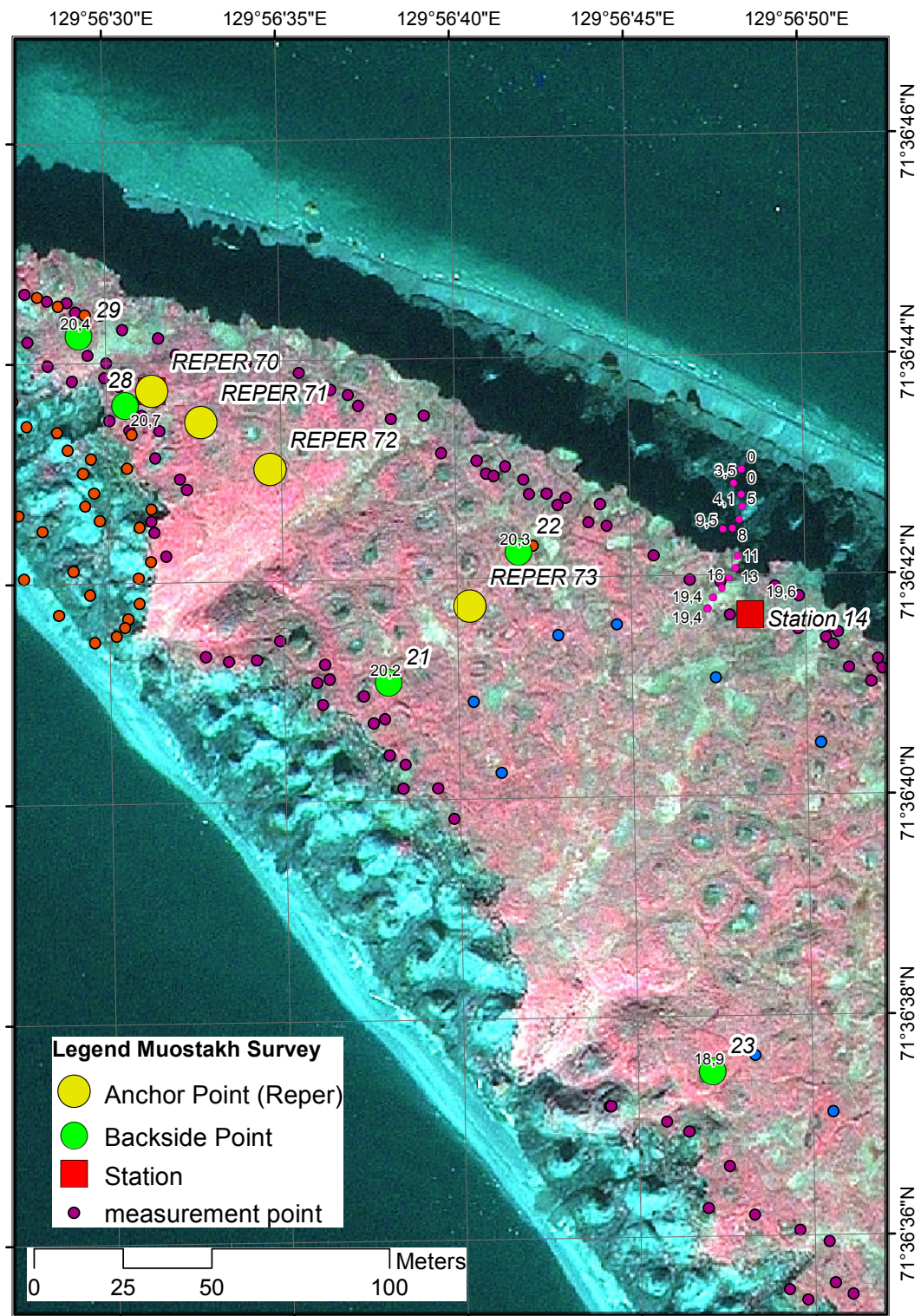


**Fig. 4.37:** Tacheometric survey on Muostakh: Free stationing of tacheometer station 14 based on a set of known backside points, point measurements on a steep cliff down to the beach labelled with elevation in m a.m.s.l. on 26<sup>th</sup> August 2011 and set up of new anchor points (*reper*) for coastal erosion determination during on-site visits.

# 5 Studies of Holocene ice wedges

*Thomas Opel & Sebastian Wetterich*

## 5.1 Scientific background and objectives

The ice-rich permafrost deposits of Northeast Siberia are characterized by different types of ground ice. Ice wedges are the most abundant type and form by the periodic repetition of wintertime frost cracking and subsequent crack-filling by snowmelt in spring. Consequently, the oxygen and hydrogen isotopic composition of the wedge-forming ice veins can be related to winter precipitation and, therefore, to winter temperatures during the time of their formation. Organic remains of ice wedges can be dated by the  $^{14}\text{C}$  method. In the last years progress has been made in ice-wedge-based paleoclimate reconstruction and it has been shown that ice wedges have the potential to provide up to centennial-scale climate information for the Late Glacial as well as Late Holocene periods in Alaska (Barrow) and Northeast Siberia (Dmitry Laptev Strait), respectively (Meyer *et al.*, 2010; Opel *et al.*, 2011). The main objective of the fieldwork conducted during the field campaign 2011 was to study Holocene ice wedges, to collect ice-wedge samples for reconstructing the regional Late Holocene climate history at Cape Mamontov Klyk and to extend the scarce spatial coverage of ice-wedge based Late Holocene paleoclimate information in the Eurasian Arctic by adding a new regional dataset. Due to the enforced change of the study region it was impossible to conduct the planned ice-wedge related work at Cape Mamontov Klyk. Consequently, the working plan was adjusted to the new study site on Muostakh Island.

## 5.2 Methods

After surveying the coastal bluffs of Muostakh Island we selected the ice wedges to be studied according to their best, i.e. perpendicular, exposure. The accessibility was limited and complicated by the steepness of the permafrost outcrops. After describing, photographing and sketching we took the ice-wedge samples using a chain saw. We sampled horizontal profiles (a) by cutting thin slices of about 2 to 3 cm width in a horizontal resolution of about 3 cm, and (b) by cutting ice blocks (about 25x15x15 cm). In addition, we took samples from recent ice vein assemblages overtopping the ice wedges and indicating modern growth. Whereas the ice slices were melted already in the field the ice blocks were transported in frozen state to the Alfred Wegener Institute (AWI) Potsdam where they will be subsampled in a cold laboratory. In total, we studied and sampled six ice wedges (App. A.1). After melting the ice slices in closed LDPE bags, meltwater for analyzing the stable-isotope composition was stored in 30 ml PE bottles, which were completely filled and tightly closed to avoid evaporation. For hydrochemical analyses in the laboratory, meltwater from selected samples was filtered using a cellulose-acetate

filtration set (pore size  $0.45\ \mu\text{m}$ ) and collected in 8-ml HDPE-flasks for anion analyses by ion chromatography, and in 15-ml PP-tubes for element (cation) analyses by ICP-OES. Samples for cation analyses were acidified with  $200\ \mu\text{l}$   $\text{HNO}_3$ . We determined electrical conductivity (EC) of the hydrochemistry samples with a WTW340i pocket meter, and pH by a Viscolor test kit (App. A.1). We collected organic material contained in the melted samples (plant remains) for age determination ( $^{14}\text{C}$  AMS) (Tab. A.1). Additionally, fresh precipitation samples ( $n = 17$ ) were collected at Cape Mamontov Klyk as well as Muostakh Island for measurement of stable isotopes and stored in the same way as the ice-wedge samples (App. A.1).

## 5.3 Description of outcrops

### 5.3.1 General stratigraphic and geomorphologic situation

The small island Muostakh Island stretches about 10 km in the NW-SE direction and less than 750 m in NE-SW direction, and is largely affected by rapid coastal erosion. The NE coast between sea level and maximum altitudes of about 19 m a.s.l. is dominated by Middle to Late Weichselian Ice Complex sequences characterized by large syngenetic ice wedges, whereas in the northern part of the SW coast besides the Ice Complex also remains of a huge alvas are exposed. On top of the Ice Complex, Holocene boggy deposits are exposed that have accumulated in small polygonal ponds. Holocene ice wedges penetrated deeply up to 8-10 m into the Ice Complex. The studied ice wedges were all located in the northern part of the NE coast (Fig. 5.1).

### 5.3.2 Ice wedge MUO11 IW1 ( $71^\circ 25' 42.1''$ N, $129^\circ 59' 41.5''$ E)

Ice wedge MUO11 IW1 was about 4 m wide, but not cut perpendicular (Fig. 5.2). From the trough above the most recent assemblage of ice veins (about 15 cm wide) overtopping the wedge body we estimated a declination of about  $45^\circ$ . The exposed vertical extension of the ice wedge was 0.7 m whereas the lower part was buried. The wedge ice was milky-white and rich in vertically oriented, 1 to 10 mm sized air bubbles as well as mineral and organic inclusions. Single ice veins were only hardly detectable and reached thicknesses of up to 1 cm.

The ice wedge was covered by 0.7 m of sediments. An active layer of 0.2 m was underlain by 0.45 m of brownish-grey silt with cryoturbation features, roots, grass and wood fragments as well as singular gravel lenses. The cryostructure exhibited non-consistently distributed horizontal ice lenses. 5 cm of grey sands represented the lowest sediment layer directly above the ice wedge. The absence of upward-bended ice veins close to the ice wedge indicated the epigenetic formation of this ice wedge. We sampled a 2.3 m long horizontal profile 1 m below the surface containing 77 samples with the last sample representing a layer of clear ice at the outermost part of the ice wedge. A few days later we cut a second profile of 2 m length in 8 blocks omitting the most right part due to overhanging sediments. Furthermore, we cut a block containing the assemblage of overtopping ice veins, representing the most recent part of the ice wedge formed after the last truncation of the ice-wedge surface.

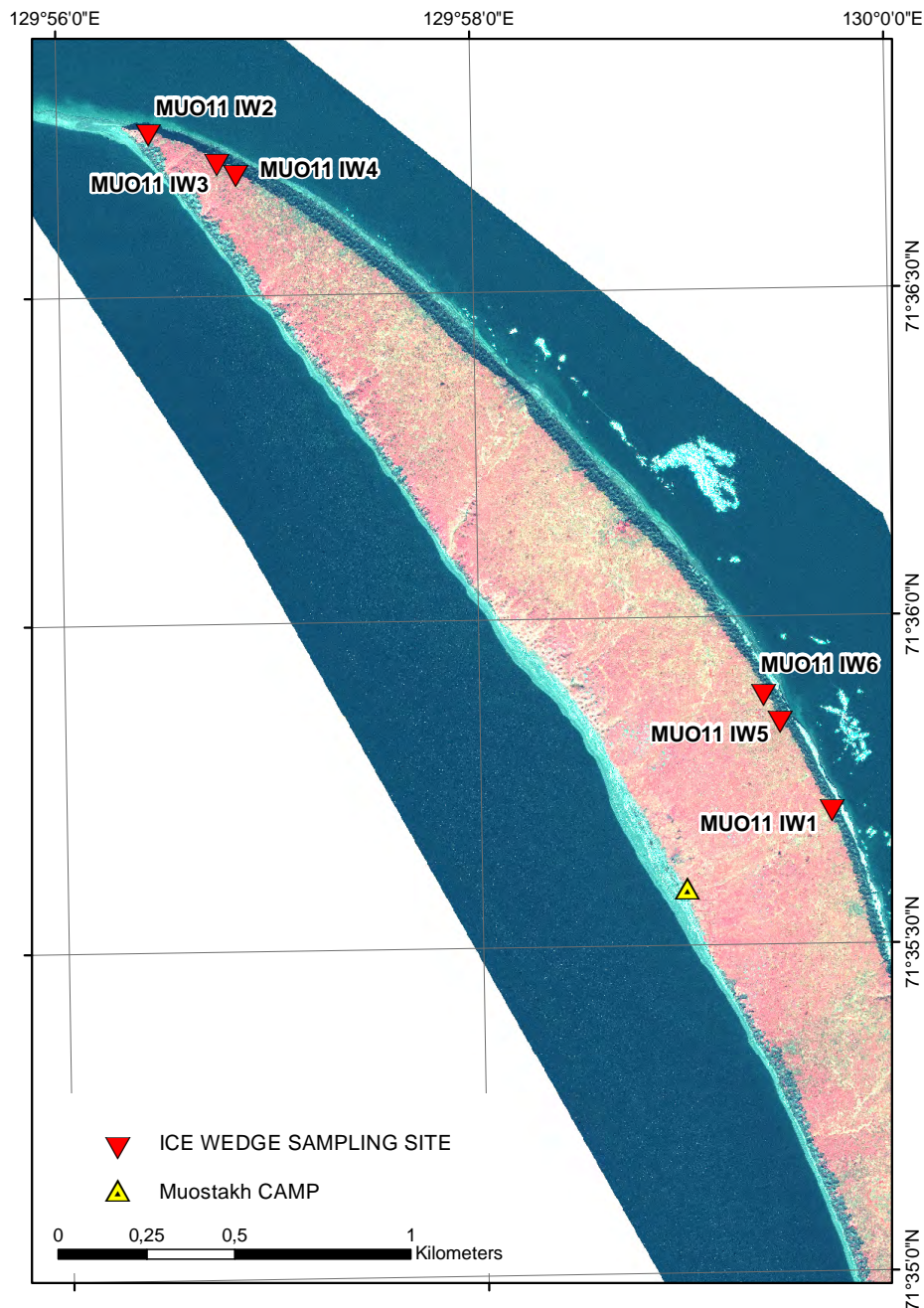


**Fig. 5.1:** Map of the northern part of Muostakh Island with study sites (background: 2010 GeoEye image).

### 5.3.3 Ice wedge MUO11 IW2 ( $71^{\circ}36'44.8''$ N, $129^{\circ}56'26.4''$ E)

Ice wedge MUO11 IW2 was about 3.8 m wide and cut perpendicular (Fig. 5.3). It was characterized by a recent ice vein assemblage of about 5 cm thickness overtopping the ice wedge about 25 cm. The exposed vertical dimension was about 2.2 m with a buried lowest ice-wedge part. The outer parts of the ice-wedge cut were repositioned due to preferentially melting. The wedge ice was milky-white and air-bubble-rich with vertically oriented bubbles (1 to 10 mm long). Single ice veins were clearly detectable with thicknesses of 2 to 10 mm. Mineral and organic inclusions were widely distributed.



Fig. 5.2: Ice wedge MUO11 IW1 (71°25'42.1" N, 129°59'41.5" E).





**Fig. 5.3:** Ice wedge MUO11 IW2 ( $71^{\circ}36'44.8''$  N,  $129^{\circ}56'26.4''$  E).

The ice wedge was covered by 70 cm of sediments. A 50 cm thick active layer of brownish organic-rich sandy silt strongly penetrated by roots was underlain by a 20 cm thick layer of brownish organic-rich sandy silts with root remains. The cryostructure was unregularly and exhibited horizontal ice layers up to 1 mm thick. Furthermore, cryoturbation patterns were detectable. The deposits the ice wedge penetrated in were greyish-brown sandy silts with gravel. They were characterized by a fine-lens-like cryostructure and showed a clear contact to the ice wedge, indicating the epigenetic character of the Holocene ice wedge within the Ice Complex deposits. We sampled two horizontal profiles across the central ice wedge part in depths of 1.2 (1.2 m wide, 37 samples) and 1.55 m (25 samples, 0.7 m wide) below surface (resolution about 3 cm). Additionally, we took samples of recent ice veins in a vertical profile: 5 samples of youngest generation overtopping the ice-wedge body and 9 samples from below until the upper horizontal profile.

#### 5.3.4 Ice wedge MUO11 IW3 ( $71^{\circ}36'42.0''$ N, $129^{\circ}56'46.3''$ E)

Ice wedge MUO11 IW3 was about 1.8 m wide and cut perpendicular (Fig. 5.4). The vertical ice-wedge extension exposed in the outcrop was about 1 m whereas the lower part was buried. The youngest ice-wedge part represented by an assemblage of recent ice veins (about 15 cm wide and 20 cm high) was detected not in the central part but some 20 cm from the left edge. However, indications for recent frost cracking were also observed at the right edge. The wedge ice was milky white and rich in vertically oriented air bubbles of 1 to 10 mm size. Single ice veins were up to 1 cm wide and contained mineral and organic inclusions. At the right edge a thick ice band of more clear ice was observed.

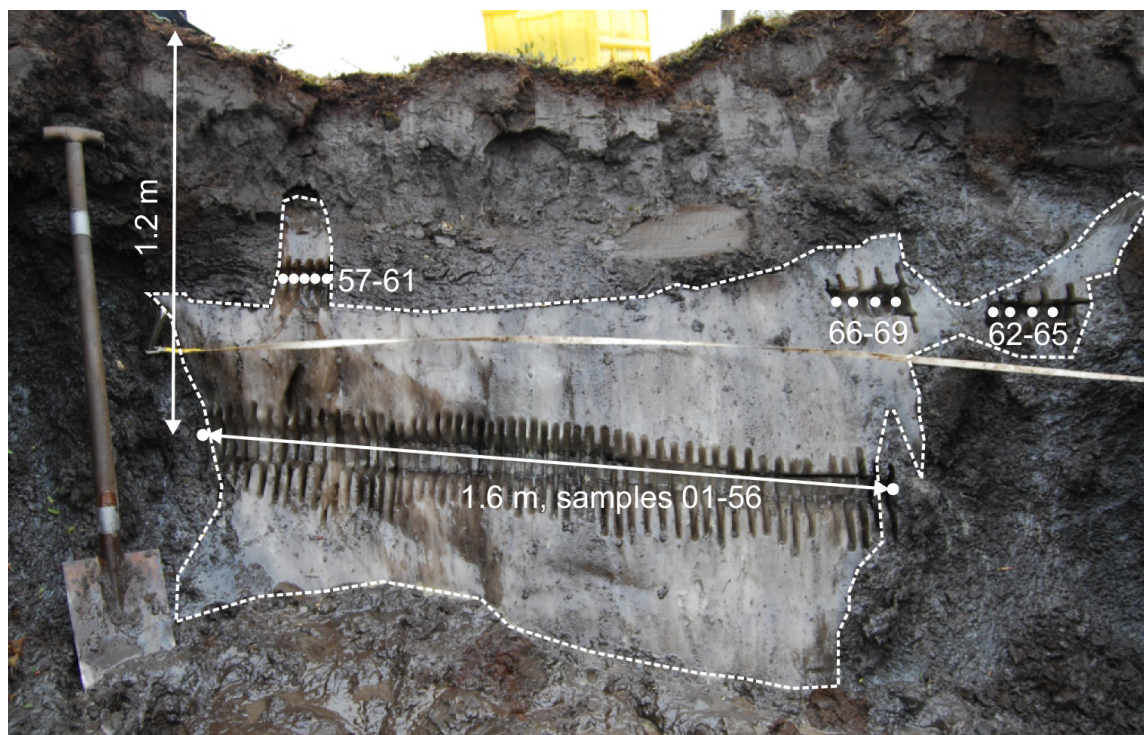


**Fig. 5.4:** Ice wedge MUO11 IW3 (71°36'42.0" N, 129°56'46.3" E).

The active layer was 30 to 45 cm thick and consisted of brownish sandy silt with some coarse sands, penetrated by roots. The 30 to 40 cm thick deposits between active layer and ice wedge consisted of greyish-brown sandy silts with single coarse sands, peat lenses and roots. The cryostructure showed horizontal coarse lenses and fine lens-like reticulated ice between them. The ice wedge penetrated in ice-rich grey sandy silts with a coarse lens-like reticulated cryostructure between horizontal ice bands. We sampled a horizontal profile of 1.6 m (56 samples) at a depth of 1.2 m below the surface. Additionally we took samples from the overtopping ice veins, from the upper right edge close to the other frost-cracking indications as well as from the ice band.

### 5.3.5 Ice wedge MUO11 IW4 (71°36'41.0" N, 129°56'51.5" E)

Ice wedge MUO11 IW4 was about 3.2 m wide and the exposed vertical dimension was 0.4 to 0.6 m (Fig. 5.5). The ice wedge was cut perpendicular and consisted of milky white ice, in particular in its central part. The wedge ice was very rich in vertically oriented air bubbles of 1 to 10 mm size and contained numerous mineral and organic inclusions. Single ice veins were 5 to 10 mm wide. No signs of recent cracking activity were found. Obviously the ice wedge was recently truncated by thawing that lowered the ice-wedge surface in the central part. The most left part of the ice body separated by a sediment wedge contained "typical" ice-wedge ice as well as a more clear ice. Similar clear ice as well as very bubble-rich ice was found above the ice wedge in the right part of the outcrop. This non ice-wedge ice might be originated by freezing of standing water, e.g. from pond water.



**Fig. 5.5:** Ice wedge MUO11 IW4 ( $71^{\circ}36'41.0''$  N,  $129^{\circ}56'51.5''$  E).

The ice wedge was covered by a 0.3 to 0.35 m thick active layer consisting of brown sandy silt, very rich in roots and other organics. No frozen sediments were found above the central ice wedge. The surrounding sediments were grey sandy silts, rich in roots and other organic material. The cryostructure exhibited horizontal coarse lens-like ice. We sampled a horizontal profile 0.7 to 0.9 m below the surface containing 98 samples. Additional samples were taken from the clear ice in the upper left as well as upper right parts of the outcrop.

### 5.3.6 Ice wedge MUO11 IW5 ( $71^{\circ}35'50.3''$ N, $129^{\circ}59'26.7''$ E)

Ice wedge MUO11 IW5 was small and only about 0.25 m wide (Fig. 5.6). The exposed vertical dimension in the outcrop was about 0.4 m with a buried lower part. The milky-white ice contained lot of air bubbles that were vertically oriented and 1 to 10 mm of size. Single ice veins were clearly detectable, up to 1 cm wide and partly a bit yellowish.

The ice wedge was truncated and exhibited no signs of recent cracking activity. It was covered by about 0.6 m brown sandy silt, strongly penetrated by roots. The upper about 0.35 m presented the active layer, the lower 0.25 m were frozen. The sediment the ice wedge penetrated in was grey, ice-rich sandy silt with horizontal ice bands up to 3 mm thick and single peat lenses. From this ice wedge we sampled one block about 0.9 m below the surface containing the entire horizontal profile as well as parts of the encompassing peat.

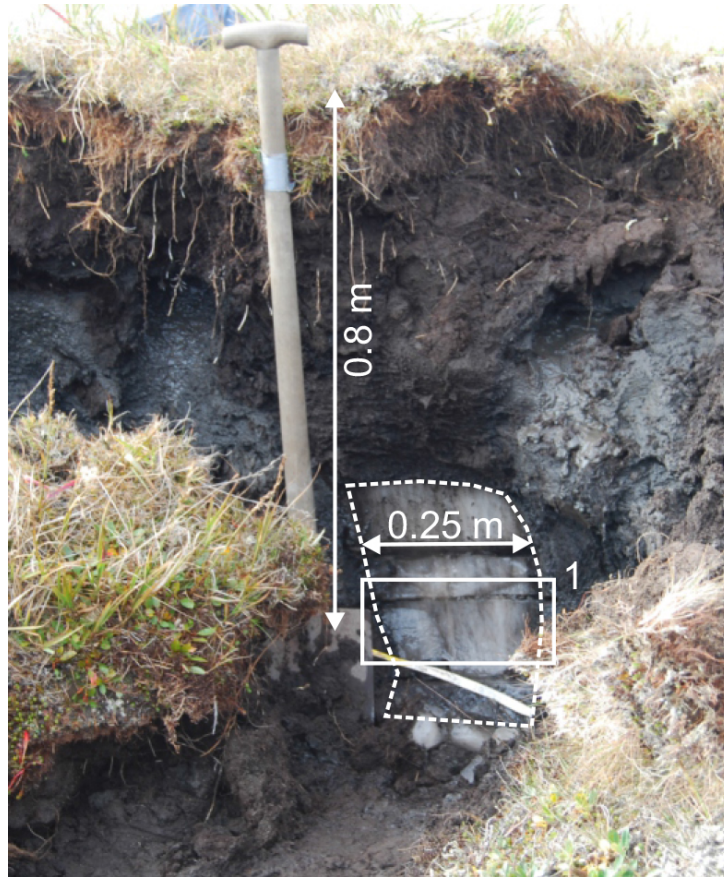


**Fig. 5.6:** Ice wedge MUO11 IW5 ( $71^{\circ}35'50.3''$  N,  $129^{\circ}59'26.7''$  E).

#### 5.3.7 Ice wedge MUO11 IW6 ( $71^{\circ}35'52.8''$ N, $129^{\circ}59'22.2''$ E)

Ice wedge MUO11 IW6 was a small and only about 0.15 m wide (Fig. 5.7). The vertical dimension in the outcrop was only about 0.3 m with the lower part buried. The wedge ice was milky and rich in vertically oriented air bubbles (1 - 10 mm). Single ice veins were up to 1 cm wide.

The ice wedge was truncated and exhibited no signs of recent cracking activity. It was covered by about 0.4 m of sediment, i.e. a 0.3 m thick active layer composed of brown sandy silt with numerous roots as well as a 0.1 m thick layer of grey ice-rich sandy silt. This was found to be the same sediment the ice wedge penetrated in. From this ice wedge we sampled one block about 0.55 m below the surface containing the entire horizontal profile as well as encompassing sediments.

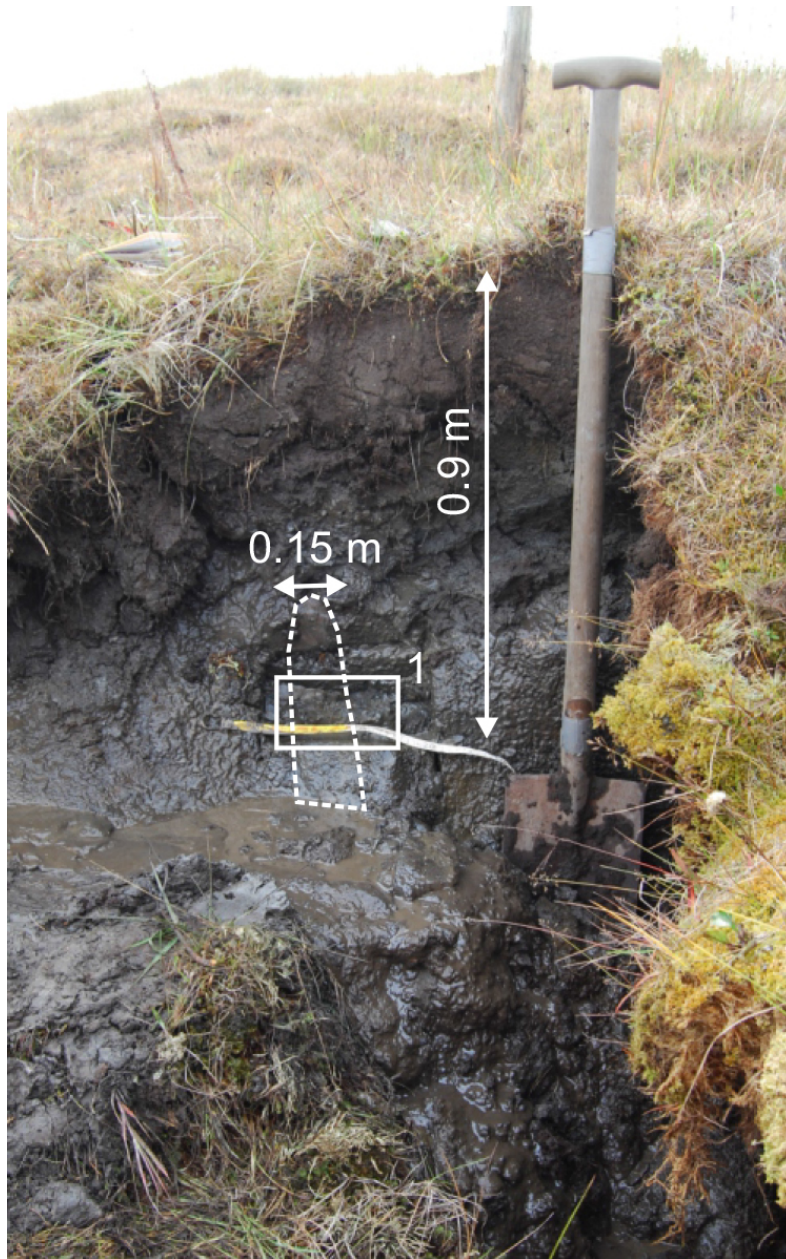


**Fig. 5.7:** Ice wedge MUO11 IW6 (71°35'52.8" N, 129°59'22.2" E).

## 5.4 Preliminary results and outlook

The fingerprint field data of pH and EC measurements along horizontal transects of the sampled ice wedges show pH values of 6.5 in almost all samples (App. A.1). The slightly acidic character of Holocene ice wedges is connected to the peaty polygon sediments in which they grow. High amounts of humic and other organic acids in pore waters in such depositional milieu are mirrored in the ice-wedge data. The general ionic content is rather low due to the atmospheric source (snow melt) feeding ice wedges, and varies if expressed as electrical conductivity in the dataset obtained on Muostakh Island between about 9 and 107  $\mu\text{S}/\text{cm}$ .

# 6 Geophysical investigations of the coastal zone

*Pier Paul Overduin, Sebastian Wetterich & Aleksandr Makarov*

## 6.1 Motivation and science goals

The 2003 and 2005 drilling expeditions to Cape Mamontov Klyk in the western Laptev Sea produced observations of the depth of the ice-bearing subsea permafrost table, temperature distributions within the sediment and sediment cores (Schirrmeister, 2004, 2007). Subsea probing in 2003 and the sediment cores drilled in 2005, in particular, provided valuable material by which insights were gained into the degradation of terrestrial permafrost following its inundation by seawater in the wake of coastal erosion (Winterfeld *et al.*, 2011). The differences in degradation rates observed between the two expeditions, although sites were located within a less-than-1 km long stretch of coastline, suggested that the distribution of the top of the ice-bearing permafrost table within the sediment was spatially highly variable. This was surprising, given the fact that a number of determining factors (coastline retreat rate, water column thermal and saline regimes, permafrost temperature and thickness) were assumed to be similar for both locations. As a result, one of the goals of the 2011 field season was to carry out geophysical surveys, both seismic and geoelectric, to study the variability of permafrost distribution at this key site laterally, using existing borehole observations for validation of geophysical results. The unexpected change of study sites from Cape Mamontov Klyk to Muostakh Island (see Introduction) necessitated changes to our goals, insofar as these were specific to the proposed site. Previous drilling expeditions to Muostakh Island in 1982 and 1983 (Kunitsky, 1989; Slagoda, 2004), however, allowed us to maintain the same approach to studying permafrost distribution using geophysical observations and their validation by comparison to borehole records. Since sediment drilling occurred two decades earlier at Muostakh Island than at Cape Mamontov Klyk, however, the additional question of whether changes in ice-bearing permafrost table position over decadal time scales could also be addressed. In contrast to Cape Mamontov Klyk, Muostakh Island offers coastal sections that differ strongly within a small area in terms of some of the determining factors for permafrost degradation rates. In particular, the coastal retreat rates of the island vary widely with coastline-normal compass direction. Data on coastal retreat rates were also generated by investigations during this expedition and by supporting remote sensing (see Chapter 4: Topographic survey of Ice Complex coasts).

Various geophysical methods have been used in a variety of settings to observe submarine permafrost indirectly. The detection of ice-bonded permafrost depends on techniques sensitive to changes in sediment ice content. Kneisel *et al.* (2008) and Yoshikawa *et al.* (2006) review geophysical techniques for ice detection in permafrost on land, including the measurement of

direct current electrical resistivity at the land surface. Using floating or seabed electrodes, this technique has been adapted to the aquatic environment and applied to submarine permafrost (Overduin *et al.*, 2012). In a marine setting, good electrode-subsurface electrical contact is provided by seawater and the target is the high electrical resistivity contrast between highly conductive, ice-free, saline marine sediments and the underlying, highly resistive, ice-bonded, terrestrial deposits. Edwards *et al.* (1988), for example, mapped resistivity variations in the subsurface using marine electromagnetic techniques in the Beaufort Sea. Our goal was to collect direct current apparent resistivities from which sediment electrical resistivities could be inverted, in order to derive the position of the transition from saline, unfrozen sediment to freshwater, ice-bearing sediment. To complement these measurements, a sub-bottom profiler was tested to provide information on sediment structure.

## 6.2 Geoelectrical DC resistivity

The geoelectric system used was the IRIS Syscal Pro Deep Marine system with 10 potential measurement channels, an injection voltage of up to 50 V and about 10 A. Injected current was powered by a set of batteries linked in series. A floating electrode array arranged as a reciprocal Schlumberger array was manufactured at the Alfred Wegener Institute. The potential electrodes were stainless steel flat plate electrodes about 30 cm in length and 10 cm in height (Fig. 6.1). Dimensions and electrode separations of the array are shown (Fig. 6.2). The reciprocal Schlumberger array measures quasi-symmetric voltages around a central current injection dipole, which in our case was 10 m. The potential and injection electrodes were connected to the cable take-outs using nuts and bolts, and were clipped to the cable to hang from it vertically. The cable was floated at the water surface using buoys and empty PET bottles. The cable was towed behind an inflatable boat powered by a 25 HP outboard motor. Towing at speeds below 7 km/h and usually slower, apparent resistivities were measured at intervals of at least 2 m, as determined by GPS position. Potential was measured with both polarities for each channel. Data were stored in an ASCII format during sampling and post-processed after the expedition.

Twelve geoelectrical profiles were collected over two partial days of sampling (Fig. 6.3). Cruise time was limited by wave conditions for all but 2 days of the time spent on Muostakh Island. High wind speeds and waves limited either boat travel in general, or made the measured potentials noisy, probably as a result of interrupted contact between electrodes and water. In total, over 17 km of profiles were collected up to 4.2 km from shore.



**Fig. 6.1:** An example of an electrode, in this case at the end of the electrode cable, take-out and buoy.

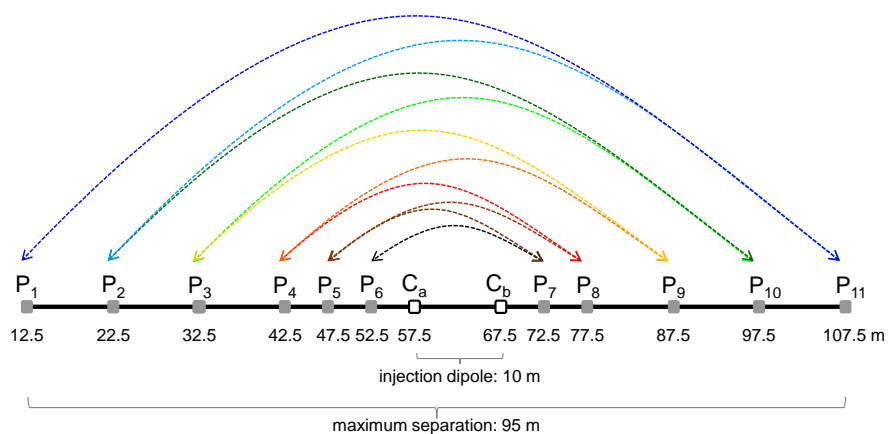


**Fig. 6.2:** Electrode geometry of the electrode streamer. P refers to a potential electrode, C to current injection electrodes. Distances given are relative to the on board reference GPS and echo-sounder position. Measurement channels are pairs of electrodes across which potential is measured; the innermost four channels (of ten) are indicated by arrows linking electrode pairs; line colours correspond to those shown in the apparent resistivity diagrams in the results section.



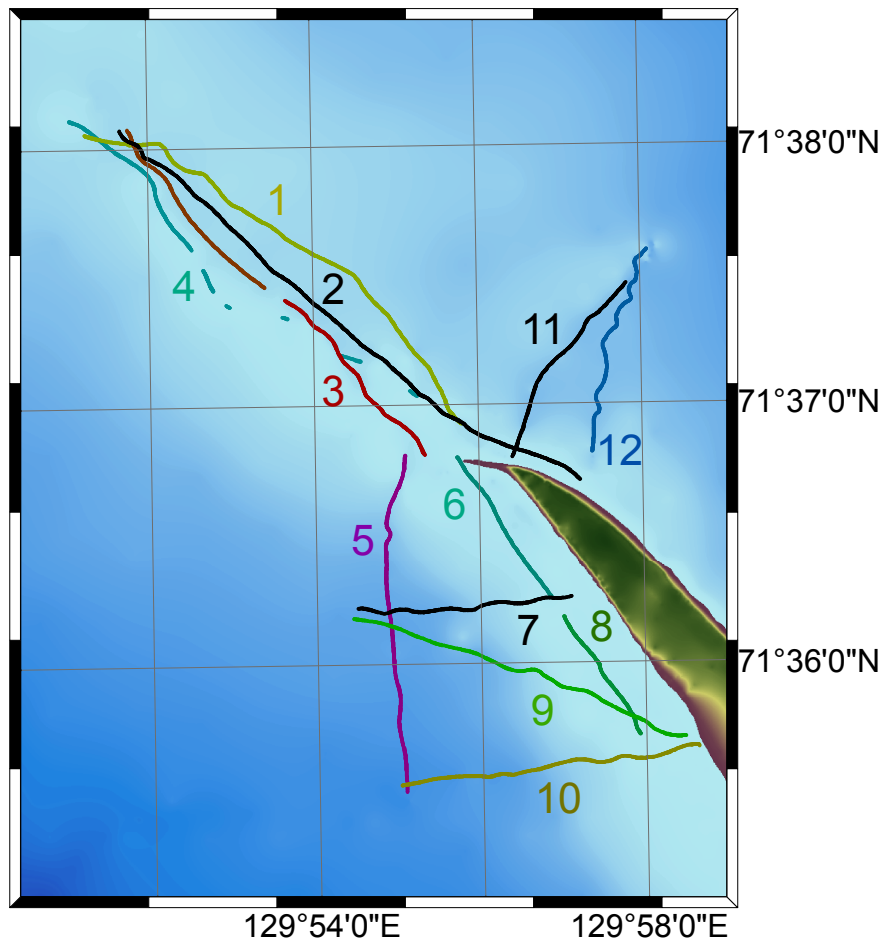


**Fig. 6.3:** The topography and bathymetry of Muostakh Island's northern tip are shown, along with the positions of the geoelectric profiles measured in 2011.

**Tab. 6.1:** List of geoelectric profiles in order of acquisition.

Profile №	Date	Time	File size [kB]	Figure	Length [km]
1	Aug. 21, 2011	09:21	552	6.4	3.4
2	Aug. 24, 2011	04:47	661626	(not shown)	4.1
3a	Aug. 24, 2011	03:21	206742	6.4	1.5
3b	Aug. 24, 2011	03:38	174581	6.4	1.5
4	Aug. 21, 2011	07:31	ca. 300	6.4	ca 1.5
5	Aug. 24, 2011	06:07	288768	6.5	2.4
6	Aug. 24, 2011	02:56	191190	6.6	1.2
7	Aug. 24, 2011	07:17	140459	6.7	1.5
8	Aug. 24, 2011	02:38	178746	6.6	1
9	Aug. 24, 2011	07:42	218643	6.5	2.5
10	Aug. 24, 2011	06:34	231743	6.5	2.1
11	Aug. 24, 2011	05:33	166300	6.7	1.5
12	Aug. 24, 2011	05:40	243486	6.7	1.5

**Tab. 6.2:** Salinity and electrical conductivity of surface water.

Date	Description	Salinity	Elec. Cond. [mS/cm]	Resistivity [ $\Omega$ m]
25.08.2011	eastern side of spit	4.2	7.89	1.27
25.08.2011	western side of spit	9.2	16.13	0.62
24.08.2011	at crossing of profiles 11 and 14	7	12.56	0.80
24.08.2011	surface water at 71°36'14" N 129°56' 33" E	8.7	15.39	0.65
24.08.2011	between LOG1 and LOG2 surface sediment samples	3.1	5.95	1.68
20.08.2011	KUN101 surface water	5.4	9.6	1.04
20.08.2011	KUN309 surface water	6.1	10.8	0.92

### 6.3 Seismic profiling

An Innomar SES 2000 compact sub-bottom profiler was used to measure shallow sediment structure. The SES2000 compact uses a frequencies in the range 4 to 15 kHz. A custom built aluminum mount was manufactured at the Alfred Wegener Institute in Bremerhaven. The mount was used to attach the SES 2000 transducer to a rubber dingy (Fig. 6.4) powered by a 25-horsepower Honda long-shaft outboard motor. The mount was attached to the dingy using driftwood spars running midship between the gunnels, and using driftwood spars from this beam to the prow. The transducer rode in front of the bow along the center line of the boat, minimizing the influence of bow waves on the transducer and avoiding asymmetric drag on the boat. The mount was constructed to permit raising the transducer during travel, in order to facilitate landing on beaches without the risk of damage to the transducer. Seismic data were collected in proprietary format and saved for post-expedition conversion and processing. The locations of five profiles collected around the northern tip of Muostakh Island are shown in Fig. 6.5.



**Fig. 6.4:** The inflatable dinghy is shown with improvised sub-bottom profiler transducer mount at the bow.

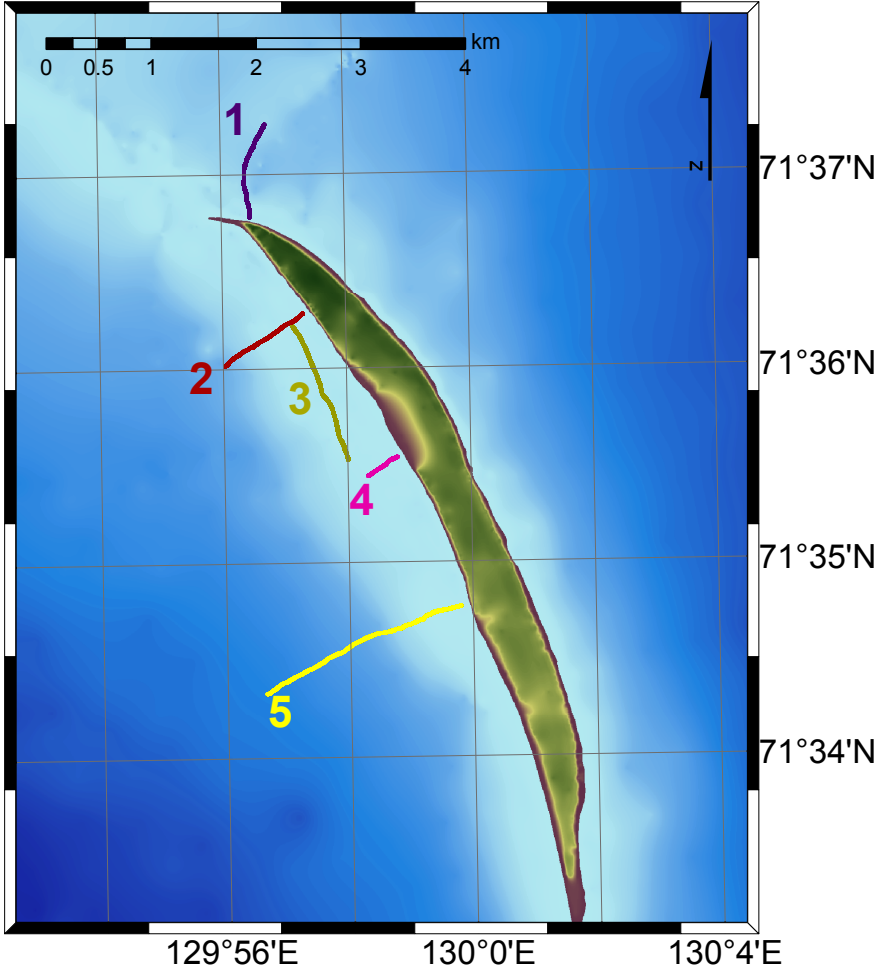


**Fig. 6.5:** The topography and bathymetry of Muostakh Island's northern tip are shown, along with the positions of the seismic profiles measured in 2011.

## 6.4 Preliminary results and outlook

The recovered geoelectrical profiles 1 to 4 cover the borehole transect drilled in 1982 and 1983 by the Melnikov Permafrost Institute of Yakutsk (Kunitsky, 1989; Slagoda, 2004). This allows us to compare our measured profiles with descriptions of the sediment cryolithology and composition from the recovered cores, and to speculate on decadal scale changes to permafrost table depth. The landward end of these profiles, and in particular profile 2, recovers apparent resistivities of sea bottom sediments that have undergone erosion and flooding since the drilling campaign. With remote sensing and survey results, we can constrain the past position of the coastline along this transect and gain insights into changes to coastal shoreface sediments immediately following flooding as a result of coastline recession. Profiles collected eastward (11, 12) and westward of the island (5-10) provide a basis for comparison of sites with differing coastal dynamics under similar synoptic conditions. Initial inspection of the sub-bottom profiles collected using the SES2000 compact device shows that the strong bottom reflection, due to the coarse sediment grain size, limited penetration depth. Data quality was further decreased by noise introduced by poor weather conditions. Future work at this location should take advantage of longer data collection periods to extend coverage spatially and over depth. Denser data distribution would provide more detail on permafrost table distribution spatially and thus on possible effects of pre-flooding permafrost landscape forms on the subsea permafrost table and its degradation following coastline recession.

# 7 Distribution of organic carbon in bottom sediments on the underwater coastal slope

*Alexander Sandakov & Mikhail Grigoriev*

## 7.1 Scientific background and objectives

The main sources of organic carbon in the East Siberian Arctic coast are composed of sediments of the Ice Complex (Grigoriev *et al.*, 2004). Due to the fact that organic carbon is a source of greenhouse gases it is of great interest to study further the redistribution of sediments on the underwater coastal slope following the destruction of the coast.

In August 2010 along the west coast of the Buor Khaya Peninsula on the underwater coastal slope the organic carbon content of the bottom sediments was determined by Sandakov *et al.* (2012). Analysis of the distribution of TOC in the submarine coastal slope revealed a fairly clear pattern, consisting of a substantial increase in concentration with increasing water depth. This distribution is explained by the active redistribution of sediments in the shallow part of the underwater coastal slope, which transfers organic matter into the steeper parts of the area.

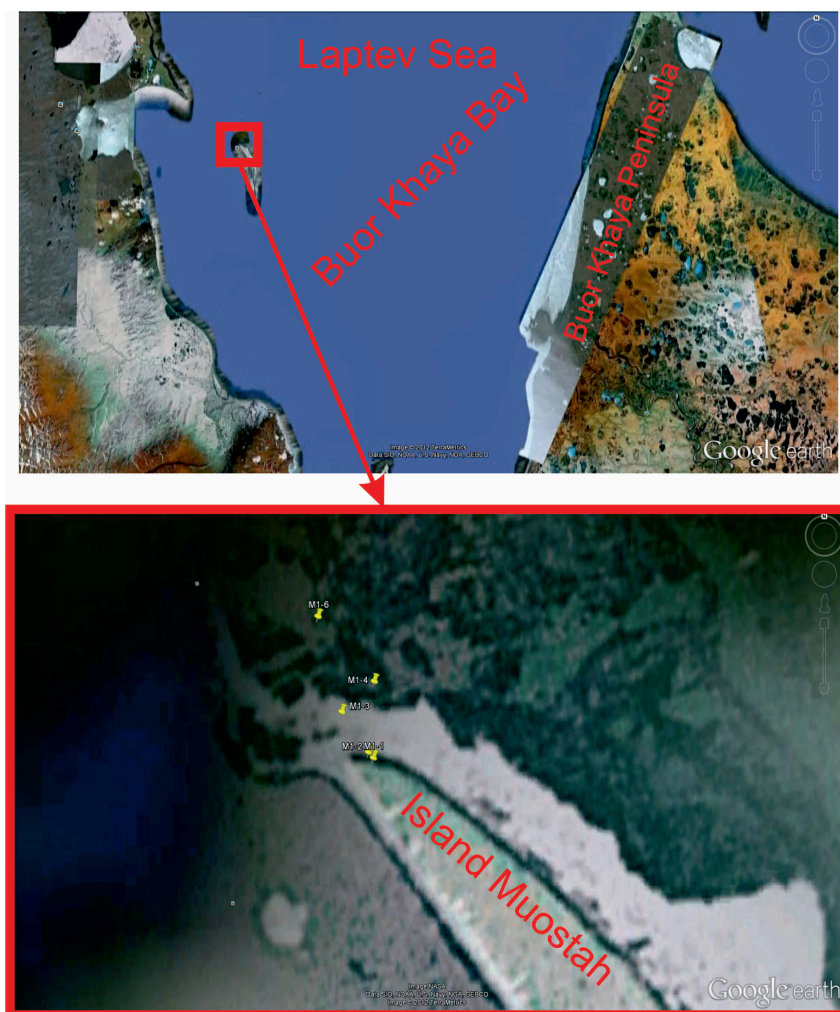
The objective of this study was to validate the distribution of TOC in sediments on the underwater coastal slope in yet another coastal setting of the Buor Khaya Gulf.

## 7.2 Field results

In August 2011 north-east of Muostakh Island ground samples were collected from the underwater coastal slope and from Ice Complex exposures (Table 7.1) along a profile (Fig. 7.1).

**Tab. 7.1:** List of Muostakh Island surface sediment samples.

Sample №	Lat	Long	Altitude m	Name of soils	Selection place
1-1	71°36.745'	129°56.430'	20,0	peat	Top of the slope
1-2	71°36.745'	129°56.430'	18,5	Silty clay loam average	slope
1-3	71°36.745'	129°56.430'	14,0	Silty sand	slope
1-4	71°36.745'	129°56.430'	12,0	Silty sand	slope
1-5	71°36.745'	129°56.430'	10,0	Fine sand	slope
1-6	71°36.745'	129°56.430'	8,0	peat	slope
1-7	71°36.745'	129°56.430'	6,0	Silty clay loam easy	slope
1-8	71°36.745'	129°56.430'	4,0	Heavy loam with organic	slope
1-9	71°36.745'	129°56.430'	1,0	Middle-sized sand	slope
1-0	71°36.745'	129°56.430'	0	Middle-sized sand	slope
M 1-1	71°36.781'	129°56.414'	-2	Fine sand	sea bottom
M 1-2	71°36.792'	129°56.381'	-3	Middle-sized sand	sea bottom
M 1-3	71°36.874'	129°56.197'	-4	Fine sand	sea bottom
M 1-4	71°36.936'	129°56.420'	-5	Silty sand with organics	sea bottom
M 1-6	71°37.068'	129°56.033'	-6	Silty sand with organics	sea bottom

**Fig. 7.1:** Map of the location of profiles



11<sup>th</sup> April – 4<sup>th</sup> May 2012

**Expedition leader:**

Dr. Mikhail N. Grigoriev

Melnikov Permafrost Institute Yakutsk  
Russian Academy of Science, Siberian Branch  
Vice-Director for Science  
Merzlotnaya St. 36, 677010 Yakutsk, Russia



# 8 Scientific Permafrost Drilling Campaign

*Mikhail N. Grigoriev, Pier Paul Overduin, Lutz Schirrmeister & Sebastian Wetterich*

## 8.1 Scientific background

The state and distribution of Laptev Sea submarine permafrost is coupled through a potential positive feedback to the global climate system through the release of greenhouse gases trapped beneath or in the permafrost, as well as through the release due to metabolism of old carbon. Based on limited observations and modeling, relict terrestrial permafrost is thought to underlie most of the Laptev Sea continental shelf (Nicol'sky *et al.*, 2012) as a result of the inundation of terrestrial permafrost formed during at least the last glacial stadion. The inundation of most of the Laptev Sea Shelf (as well as other arctic shelf) area following the last glacial maximum is the result of sea level rise but includes the influences of tectonics, coastal erosion and subsidence. Permafrost distribution beneath the inundated land area is influenced by the distribution and temperature of the permafrost before flooding, and by processes acting during and following inundation. We seek to understand the processes affecting permafrost during and immediately after inundation, when observed degradation rates are highest. Using these results, we plan to develop scenarios of submarine permafrost development to explore the role of the Laptev Sea as a global climate system component.

Our objective is to obtain sediment records and temperature observations of both onshore and offshore permafrost, and to investigate drivers of permafrost degradation in the near-shore zone (water depths below 10) along the western coastline of Buor Khaya Peninsula in the central Laptev Sea. A 2010 expedition to the Buor Khaya Peninsula investigated coastal dynamics and paleo-environmental records of change in the region (Wetterich *et al.*, 2011). During that expedition, geophysical surveys of sub-bottom electrical resistivity yielded initial estimates of ice-bonded permafrost distribution in the near-shore zone for two regions of the peninsula's western coast: the mouth of the Orto-Stan River and a region approximately 18 kilometers to the south of the Orto-Stan's mouth. The expedition described in this report draws upon these results to relate near-shore permafrost degradation to sediment type and depositional history, and to coastal dynamics. Specifically, the distribution of subsea permafrost and its degradation rate following inundation will be estimated and related to variability in erosion rates and boundary conditions at the sea bottom.

These results can be related to those from other sites. Combining results of drilling locations from differing settings will provide material for laboratory-based validation of both acoustic and electrical data. The material will be used to provide a paleo-reconstruction of environmental conditions in the region, including details of the progress of submarine permafrost degradation. Sampling of the near shore sediments provides refinement of coastal flux estimates and provides a basis for a sedimentary budget for coastal fluxes from the on- and offshore.

## 8.2 Acknowledgements

This project (Chapter 8: Scientific Permafrost Drilling Campaign) was carried out as a part of the Helmholtz Association of Research Centers Joint Russian German Research Group on the Sensitivity of the Arctic Coast to Change at AWI, and is a direct contribution to the Helmholtz Association's Research Program „Marine, Coastal and Polar Systems: Polar Regions and Coasts in a changing Earth System (PACES)“ as an activity of Topic 1 - Work Package 5: The role of degrading permafrost and carbon turnover in the coastal, shelf and deep sea environment. SPOT Planet Action – an Astrium GEO initiative – provided quasi-simultaneous acquisition of remote sensing data for monitoring of sea ice conditions through the project “Coastal erosion in East Siberia”. The Potsdam Research Cluster for Georisk Analysis, Environmental Change and Sustainability (PROGRESS) contributed personnel and analyses to support this expedition. A co-operative agreement with a group lead by Dr. Igor Semiletov (International Arctic Research Center, University of Alaska Fairbanks and Laboratory of Geochemistry in the Polar Regions, Pacific Oceanological Institute (POI), Vladivostok) made it possible to combine land and marine drilling efforts. The logistic services required for such an expedition are considerable and were provided by the Hydrobase (state hydrographic service) of Tiksi.

## 8.3 Itinerary

April 11, 2012	German participants fly from Berlin to Yakutsk, Russia
April 12, 2012	German and Russian participants fly from Yakutsk to Tiksi
April 13-16, 2012	Technical and logistic preparation
April 17, 2012	Departure of sled caravan from Tiksi
April 18, 2012	Arrival at western coast of Buor Khaya Peninsula (distance travelled 166 km)
April 19-23, 2012	Marine drill site BK-2
April 24-27, 2012	Terrestrial drill site BK-9
April 28, 2012	Departure from Buor Khaya Peninsula for Tiksi
April 30, 2012	Arrival in Tiksi
May 1-2, 2012	Unpacking, storage, sample preparation and inventory in Tiksi; planning and preparation of 2013 expeditions together with Lena Delta Reserve and Hydrobase
May 3-4, 2012	Travel from Tiksi to Berlin via Yakutsk

The group consisted of 11 members from three organisations, the Alfred Wegener Institute Helmholtz Centre for Polar and Marine Research in Potsdam, Germany (AWI), the Melnikov Permafrost Institute in Yakutsk, Siberian Branch of the Russian Academy of Sciences, Russia (PIY), and the Tiksi Hydrobase (Fig. 8.1).



**Fig. 8.1:** Expedition participants (from left to right): \* Dmitry Mashkov (chief engineer, Tiksi Hydrobase), Aleksandr Grigorievich Shiyan, URB-4T driver (Tiksi Hydrobase), \* Dmitry Melnichenko (director, Tiksi Hydrobase), Aleksandr Maslov, drillmaster (PIY), Viktor Dobrobaba, camp and caravan leader (Tiksi Hydrobase), Sebastian Wetterich, scientist (AWI), Valery Kulikov, Balok manager, cook (Tiksi Hydrobase), Aleksandr Safin, caterpillar driver (Tiksi Hydrobase), Pier Paul Overduin, scientist (AWI), Mikhail Grigoriev, expedition leader (PIY), Viktor Bayderin, vezdekhod driver (Tiksi Hydrobase), Sergey Kamarin, drill site operator (Tiksi Hydrobase), Lutz Schirmeister, scientist (AWI), \* did not accompany field expedition

## 8.4 Study Area and Methods

The main study site was a transect of boreholes and ice holes about 16 km south of the mouth of the Orto-Stan River on the western shore of Buor Khaya Bay. Our investigations were restricted to the near-shore zone, which at this site is defined as the zone including water depths of less than 5 m. The 5 m isobath lies within 1 km of the western Buor Khaya Peninsula coastline. The transect ran from about 750 m offshore ( $72^{\circ}25'20.4''$  N,  $132^{\circ}05'04.9''$  E) to a borehole site at the peak of a small Yedomia hill being eroded at the coast ( $71^{\circ}25'13.0''$  N,  $132^{\circ}06'38.0''$  E). Bathymetry was measured at 8 locations (BK1 to BK7, BK9) and water was sampled, if it was encountered, at 6 ice holes (BK1, BK2, and BK4 to BK7) drilled by Jiffy ice drill (6 inch diameter). Bathymetry was measured by lowering a weighted, graduated line to the seabed. Water was sampled at approximately 1 m intervals from the surface to the seabed, and water electrical conductivity, salinity and temperature were measured, either in the samples or in the water column directly, in either case using a WTW Cond 340i conductivity meter with a 6 m sensor cable.

Sampling of unfrozen and frozen sediments in marine sediments was done using a portable drill rig (URB-4T, Vorovskii Factory for Drilling Equipment, Ekaterinaburg, Russia, Fig. 8.2) from the sea ice surface and terrestrial permafrost was collected using a smaller drill rig (KMB-3, Geotekhnika, Moscow, Russia, Fig. 8.3). In both cases, drilling was controlled by Aleksandr Maslov, assisted by a team of 5 people, of whom 2 functioned as drillers and 3 were primarily responsible for sediment handling, description, sampling and conservation.

Sediment cores and samples were described concerning color, plant inclusions, visible sediment and ice structures. Samples were either frozen after sampling, by being left exposed to ambient air temperatures, or they were already frozen. Frozen samples were packaged in sample bags or tubes and stored in Styrofoam boxes.

The URB-4T is a self-propelled caterpillar vehicle with an approximately 8 m drill tower. Casing for the borehole measured 146 mm in diameter and was lowered during the drilling process (at site BK2) to a depth of 32 m b.s.l. Drilling for sediment core took place inside and below this casing with diameters of 108 and 89 mm. Sediment was removed from the up to 4 m long core barrel using a combination of core barrel heating (flame source) and compressed air to blow the sediment out of the barrel.

Available KMB casing diameters were 127, 108, 89 and 73 mm. Drilling occurred in a dry hole without casing starting with 127 mm diameter. The drill was set up on the ground surface and was stabilized by a log and some metal beams that ran between the drill's stanchions. To anchor the drill, a large sled and a caterpillar tread vehicle were parked on the log and beams, respectively, on either side of the drill. The space between the two was somewhat protected from the wind, which protection was improved by a tent wall on a third side.

Sediment temperatures in the marine borehole (BK2) were measured using two sets of thermistors: a 40 m Geoprecision thermistor strings and two thermistor strings from PIY, stretching from 1 to 20 m and from 41 to 50 m b.s.l. The 40 m Geoprecision thermistor string had digital sensors mounted at depths of 0, 0.2, 0.5, 1.0, 2.0, 5.0, 8.0, 10.0, 12.0, 15.0, 20.0, 25.0, 30.0, 35.0 and 40.0 m below the upper end of the casing. Depths are thus directly comparable to core depths given in the descriptions of marine sediments, and roughly correspond to m bsl, not accounting for tidal fluctuation (on the order of 10 cm amplitude).

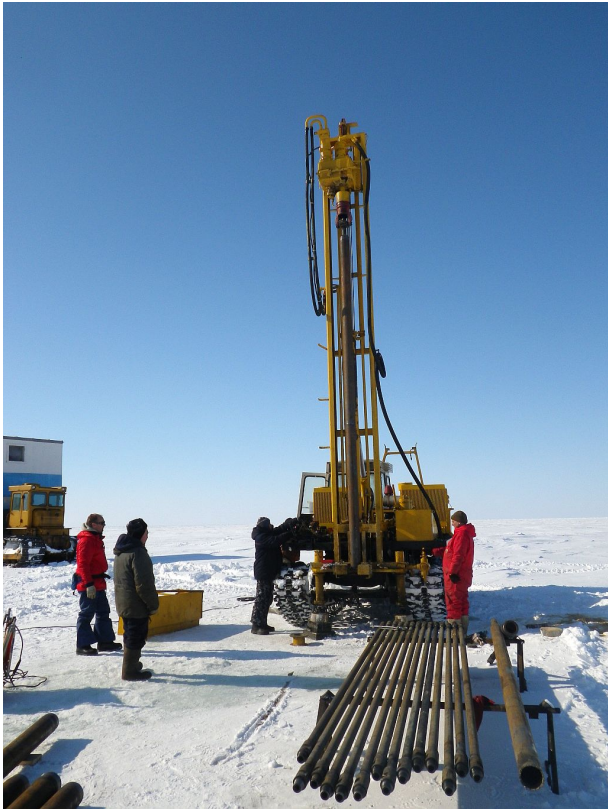


Fig. 8.2: A photograph of the URB-4T drill rig at the BK2 marine drill site.



Fig. 8.3: A photograph of the KMB drill rig at the BK8 terrestrial drill site.

## 8.5 Results

### 8.5.1 Marine drilling

Drilling at site BK2 began from the sea ice surface. The sea ice was destroyed by drilling, and no samples were taken. The sea ice was 2.07 m thick, 0.12 m of which floated above the sea water surface. The water depth was 4.03 m, so that the sub-ice water column was 2.08 m high. Unfrozen sediment was encountered at the sea bed, but recovery rates were low, since the sediment had high water content near the sea bed. The top of ice-bonded sediments was encountered at 28.75 m b.s.l., with 24.68 m of overlying unfrozen sediment. Of the total borehole depth of approximately 51.70 m, 4.3 m were water column, 34.67 m were recovered sediment and 16.33 m were not recovered, most of this between the sea bed and the top of the ice-bonded permafrost. This represents a recovery rate of 72 % overall, and of 67 % for the unfrozen sediment record (Fig. 8.4). Temperatures were measured in the borehole shortly after drilling using two temperature chains (from AWI and PIY). Temperatures recorded with the AWI thermistor string recorded permafrost temperatures between -14 °C and +1 °C three days after drilling stopped (Fig. 8.7& 8.8).

### 8.5.2 Terrestrial drilling

Drilling at site BK8, on top of the Yedoma upland, took place with the use of AWI's KMB drill rig. To secure the rig against torque, driftwood logs were laid between the struts of the drill and weighted down at either end by the sled with drilling casing and by the all-terrain vehicle. This additionally provided some protection from the wind. Core recovery began at the ground surface and continued down to the maximum borehole depth of 18.9 m (Fig. 8.5). Ice wedge ice was encountered between 3.2 m and 8.5 m and was collected. Drilling ceased due to the slow speed of progress and time constraints for the return trip. Temperatures measured in the borehole shortly after drill and before thermal equilibration can expect to have been reached recorded permafrost temperatures between -9 °C and -17 °C, with a permafrost temperature at the depth of zero seasonal amplitude of around -10.1 °C (Fig. 8.7).

### 8.5.3 Sea ice bore holes

Eight holes were drilled through the sea ice, water column measurements were made at the 7 holes which had water (Tab. 8.1) and samples were collected at 6 of the holes (List C & Fig. 8.6). Results showed some variability in sea water salinity and electrical conductivity, between 5.9 and 21.2 per mille ‰ and between 10.9 and 35.7 mS/cm, respectively. There was some initial insecurity regarding the measurements, for example, at site BK2, since an instable salinity profile was detected. This may have been due to the effects of drilling, either through the release of fresher or saltier water from the sea ice during drilling, through disturbance of the water column by the ice auger and/or by ice forming in the measurement cell of the conductivity sensor. As a result, additional measurements were made on water samples in the mobile accommodation (balok) on April 23, 2012. The results are presented in Table 8.2.

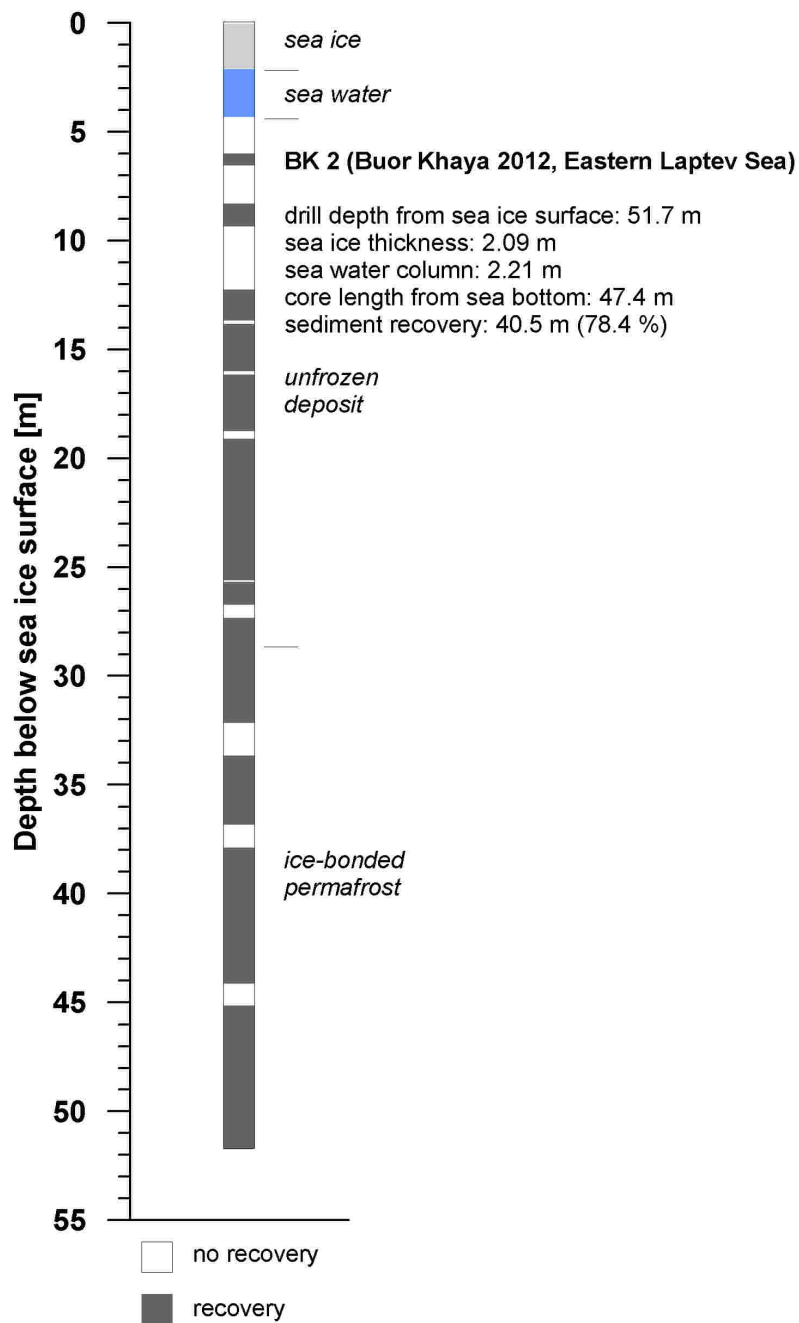


**Fig. 8.4:** The sediment recovery at borehole BK2 (offshore), showing the overlying sea ice and sea water and the recovered sediment sequences (gray). The boundary between overlying unfrozen sediment and underlying ice-bonded sediment is indicated with a dash to the right of the profile (between 28 and 29 m b.s.l.).

**Tab. 8.1:** Sea ice hole positions and water column data.

Site	Depth [m b.s.l.]	Conductivity [mS/cm]	Salinity [‰]	Temperature [°C]
<b>BK1</b>	0	21.6	12.5	0.1
	2	23.5	13.4	-1.2
	bottom	22.9	12.9	-1.5
Position: 71°25'18.4" N, 132°05'20.4" E			Water depth: 3.6 m	
Surface elevation: 0.15 m a.s.l.			Ice thickness: 2.12 m	
<b>BK2</b>	0	22.8	13.5	-1.7
	2	21.3	12.1	-1.5
	3	15.3	8.5	-1.6
	bottom	10.9	5.9	-1.6
Position: 71°25'20.3" N, 132°05'05.3" E			Water depth: 4.3 m	
Surface elevation: 0.17 m a.s.l.			Ice thickness: 2.09 m	
<b>BK3</b>	0	21.2	12.9	-1.3
	1	35.6	21.2	-1.1
	2	35.6	21.1	-1.1
	3	34.9	20.4	-1
	bottom	34.9	20.4	-1
Position: 71°42'196" N, 132°08'791" E			Water depth: 3.4 m	
Surface elevation: 0.11 m a.s.l.			Ice thickness: 2.05 m	
<b>BK4</b>	0	33.9	20.4	-1.1
	1	35.7	21.2	-1.1
	2	35.5	21.1	-1.1
	bottom	35.4	21	-1.1
Position: 71°42'193" N, 132°09'206" E			Water depth: 2.95 m	
Surface elevation: 0.17 m a.s.l.			Ice thickness: 2.00 m	
<b>BK5</b>	0	35.3	21	-1.1
	1	35.3	21	-1.1
	2	35.3	21	-1.1
	bottom	35.3	20.9	-1.1
Position: 71°42'182" N, 132°09'515" E			Water depth: 2.50 m	
Surface elevation: 0.52 m a.s.l.			Ice thickness: 2.20 m	
<b>BK6</b>	0	19.5	11.2	-1.1
	1	35.9	21.4	-1.1
	bottom	35.5	21.1	-1.1
Position: 71°42'171" N, 132°09'801" E			Water depth: 2.10 m	
Surface elevation: 0.14 m a.s.l.			Ice thickness: 1.90 m	
<b>BK7</b>	0	35.4	21	-1.2
	1	38.8	23.3	-1.2
	bottom	19.3	10.9	-1.2
Position: 71°42'155" N, 132°10'081" E			Water depth: (no water column)	
Surface elevation: 0.57 m a.s.l.			Ice thickness: 1.70 m	



**BK 8 (Buor Khaya 2012, Eastern Laptev Sea)**

drill depth from Yedoma surface: 18.9 m

core length: 18.9 m

sediment recovery: 18.9 m (100 %)

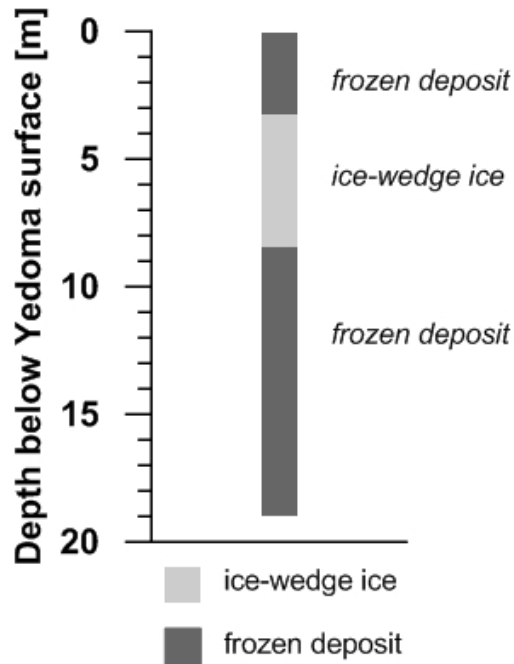


**Fig. 8.5:** The sediment recovery record for borehole BK8 (onshore) shows the recovered sediment sequences (gray) and ice wedge ice (light gray).

**Tab. 8.2:** Water sample electrical conductivity and salinity measurements from April 23, 2012.

Site	depth [m]	electrical conductivity [mS/cm]	salinity [‰]
BK4	0.0	33.9	20.4
	2.0	32.9	20.1
	2.35	33.7	20.4
BK5	0.0	32.8	20.3
	1.9	33.3	20.3
BK6	0.0	34.2	21
	1.5	33.6	20.6
BK7	0.0	37.2	23.1
	1.0	36.8	22.8

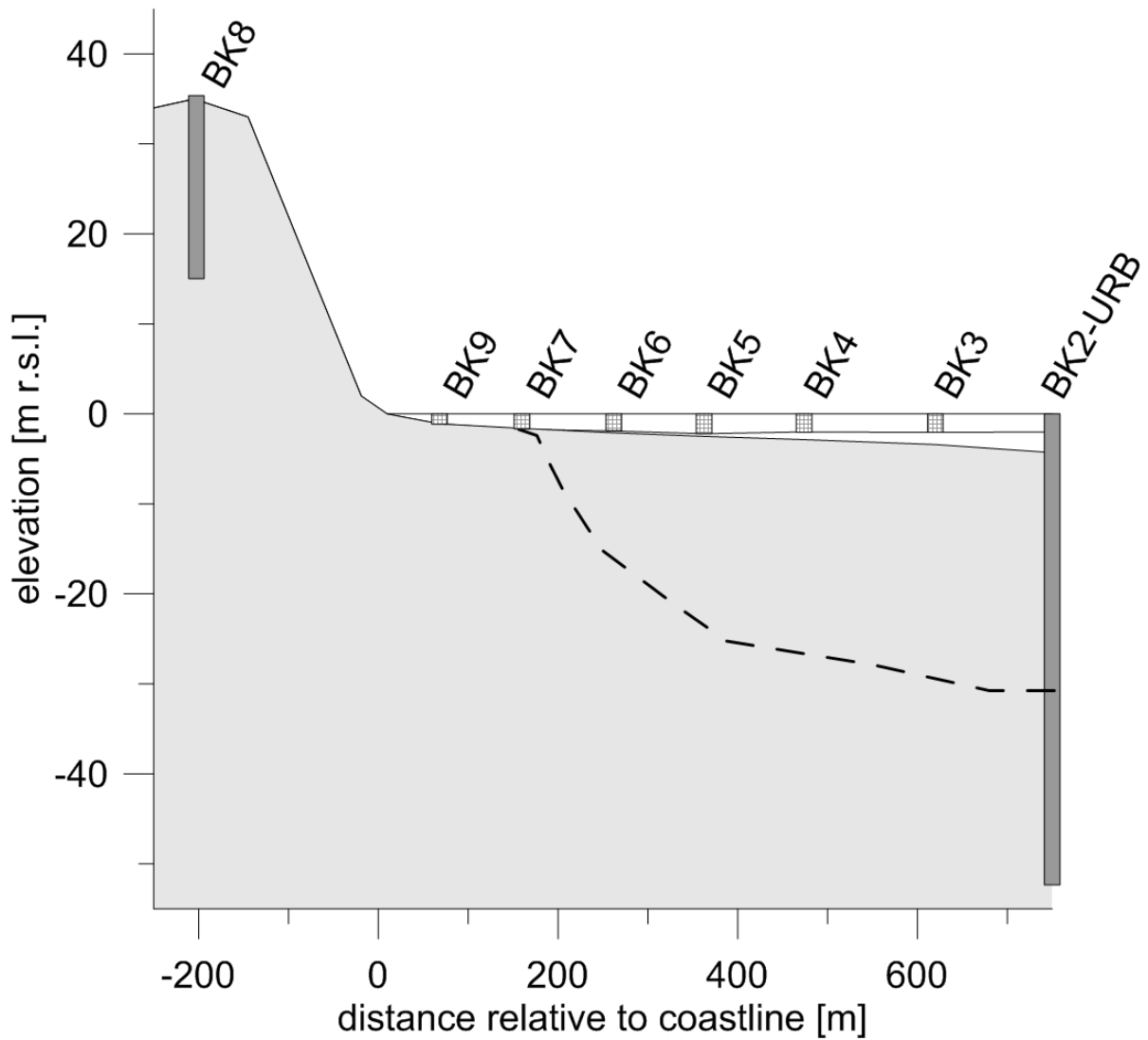


**Fig. 8.6:** Shoreface profile and distribution of sampling sites relative to the coastline and sea level. Boreholes are shown as darker gray bars, while ice holes are shown hatched. The upper surface of ice-bonded permafrost was observed at BK2-URB and its position elsewhere is surmised. The vertical scale is exaggerated by a factor of ten.

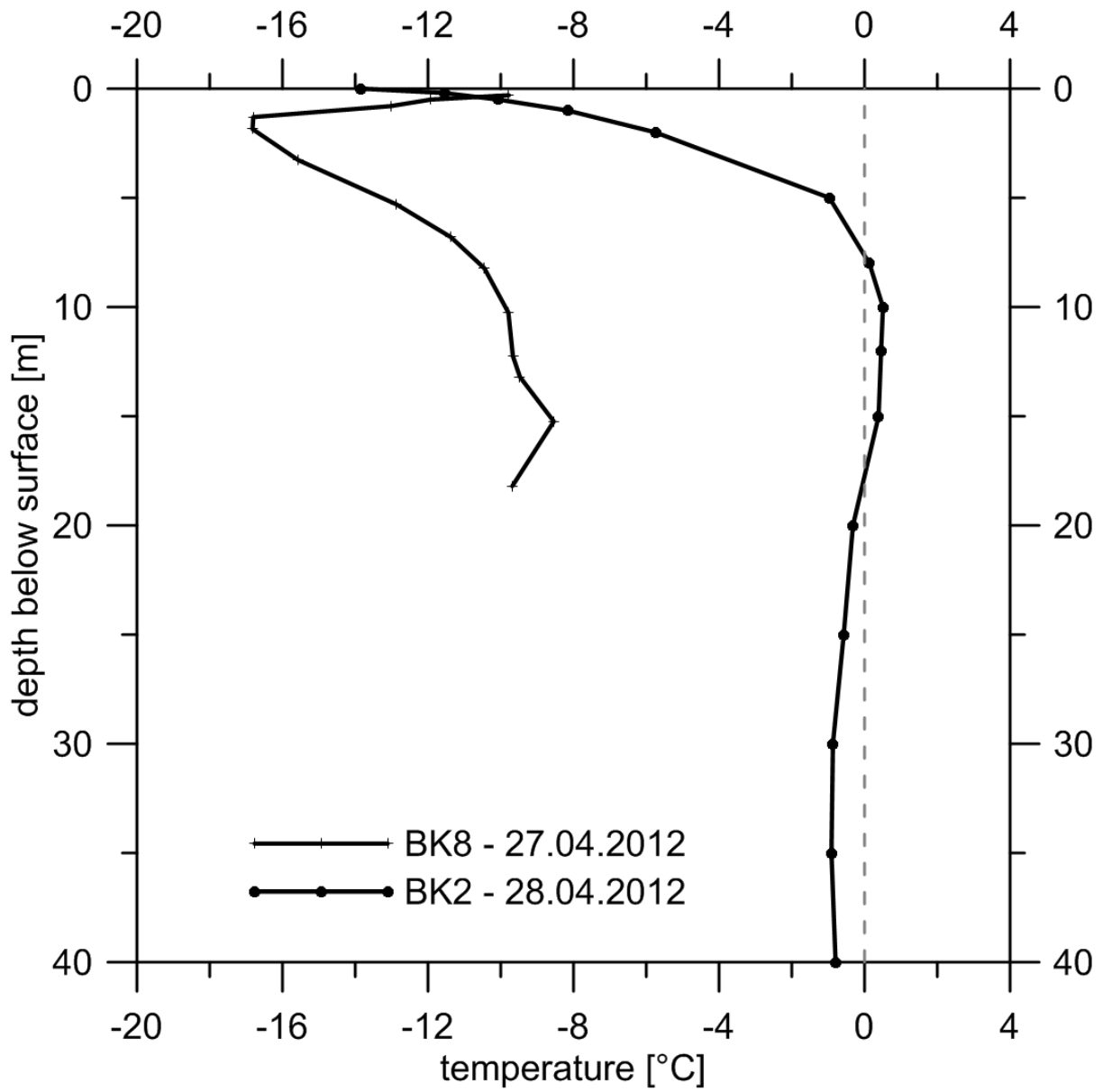


**Fig. 8.7:** Borehole temperatures measured using GeoPrecision thermistor strings with PT1000 sensors in the boreholes BK2 and BK8.

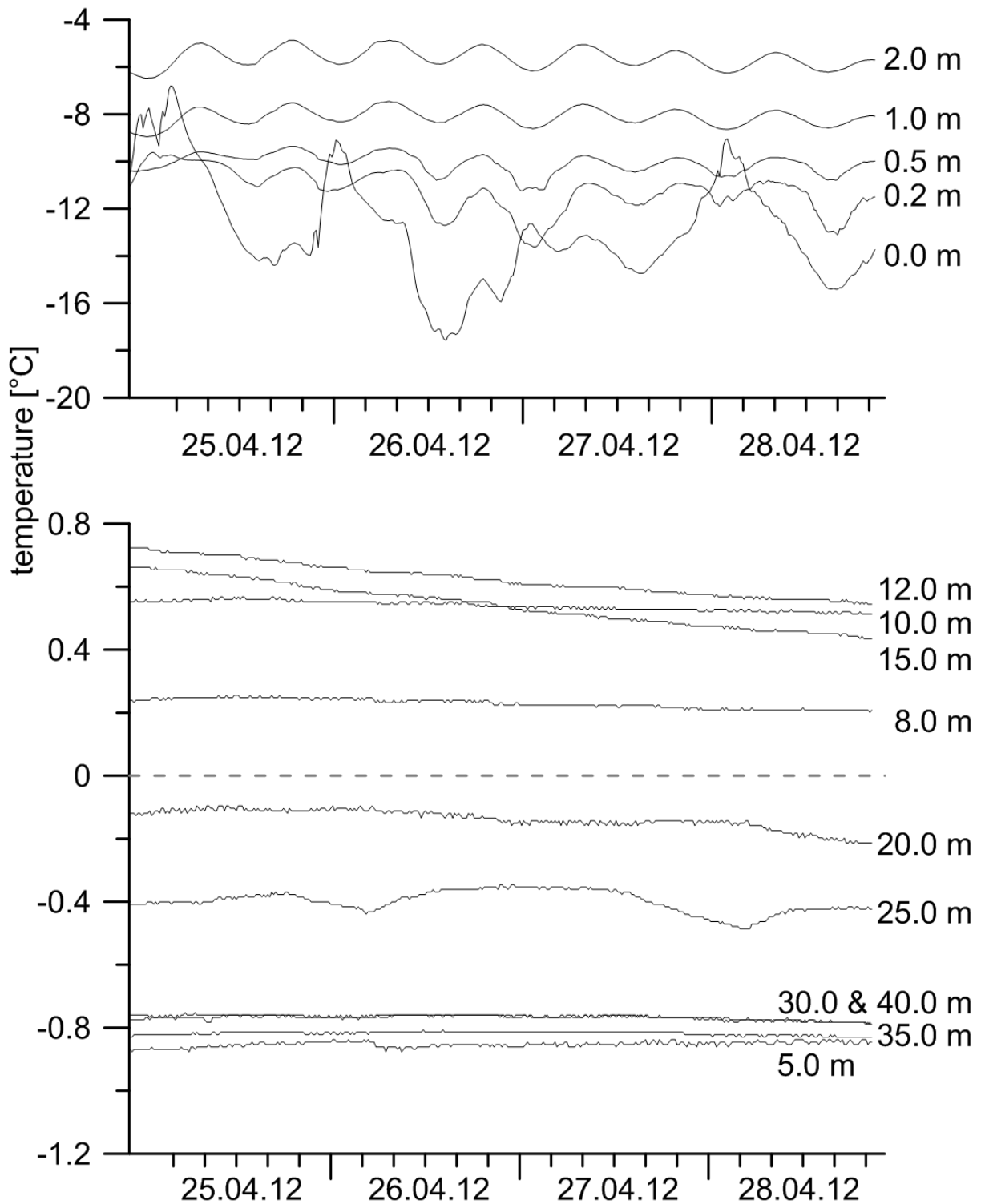


**Fig. 8.8:** The change in temperature over time at borehole BK2 for the four days immediately following drilling. The upper graph shows the temperatures recorded in the borehole for depths corresponding to sea ice and water column. The lower graph shows temperatures recorded at depths within the sediment column.

## References

- ARE, F. E., GRIGORIEV, M. N., HUBBERTEN, H.-W., RACHOLD, V., RAZUMOV, S. O., & SCHNEIDER, W. 2000. Coastal erosion studies in the Laptev Sea. *Chap. 4.3, pages 65–74 of: RACHOLD, V. (ed), Russian-German Cooperation System Laptev Sea: The Expedition Lena 1999*. Reports on Polar and Marine Research, vol. 354. Alfred Wegener Institute. (cited on page 16)
- EDWARDS, R. N., WOLFGAM, P. A., & JUDGE, A. S. 1988. The ICE-MOSERS Experiment: Mapping permafrost zones electrically beneath the Beaufort Sea. *Marine Geophysical Researches*, 9, 265–290. (cited on page 65)
- GRIGORIEV, M. N. 2004. Studies of coastal dynamics and sub-sea permafrost. *Chap. 4.7, pages 139–150 of: SCHIRRMEISTER, L. (ed), Expeditions in Siberia 2003*. Reports on Polar and Marine Research, vol. 489. Alfred Wegener Institute. (cited on page 16)
- GRIGORIEV, M. N., ARE, F. E., HUBBERTEN, H.-W., RACHOLD, V., RAZUMOV, S. O., & SCHNEIDER, W. 2003. Onshore coastal studies - coastal dynamics at key sites of the New Siberian Islands, Dmitry Laptev Strait, and Buor Khaya Bay. *Chap. 5.3.3, pages 326–329 of: GRIGORIEV, M. N., RACHOLD, V., BOLSHIYANOV, D. YU., PFEIFFER, E.-M., SCHIRRMEISTER, L., WAGNER, D., & HUBBERTEN, H.-W. (eds), Russian-German Cooperation System Laptev Sea: The Expedition Lena 2002*. Reports on Polar and Marine Research, vol. 466. Alfred Wegener Institute. (cited on page 16)
- GRIGORIEV, M.N., RACHOLD, V., ARE, F.E., HUBBERTEN, H.-W., RAZUMOV, S.O., & SCHNEIDER, W. 2001. Coastal dynamics in the western Laptev Sea. *Chap. 4.3, pages 54–64 of: RACHOLD, V., & GRIGORIEV, M.N. (eds), Russian-German Cooperation System Laptev Sea: The Expedition Lena 2000*. Reports on Polar and marine Research, vol. 388. Alfred Wegener Institute. (cited on page 16)
- GRIGORIEV, M.N., RACHOLD, V., SCHIRRMEISTER, L., & HUBBERTEN, H.-W. 2004. Organic carbon input to the Arctic Seas through coastal erosion. *Chap. 2.3, pages 37–65 of: STEIN, R., & MACDONALD, R.W. (eds), The organic carbon cycle in the Arctic Ocean: present and past*. Springer, Berlin. (cited on page 72)
- GROSSE, G. 2004. Multi-sensor optical remote sensing of periglacial tundra landscapes. *Chap. 4.4, pages 75–91 of: SCHIRRMEISTER, L. (ed), Expeditions in Siberia 2003*. Reports on Polar and Marine Research, vol. 489. Alfred Wegener Institute. (cited on page 19)
- GÜNTHER, F., OVERDUIN, P. P., & SANDAKOV, A. 2011. Topographical surveys for coastal dynamics studies. *Chap. 4, pages 17–34 of: WETTERICH, S., OVERDUIN, P. P., & GRIGORIEV, M. N. (eds), The Expedition Eastern Laptev Sea – Buor Khaya Peninsula 2010*. Reports on Polar and Marine Research, vol. 629. Alfred Wegener Institute. (cited on pages 16 and 17)

- KNEISEL, C., HAUCK, C., FORTIER, R., & MOORMAN, B. 2008. Advances in geophysical methods for permafrost investigations. *Permafrost and Periglacial Processes*, **19**, 157–178. (cited on page 64)
- KUNITSKY, V. V. 1989. *Kriolitologiya Nizovya Leny (Cryolithology of the Lower Lena)*. Melnikov Permafrost Institute, Russian Academy of Sciences, Siberian Branch, Yakutsk, Russia. (cited on pages 64 and 71)
- MEYER, H., SCHIRRMEISTER, L., YOSHIKAWA, K., OPEL, T., WETTERICH, S., HUBBERTEN, H.-W., & BROWN, J. 2010. Permafrost evidence for severe winter cooling during the Younger Dryas in northern Alaska. *Geophysical Research Letters*, **37**, L03501. (cited on page 55)
- NICOLSKY, D. J., ROMANOVSKY, V. E., ROMANOVSKII, N. N., KHOLODOV, A. L., SHAKHOVA, N. E., & SEMILETOV, I. P. 2012. Modeling sub-sea permafrost in the East Siberian Arctic Shelf: The Laptev Sea region. *Journal of Geophysical Research*, **117**(F3), F03028. (cited on page 75)
- OPEL, T., DEREVIAGIN, A., MEYER, H., SCHIRRMEISTER, L., & WETTERICH, S. 2011. Paleoclimatic information from stable water isotopes of Holocene ice wedges at the Dmitrii Laptev Strait (Northeast Siberia). *Permafrost and Periglacial Processes*, **22**, 84–100. (cited on page 55)
- OVERDUIN, P. P., WESTERMANN, S., YOSHIKAWA, K., HABERLAU, T., ROMANOVSKY, V., & WETTERICH, S. 2012. Geoelectric observations of the degradation of nearshore submarine permafrost at Barrow (Alaskan Beaufort Sea). *Journal of Geophysical Research*, **117**, F02004. (cited on page 65)
- OVERDUIN, P.P., GRIGORIEV, M.N., JUNKER, R., RACHOLD, V., KUNITSKY, V.V., BOLSHIYANOV, D.YU., & SCHIRRMEISTER, L. 2007. Russian-German Cooperation System Laptev Sea: The Expedition COAST 1. *Pages 5–39 of: SCHIRRMEISTER, L. (ed), Expeditions in Siberia 2005*. Reports on Polar and Marine Research, vol. 550. Alfred Wegener Institute. (cited on pages 1 and 4)
- SANDAKOV, A. V., GRIGORIEV, M. N., GÜNTHER, F., & OVERDUIN, P. P. 2012. The wash-out of organic carbon from degrading shores and its distribution at the under-water coastal slope (Buor Khaya Peninsula, Laptev Sea). *Pages 494–495 of: DROZDOV, D. S. (ed), Proceedings of the Tenth International Conference on Permafrost, resources and risks of permafrost areas in a changing world, Salekhard, Yamal-Nenets Autonomous District, Russia, June 25-29, 2012*, vol. Extended abstracts 4/2. The Fort Dialog-Iset Publisher, Tyumen, Ekaterinburg. (cited on page 72)
- SCHIRRMEISTER, L. (ed). 2004. *Expeditions in Siberia in 2003*. Reports on Polar and Marine Research, vol. 489. Alfred Wegener Institute. (cited on page 64)
- SCHIRRMEISTER, L. (ed). 2007. *Expeditions in Siberia 2005*. Reports on Polar and Marine Research, vol. 550. Alfred Wegener Institute. (cited on page 64)
- SCHIRRMEISTER, L., & GRIGORIEV, M. N. 2004. Russian-German Cooperation System Laptev Sea: The Expedition Lena Anabar 2003, Periglacial Studies around Cape Mamontov Klyk. *Chap. 4, pages 61–209 of: SCHIRRMEISTER, L. (ed), Expeditions in Siberia 2003*. Reports on Polar and Marine Research, vol. 489. Alfred Wegener Institute. (cited on page 1)

- SCHIRRMEISTER, L., GROSSE, G., KUNITSKY, V., MAGENS, D., MEYER, H., DEREVIAGIN, A., KUZNETSOVA, T., ANDREEV, A., BABIY, O., KIENAST, F., GRIGORIEV, M., OVERDUIN, P. P., & PREUSSER, F. 2008. Periglacial landscape evolution and environmental changes of Arctic lowland areas for the last 60 000 years (western Laptev Sea coast, Cape Mamontov Klyk). *Polar Research*, **27**(2), 249–272. (cited on page 17)
- SLAGODA, E. A. 2004. *Kriolitogennye otlozheniya primorskoi ravniny morya Laptevykh: litologiya i mikromorfologiya (poluostrov Bykovskiy i ostrov Muostakh) - Cryolithogenic sediments of the Laptev Sea coastal lowland: lithology and micromorphology (Bykovsky Peninsula and Muostakh Island)*. Ekspres, Tyumen. (cited on pages 64 and 71)
- VIEHBERG, F. A. 2002. A new and simple method for qualitative sampling of meiobenthos-communities. *Limnologica*, **32**, 350–351. (cited on page 12)
- WETTERICH, S., & SCHIRRMEISTER, L. 2008. Limnological studies in the Dmitrii Laptev Strait region. *Chap. 5.2, pages 155–163 of: BOIKE, J., BOLSHIYANOV, D. YU., SCHIRRMEISTER, L., & WETTERICH, S. (eds), The Expedition Lena - New Siberian Islands 2007*. Reports on Polar and Marine Research, vol. 584. Alfred Wegener Institute. (cited on page 12)
- WETTERICH, S., & SCHIRRMEISTER, L. 2011a. Limnological sampling of polygon ponds on Buor Khaya Peninsula. *Chap. 3, pages 11–16 of: WETTERICH, S., OVERDUIN, P. P., & GRIGORIEV, M. N. (eds), Russian-German Cooperation SYSTEM LAPTEV SEA: The expedition Eastern Laptev Sea - Buor Khaya Peninsula 2010*. Reports on Polar and Marine Research, vol. 629. Alfred Wegener Institute. (cited on page 12)
- WETTERICH, S., & SCHIRRMEISTER, L. 2011b. Limnological studies in modern periglacial waters on the Lower Kolyma plain. *Chap. 4, pages 21–26 of: WETTERICH, S., SCHIRRMEISTER, L., & KHOLODOV, A. L. (eds), The joint Russian-German Expedition BERINGIA/KOLYMA 2008*. Reports on Polar and Marine Research, vol. 636. Alfred Wegener Institute. (cited on page 12)
- WETTERICH, S., SCHIRRMEISTER, L., MEYER, H., VIEHBERG, F. A., & MACKENSEN, A. 2008. Arctic freshwater ostracods from modern periglacial environment in the Lena River Delta Siberian Arctic, Russia): Geochemical applications for palaeoenvironmental reconstructions. *Journal of Paleolimnology*, **39**, 417–449. (cited on page 12)
- WETTERICH, S., OVERDUIN, P. P., & GRIGORIEV, M. N. (eds). 2011. *Russian-German Cooperation System Laptev Sea: The Expedition Eastern Laptev Sea - Buor Khaya Peninsula 2010*. Reports on Polar and Marine Research, vol. 629. Alfred Wegener Institute for Polar and Marine Research, Bremerhaven. (cited on page 75)
- WINTERFELD, M., SCHIRRMEISTER, L., GRIGORIEV, M. N., KUNITSKY, V. V., ANDREEV, A., MURRAY, A., & OVERDUIN, P. P. 2011. Coastal permafrost landscape development since the Late Pleistocene in the western Laptev Sea, Siberia. *Boreas*, **40**(4), 697–713. (cited on pages 4 and 64)
- YOSHIKAWA, K., LEUSCHEN, C., IKEDA, A., HARADA, K., GOGINENI, P., HOEKSTRA, P., HINZMAN, L., SAWADA, Y., & MATSUOKA, N. 2006. Comparison of geophysical investigations for detection of massive ground ice (pingo ice). *Journal of Geophysical Research*, **111**, E06S19. (cited on page 64)

# List of figures

1.1	Location of study sites . . . . .	2
1.2	Photograph of the Mamontov Klyk 2011 expedition group members . . . . .	3
2.1	Photograph and diagram of borehole casing . . . . .	5
2.2	Schematic diagram of borehole casing . . . . .	6
2.3	Temperature data from COAST C1 borehole . . . . .	7
2.4	Borehole temperature outlier data example . . . . .	8
2.5	Second example of borehole temperature outlier data . . . . .	8
2.6	Minimum, mean, maximum and outlier maximum borehole temperatures . . . . .	9
3.1	Photographs of polygon types . . . . .	12
3.2	Polygon temperature data . . . . .	14
4.1	Photographs of topographic survey setup . . . . .	18
4.2	Photograph of a topographic fixed and marked backside point . . . . .	18
4.3	Oblique view of the Cape Mamontov Klyk topography . . . . .	19
4.4	Map of topographic survey points at Cape Mamontov Klyk . . . . .	20
4.5	Map of topographic survey points at Cape Mamontov Klyk . . . . .	21
4.6	Topographic survey of coastal cliffs on Muostakh Island . . . . .	23
4.7	Slope profile locations on Muostakh Island . . . . .	24
4.8	Examples of coastal slope profiles . . . . .	25
4.9	Tacheometric survey on Muostakh Island I . . . . .	26
4.10	Tacheometric survey on Muostakh Island II . . . . .	27
4.11	Tacheometric survey on Muostakh Island III . . . . .	28
4.12	Tacheometric survey on Muostakh Island IV . . . . .	29
4.13	Tacheometric survey on Muostakh Island V . . . . .	30
4.14	Tacheometric survey on Muostakh Island VI . . . . .	31
4.15	Tacheometric survey on Muostakh Island VII . . . . .	32
4.16	Tacheometric survey on Muostakh Island VIII . . . . .	33
4.17	Tacheometric survey on Muostakh Island IX . . . . .	34
4.18	Tacheometric survey on Muostakh Island X . . . . .	35
4.19	Tacheometric survey on Muostakh Island XI . . . . .	36
4.20	Tacheometric survey on Muostakh Island XII . . . . .	37
4.21	Tacheometric survey on Muostakh Island XIII . . . . .	38
4.22	Tacheometric survey on Muostakh Island XIV . . . . .	39
4.23	Tacheometric survey on Muostakh Island XV . . . . .	40
4.24	Tacheometric survey on Muostakh Island XVI . . . . .	41
4.25	Tacheometric survey on Muostakh Island XVII . . . . .	42
4.26	Tacheometric survey on Muostakh Island XVIII . . . . .	43
4.27	Tacheometric survey on Muostakh Island XIX . . . . .	44



---

4.28	Tacheometric survey on Muostakh Island XX	45
4.29	Tacheometric survey on Muostakh Island XXI	46
4.30	Tacheometric survey on Muostakh Island XXII	47
4.31	Tacheometric survey on Muostakh Island XXIII	48
4.32	Tacheometric survey on Muostakh Island XXIV	49
4.33	Tacheometric survey on Muostakh Island XXV	50
4.34	Tacheometric survey on Muostakh Island XXVI	51
4.35	Establishment of station 13 at Musotakh Island's north end	52
4.36	Elevation determinations at Muostakh Island's northern end	53
4.37	Establishment of reference points at Muostakh Island's northern end	54
5.1	Ice wedge study sites	57
5.2	Ice wedge MUO11 IW1	58
5.3	Ice wedge MUO11 IW2	59
5.4	Ice wedge MUO11 IW3	60
5.5	Ice wedge MUO11 IW4	61
5.6	Ice wedge MUO11 IW5	62
5.7	Ice wedge MUO11 IW6	63
6.1	Photograph of geoelectric cable electrode	66
6.2	Electrode array geometry	66
6.3	Geoelectric profile position at Muostakh Island	67
6.4	Photograph of seismic system mount	69
6.5	Map of seismic profile positions	70
7.1	Map of surface sediment sample locations	73
8.1	Drilling expedition participants	77
8.2	Photograph of URB-4T drill rig	79
8.3	Photograph of the KMB drill rig	79
8.4	Sediment recovery at the offshore Buor Khaya site (BK2)	81
8.5	Sediment recovery at the onshore Buor Khaya site (BK8)	83
8.6	schematic diagram of the Buor Khaya shoreface profile	84
8.7	Borehole temperature profiles at Buor Khaya	85
8.8	Temperature changes at BK2 following drilling	86

## List of tables

2.1	Mamontov Klyk borehole thermistor string . . . . .	5
3.1	Geographical features of the studied waters . . . . .	13
3.2	Morphological and sedimentological features of the studied waters . . . . .	13
3.3	Physico-chemical features of the studied waters . . . . .	14
4.1	Summary of topographic survey on Cape Mamontov Klyk . . . . .	21
4.2	Summary of topographic survey on Muostakh Island . . . . .	25
6.1	List of geoelectic profiles in order of acquisition. . . . .	67
6.2	Salinity and electrical conductivity of surface water. . . . .	68
7.1	List of Muostakh Island surface sediment samples . . . . .	73
8.1	Sea ice hole positions and water column data . . . . .	82
8.2	Surface water electrical conductivity and salinity measurements . . . . .	83

# A Appendix Ice Wedges

List of Holocene ice-wedge samples for stable water isotope analysis from Muostakh Island

Sample №	Hydrochemistry	pH	EC [ $\mu\text{S}/\text{cm}$ ]	Organic Material?
Ice wedge MUO11 IW1				
MUO11 IW1-001	-	-	-	x
MUO11 IW1-002	-	-	-	x
MUO11 IW1-003	-	-	-	x
MUO11 IW1-004	x	6.5	84.1	x
MUO11 IW1-005	-	-	-	x
MUO11 IW1-006	-	-	-	-
MUO11 IW1-007	-	-	-	x
MUO11 IW1-008	-	-	-	x
MUO11 IW1-009	-	-	-	x
MUO11 IW1-010	-	-	-	-
MUO11 IW1-011	-	-	-	x
MUO11 IW1-012	-	-	-	x
MUO11 IW1-013	-	-	-	-
MUO11 IW1-014	x	6.5	68.3	-
MUO11 IW1-015	-	-	-	x
MUO11 IW1-016	-	-	-	x
MUO11 IW1-017	-	-	-	x
MUO11 IW1-018	-	-	-	x
MUO11 IW1-019	-	-	-	x
MUO11 IW1-020	-	-	-	x
MUO11 IW1-021	-	-	-	x
MUO11 IW1-022	-	-	-	x
MUO11 IW1-023	-	-	-	x
MUO11 IW1-024	x	6.5	51.8	x
MUO11 IW1-025	-	-	-	-
MUO11 IW1-026	-	-	-	x
MUO11 IW1-027	-	-	-	x
MUO11 IW1-028	-	-	-	x
MUO11 IW1-029	-	-	-	-
MUO11 IW1-030	-	-	-	x
MUO11 IW1-031	-	-	-	x
MUO11 IW1-032	-	-	-	x

*continuation on next side*

List of Holocene ice-wedge samples for stable water isotope analysis from Muostakh Island - continuation

Sample №	Hydrochemistry	pH	EC [ $\mu\text{S}/\text{cm}$ ]	Organic Material?
MUO11 IW1-033	-	-	-	-
MUO11 IW1-034	x	6.5	61.9	-
MUO11 IW1-035	-	-	-	x
MUO11 IW1-036	-	-	-	x
MUO11 IW1-037	-	-	-	-
MUO11 IW1-038	-	-	-	x
MUO11 IW1-039	-	-	-	x
MUO11 IW1-040	-	-	-	x
MUO11 IW1-041	-	-	-	x
MUO11 IW1-042	-	-	-	x
MUO11 IW1-043	-	-	-	x
MUO11 IW1-044	x	6.5	107.3	x
MUO11 IW1-045	-	-	-	x
MUO11 IW1-046	-	-	-	-
MUO11 IW1-047	-	-	-	x
MUO11 IW1-048	-	-	-	x
MUO11 IW1-049	-	-	-	x
MUO11 IW1-050	-	-	-	x
MUO11 IW1-051	-	-	-	x
MUO11 IW1-052	-	-	-	x
MUO11 IW1-053	-	-	-	x
MUO11 IW1-054	x	6.5	44.2	x
MUO11 IW1-055	-	-	-	x
MUO11 IW1-056	-	-	-	x
MUO11 IW1-057	-	-	-	x
MUO11 IW1-058	-	-	-	x
MUO11 IW1-059	-	-	-	x
MUO11 IW1-060	-	-	-	x
MUO11 IW1-061	-	-	-	x
MUO11 IW1-062	-	-	-	-
MUO11 IW1-063	-	-	-	x
MUO11 IW1-064	x	6.5	31.5	x
MUO11 IW1-065	-	-	-	x
MUO11 IW1-066	-	-	-	x
MUO11 IW1-067	-	-	-	-
MUO11 IW1-068	-	-	-	-
MUO11 IW1-069	-	-	-	-
MUO11 IW1-070	-	-	-	-
MUO11 IW1-071	-	-	-	x
MUO11 IW1-072	-	-	-	x
MUO11 IW1-073	-	-	-	x

*continuation on next side*

List of Holocene ice-wedge samples for stable water isotope analysis from Muostakh Island - continuation

Sample №	Hydrochemistry	pH	EC [ $\mu\text{S}/\text{cm}$ ]	Organic Material?
MUO11 IW1-074	x	6.5	39.9	x
MUO11 IW1-075	-	-	-	-
MUO11 IW1-076	-	-	-	x
MUO11 IW1-077	-	-	-	-
MUO11 IW1-1	<i>Frozen block for subsampling in cold laboratory</i>			
MUO11 IW1-2	<i>Frozen block for subsampling in cold laboratory</i>			
MUO11 IW1-3	<i>Frozen block for subsampling in cold laboratory</i>			
MUO11 IW1-4	<i>Frozen block for subsampling in cold laboratory</i>			
MUO11 IW1-5	<i>Frozen block for subsampling in cold laboratory</i>			
MUO11 IW1-6	<i>Frozen block for subsampling in cold laboratory</i>			
MUO11 IW1-7	<i>Frozen block for subsampling in cold laboratory</i>			
MUO11 IW1-8	<i>Frozen block for subsampling in cold laboratory</i>			
MUO11 IW1-9	<i>Frozen block for subsampling in cold laboratory</i>			
Ice wedge MUO11 IW3				
MUO11 IW3-001	-	-	-	-
MUO11 IW3-002	-	-	-	-
MUO11 IW3-003	-	-	-	-
MUO11 IW3-004	x	6.5	60.5	-
MUO11 IW3-005	-	-	-	-
MUO11 IW3-006	-	-	-	x
MUO11 IW3-007	-	-	-	x
MUO11 IW3-008	-	-	-	x
MUO11 IW3-009	-	-	-	x
MUO11 IW3-010	-	-	-	x
MUO11 IW3-011	-	-	-	-
MUO11 IW3-012	-	-	-	-
MUO11 IW3-013	x	6.5	62.8	-
MUO11 IW3-014	-	-	-	-
MUO11 IW3-015	-	-	-	x
MUO11 IW3-016	-	-	-	-
MUO11 IW3-017	-	-	-	-
MUO11 IW3-018	-	-	-	-
MUO11 IW3-019	-	-	-	-
MUO11 IW3-020	-	-	-	-
MUO11 IW3-021	-	-	-	-
MUO11 IW3-022	-	-	-	-
MUO11 IW3-023	x	6.5	63.7	-
MUO11 IW3-024	-	-	-	-
MUO11 IW3-025	-	-	-	x
MUO11 IW3-026	-	-	-	x

*continuation on next side*

List of Holocene ice-wedge samples for stable water isotope analysis from Muostakh Island - continuation

Sample №	Hydrochemistry	pH	EC [ $\mu\text{S}/\text{cm}$ ]	Organic Material?
MUO11 IW3-027	-	-	-	-
MUO11 IW3-028	-	-	-	x
MUO11 IW3-029	-	-	-	-
MUO11 IW3-030	-	-	-	-
MUO11 IW3-031	-	-	-	x
MUO11 IW3-032	-	-	-	x
MUO11 IW3-033	x	6.5	76.4	-
MUO11 IW3-034	-	-	-	-
MUO11 IW3-035	-	-	-	-
MUO11 IW3-036	-	-	-	x
MUO11 IW3-037	-	-	-	-
MUO11 IW3-038	-	-	-	-
MUO11 IW3-039	-	-	-	x
MUO11 IW3-040	-	-	-	x
MUO11 IW3-041	-	-	-	-
MUO11 IW3-042	-	-	-	x
MUO11 IW3-043	x	6.5	94.8	x
MUO11 IW3-044	-	-	-	x
MUO11 IW3-045	-	-	-	x
MUO11 IW3-046	-	-	-	x
MUO11 IW3-047	-	-	-	x
MUO11 IW3-048	-	-	-	x
MUO11 IW3-049	-	-	-	-
MUO11 IW3-050	-	-	-	x
MUO11 IW3-051	-	-	-	x
MUO11 IW3-052	x	6.5	47.6	-
MUO11 IW3-053	-	-	-	x
MUO11 IW3-054	-	-	-	x
MUO11 IW3-055	-	-	-	-
MUO11 IW3-056	-	-	-	-
MUO11 IW3-057	-	-	-	-
MUO11 IW3-058	-	-	-	-
MUO11 IW3-059	x	6.0	64.6	-
MUO11 IW3-060	-	-	-	x
MUO11 IW3-061	-	-	-	-
MUO11 IW3-062	-	-	-	-
MUO11 IW3-063	x	6.5	62.9	-
MUO11 IW3-064	-	-	-	-
MUO11 IW3-065	-	-	-	-
MUO11 IW3-066	-	-	-	-
MUO11 IW3-067	-	-	-	-

*continuation on next side*

List of Holocene ice-wedge samples for stable water isotope analysis from Muostakh Island - continuation

Sample №	Hydrochemistry	pH	EC [ $\mu\text{S}/\text{cm}$ ]	Organic Material?
MUO11 IW3-068	x	6.5	55.7	x
MUO11 IW3-069	-	-	-	-
Ice wedge MUO11 IW4				
MUO11 IW4-001	-	-	-	-
MUO11 IW4-002	-	-	-	-
MUO11 IW4-003	x	6.5	25.1	-
MUO11 IW4-004	-	-	-	-
MUO11 IW4-005	-	-	-	x
MUO11 IW4-006	-	-	-	x
MUO11 IW4-007	-	-	-	x
MUO11 IW4-008	-	-	-	-
MUO11 IW4-009	-	-	-	x
MUO11 IW4-010	-	-	-	-
MUO11 IW4-011	-	-	-	x
MUO11 IW4-012	-	-	-	x
MUO11 IW4-013	x	6.5	30.7	x
MUO11 IW4-014	-	-	-	x
MUO11 IW4-015	-	-	-	x
MUO11 IW4-016	-	-	-	x
MUO11 IW4-017	-	-	-	x
MUO11 IW4-018	-	-	-	x
MUO11 IW4-019	-	-	-	-
MUO11 IW4-020	-	-	-	x
MUO11 IW4-021	-	-	-	x
MUO11 IW4-022	-	-	-	-
MUO11 IW4-023	x	6.5	29.6	-
MUO11 IW4-024	-	-	-	-
MUO11 IW4-025	-	-	-	-
MUO11 IW4-026	-	-	-	-
MUO11 IW4-027	-	-	-	-
MUO11 IW4-028	-	-	-	x
MUO11 IW4-029	-	-	-	x
MUO11 IW4-030	-	-	-	x
MUO11 IW4-031	-	-	-	x
MUO11 IW4-032	-	-	-	x
MUO11 IW4-033	x	6.5	38.8	x
MUO11 IW4-034	-	-	-	x
MUO11 IW4-035	-	-	-	x
MUO11 IW4-036	-	-	-	x
MUO11 IW4-037	-	-	-	x

*continuation on next side*

List of Holocene ice-wedge samples for stable water isotope analysis from Muostakh Island - continuation

Sample №	Hydrochemistry	pH	EC [ $\mu\text{S}/\text{cm}$ ]	Organic Material?
MUO11 IW4-038	-	-	-	x
MUO11 IW4-039	-	-	-	x
MUO11 IW4-040	-	-	-	x
MUO11 IW4-041	-	-	-	x
MUO11 IW4-042	-	-	-	x
MUO11 IW4-043	x	6.5	42.8	x
MUO11 IW4-044	-	-	-	x
MUO11 IW4-045	-	-	-	x
MUO11 IW4-046	-	-	-	x
MUO11 IW4-047	-	-	-	x
MUO11 IW4-048	-	-	-	-
MUO11 IW4-049	-	-	-	x
MUO11 IW4-050	-	-	-	x
MUO11 IW4-051	-	-	-	x
MUO11 IW4-052	-	-	-	x
MUO11 IW4-053	x	6.5	45.0	-
MUO11 IW4-054	-	-	-	-
MUO11 IW4-055	-	-	-	-
MUO11 IW4-056	-	-	-	x
MUO11 IW4-057	-	-	-	x
MUO11 IW4-058	-	-	-	x
MUO11 IW4-059	-	-	-	x
MUO11 IW4-060	-	-	-	x
MUO11 IW4-061	-	-	-	x
MUO11 IW4-062	-	-	-	x
MUO11 IW4-063	x	6.5	32.0	x
MUO11 IW4-064	-	-	-	x
MUO11 IW4-065	-	-	-	x
MUO11 IW4-066	-	-	-	x
MUO11 IW4-067	-	-	-	x
MUO11 IW4-068	-	-	-	x
MUO11 IW4-069	-	-	-	x
MUO11 IW4-070	-	-	-	x
MUO11 IW4-071	-	-	-	x
MUO11 IW4-072	-	-	-	x
MUO11 IW4-073	x	6.5	32.4	x
MUO11 IW4-074	-	-	-	x
MUO11 IW4-075	-	-	-	x
MUO11 IW4-076	-	-	-	-
MUO11 IW4-077	-	-	-	x
MUO11 IW4-078	-	-	-	x

*continuation on next side*



List of Holocene ice-wedge samples for stable water isotope analysis from Muostakh Island - continuation

Sample №	Hydrochemistry	pH	EC [ $\mu\text{S}/\text{cm}$ ]	Organic Material?
MUO11 IW4-079	-	-	-	x
MUO11 IW4-080	-	-	-	-
MUO11 IW4-081	-	-	-	x
MUO11 IW4-082	-	-	-	x
MUO11 IW4-083	x	6.5	46.5	x
MUO11 IW4-084	-	-	-	x
MUO11 IW4-085	-	-	-	x
MUO11 IW4-086	-	-	-	-
MUO11 IW4-087	-	-	-	-
MUO11 IW4-088	-	-	-	x
MUO11 IW4-089	-	-	-	x
MUO11 IW4-090	-	-	-	x
MUO11 IW4-091	-	-	-	x
MUO11 IW4-092	-	-	-	x
MUO11 IW4-093	-	-	-	x
MUO11 IW4-094	x	6.5	34.6	x
MUO11 IW4-095	-	-	-	x
MUO11 IW4-096	-	-	-	-
MUO11 IW4-097	-	-	-	-
MUO11 IW4-098	-	-	-	x
MUO11 IW4-099	x	6.5	8.9	x
MUO11 IW4-100	-	-	-	x
MUO11 IW4-101	-	-	-	x
MUO11 IW4-102	-	-	-	x
MUO11 IW4-103	x	6.5	9.2	x
MUO11 IW4-104	-	-	-	x
Ice wedge MUO11 IW5				
MUO11 IW5-1	<i>Frozen block for subsampling in cold laboratory</i>			
Ice wedge MUO11 IW6				
MUO11 IW6-1	<i>Frozen block for subsampling in cold laboratory</i>			
<i>end of table</i>				

List of precipitation samples from Cape Mamontov Klyk and Muostakh Island.

Sample №	Date	Time	Remarks
Cape Mamontov Klyk			
MAK11-rain-01	15.08.2011	11:00	strong wind from E
MAK11-rain-02	15.08.2011	21:00	wind from E
MAK11-rain-03	16.08.2011	14:00	-
MAK11-rain-04	16.08.2011	16:00	-
MAK11-rain-05	17.08.2011	05:00	-
MAK11-rain-06	17.08.2011	08:00	-
MAK11-rain-07	17.08.2011	09.30	-
Muostakh Island			
MUO11-rain-01	20.08.2011	22:00	wind from S/SW
MUO11-rain-02	20.08.2011	22:30	wind from SE
MUO11-rain-03	20.08.2011	23:00	wind from SE
MUO11-rain-04	21.08.2011	18:30	shower
MUO11-rain-05	23.08.2011	09:00	-
MUO11-rain-06	23.08.2011	11:00	-
MUO11-rain-07	23.08.2011	14:00	-
MUO11-rain-08	23.08.2011	17:00	-
MUO11-rain-09	26.08.2011	08:00	-
MUO11-rain-10	28.08.2011	11:00	-

## B Appendix Core Logs

Log protocol						
		Hole: BK2 (URB 108 mm)				
Depth		Rock type	Notes			
from	to	sediment (see litho codes)	Additional observations			
20.04.12	0	2,07	Sea ice	No sampling (warelevel 12 cm below surface)	BK 2-1	
	2,07	4,15	Sea water			
	4,15	6,00	no recovery			
	6,00	6,44	fine sand, unfrozen, salty, light-grey, not layered, single organic remains	BK 2-1 6,52 → 6,00 m tube sample		
	6,44	6,52	Light-grey, sandy-silty (1cm thick) dark organic (2 -3 mm thick) alternating bedding, salty, unfrozen	BK 2-1 6,52 → 6,00 m tube sample		
	6,52	8,25	no recovery			
	8,25	8,45	fine sand, silty, grey, unfrozen, salty, plant remains, compressed	BK 2-2 8,45 → 8,25 m bag sample		BK 2-2
	8,45	9,35	alternating bedding: finesand, silt(grey) organic (dark) wood remains (?) unfrozen, break locationsat fine layers	BK 2-2 9,35 → 8,45 m tube sample (9m methane)		
	9,35	12,25	no recovery			BK 2-3
	12,25	13,75	Medium-grained sand, plant remains, <u>not</u> salty, unfrozen, no bedding; Casing down to 13,75 m after coring	BK 2-3 (bags) 12,85 → 12,75 m 12,75 → 12,65 m 12,65 → 12,55 m 12,55 → 12,45 m 12,45 → 12,35 m 12,35 → 12,25 m BK 2-3 13,75 → 12,50 m (drill cuttings) BK 2-3 (tube) 13,65 → 12,85		
13,25	13,25		BK 2 13,25m methane (Dennis)			
21.04.12	13,80	13,95	Grey, mid-grained sand, unfrozen, not salty, no organic, moist, not bedded	no photo BK 2-4 (bags) 13,95 → 13,90 13,90 → 13,85 13,85 → 13,80	BK 2-4	

Core Log Buor Khaya - Core BK2

Log protocol					
		Hole: BK2 (URB 108 mm)			
Depth		Rock type	Notes		
from	to	sediment (see litho codes)	Additional observations		
21.04.12	13,95	15,25	unfrozen, dark-grey, fine-grained sand, moist	BK 2-5 (bags) 15,25 → 15,20 15,20 → 15,15 15,15 → 15,10 15,10 → 15,05 15,05 → 14,95 14,95 → 14,85 14,85 → 14,75 14,75 → 14,65 14,65 → 14,55 14,55 → 14,45 14,45 → 14,35 14,35 → 14,25 14,25 → 14,15 14,15 → 14,05 14,05 → 13,95	BK 2-5
	15,25	15,35	coarse grained sand, unfrozen, salty	BK 2-6 (bag) 15,35 → 15,25	BK 2-6
	15,35	15,45	macro wood remains (pieces) pebble (length axis 2cm), grey, silty, unfrozen, black layers	BK 2-6 (bag) 15,45 → 15,35	
	15,45	15,60	not salty, grey, unfrozen, coarse-grained sand, fine gravel	BK 2-7 (bag) 15,60 → 15,45	BK 2-7
	15,60	15,90	mid-grained sand, grey-brown, not salty, dry, unfrozen, „warm“, no organic	BK 2-8 (bags) 15,90 → 15,80 15,80 → 15,70 15,70 → 15,60	BK 2-8
	15,90	16,00	fine-grained sand, grey brown, not salty, dry, unfrozen, „warm“, no organic	BK 2-8 (bag) 16,00 → 15,90	
	16,00	16,15	no recovery		
	above	Above 15,60		BK 2-8 above 15,60 Drill Cuttings	
	17,50	17,85	mid-grained sand, dry, unfrozen, grey, plant remains between 17,65 → 17,50; Organic layers ca. 1cm thick	BK 2-9 (bags) 17,85 → 17,70 17,70 → 17,65 17,65 → 17,50	BK 2-9

Core Log Buor Khaya - Core BK2

Log protocol					
		Hole: BK2 (URB 108 mm)			
Depth		Rock type	Notes		
from	to	sediment (see litho codes)	Additional observations		
21.04.12	17,85	18,15	grey, mid-grained sand, plant remains	BK 2-9 (bags) 18,15 → 18,00 18,00 → 17,85 18 m methane 18,20 sample Misha	BK 2-9
	18,15	18,50	grey, dry, unfrozen, mid-grained sand	BK 2-9 (bags) 18,50 → 18,35 18,35 → 18,15	
	18,50	18,55	grey, dry, unfrozen, coarse-grained sand (with modern snow)	BK 2-9 (bag) 18,55 → 18,50	
	18,55	18,6	grey, dry, unfrozen, coarse-grained sand (with modern snow)	BK 2-9 (bag) 18,60 → 18,55	
	18,60	18,65	grey, dry, unfrozen, coarse-grained sand (with modern snow)	BK 2-9 (bag) 18,65 → 18,60	
	18,65	18,75	grey, bedded, fine to mid-grained sand, dry, unfrozen, no organics (with modern snow)	BK 2-9 (bag) 18,75 → 18,65	
	18,75	19,10	no recovery		BK 2-10
	19,10	19,60	coarse grained sand, grey, not bedded, no organic, unfrozen	BK 2-10 (bag) 19,60 → 19,10	
	19,60	20,25	mid-grained sand, grey, weakly bedded, single coarse wood remains	BK 2-10 19,95 → 19,60 no recovery! 20,25 → 19,95 tube	
	20,25	20,60	Mid-grained sand, grey, weakly bedded, single coarse wood remains	BK 2-10 (tube) 20,75 → 20,25	
	20,60	21,90	unfrozen, dark-grey, grey sand-silt alternate bedding, sand layer 5-10 mm, silt layer 1-2 mm, plant detrius layer	BK 2-10 21,90 → 21,75 bag 21,75 → 21,50 bag 21,50 → 20,75 tube	
	21,85	22,10	fine sand, silt, bedded, unfrozen, single plant remains	BK 2-10 (bags) 22,10 → 22,05 22,05 → 21,90 21,90 → 21,75	
	22,10	22,60	no recovery		

Core Log Buor Khaya - Core BK2

Log protocol					
		Hole: BK2 (URB 108 mm)			
Depth		Rock type	Notes		
from	to	sediment (see litho codes)	Additional observations		
21.04.12	22,60	25,00	fine sand, bedded, single organic remains, lightgrey-brown, oxidation spots around plant remains	BK 2-10 (bag) 25,00 → 24,70 (tube) 24,70 → 24,40 (bag) 24,40 → 24,20 (bag) 24,20 → 23,75 (bag) 23,75 → 23,45 (bag) 23,45 → 23,15 (tube) 23,15 → 22,10 no recovery	BK 2-11
	25,00	26,70	not frozen, grey, bedded, mid-grained sand, organic layers	BK 2-11 (tube) 26,70 → 26,25 26,25 → 25,65 25,60 → 25,00	
	26,70	28,75	not frozen, grey, mid – to coarse grained sand, singel small gravel, no organic, not bedded	BK 2-12 28,75 → 28,45 (bag) 28,45 → 28,20 (bag) 28,20 → 27,55 (tube) 27,55 → 27,30 (bag) 27,30 → 26,70 (no recovery)	BK 2-12
	28,75	29,55	frozen, organic remains, lightbrown, midgrained grey sand, microlens-like KT	BK 2-12 (tube) 29,65 → 28,75	
	29,55	29,65	frozen fine-grained sand, no organics, microlens-like KT		
	29,65	32,15	frozen, grey, microlens-like KT, makro wood remains, mid-grained sand	BK 2-13 (tubes) 32,15 → 31,30 31,30 → 30,85 30,85 → 30,00 30,00 → 29,65	BK 2-13
22.04.12	32,15	33,65	no recovery		
	33,65	34,20	frozen, lightgrey fine-grainedsand and silt and plant detritus, cross bedded with mid-grained sand, nummerous wood remains,microlens-like KT, each bed about 5cm thick	BK 2-14 (tube) 34,20 → 33,65	BK 2-14
	34,20	34,65	mid-grained sand, grey-brown, plant detritus layers, massive KT, pebble at ca. 34,55	BK 2-15 (tubes) 36,80 → 36,00	BK 2-15
34,65	35,50	fine-grained sand, bedded plant detritus layers 1mm thick,massive KT	36,00 → 35,44		

Core Log Buor Khaya - Core BK2

B Appendix Core Logs

Log protocol					
		Hole: BK2 (URB 108 mm)			
Depth		Rock type	Notes		
from	to	sediment (see litho codes)	Additional observations		
22.04.12	35,50	36,80	mid-grained sand, grey, not bedded, no organic, massive KT	35,44 → 35,04 35,04 → 34,20	BK 2-15
	36,80	37,85	no recovery		BK 2-16
	37,85	38,10	weakly bedded, silt to clay, massive KT, sharp contact to underlying sand		
	38,10	39,80	grey fine sand, microlens-like KT, few organic remains, weakly bedded, sharp contact to underlying silt within one core piece	BK 2-16 (tube) 40,55 → 39,70 39,70 → 38,74 38,74 → 37,85	
	39,80	40,06	bedded silt to clay, dark grey, massive KT, no organic	Drill cuttings from above 40,55 m	
	40,06	40,39	fine-grained sand, single plant detritus layers, massive KT, light grey, gradual transition to overlying silts		BK 2-17
	40,39	40,55	Light-grey clay, crossbedded massive KT		
	40,55	40,90	light-grey fine-grained sand, massive KT, single plant detritus layers	BK 2-17 (bags) 40,90 → 40,80 40,80 → 40,65 40,65 → 40,55	
	40,55	40,65	no recovery		BK 2-18
	40,65	41,65	fine-grained sand, light grey, not bedded, massive KT, no organic		
	41,65	41,80	fine-grained sand, light grey, numerous plant detritus layers, cross(?) bedded	BK 2-18 (tubes) 44,10 → 43,30 43,30 → 42,35	
	41,80	42,30	clay to silt, dark grey, bedded (laminated), massive KT, no organics	42,35 → 41,50 41,50 → 40,65	
	42,30	44,10	fine-grained sand, grey, single layers of plant detritus, not bedded, massive KT		BK 2-19
	44,10	45,10	no recovery		
45,10	46,80	light-grey mid-grained sand, almost no organic, only plant detritus layers at 45,15m, not bedded, massive KT	BK 2-19 (tubes) 48,40 → 47,50		
23.04.12	46,80	46,90	grey, coarse-grained sand, light brown coarse wood remains, massive KT	47,50 → 46,50 46,50 → 45,90	BK 2-19
	46,90	47,60	grey, mid-grained sand, not bedded, massive KT, pebble at 47,34m, no organics	45,95 → 45,10	

Core Log Buor Khaya - Core BK2

Log protocol					
		Hole: BK2 (URB 108 mm)			
Depth		Rock type	Notes		
from	to	sediment (see litho codes)	Additional observations		
23.04.12	47,60	47,70	laminated silt layers, 2-4mm, plant detritus layers 1mm, graduate bedding towards underlying mid-grained sand, massive KT	(previous page)	BK 2-19
	47,70	48,40	Light-grey mid-grained sand, single organic remains, not bedded, massive KT		
	48,40	50,90	bedded, grey, fine-grained sand, plant detritus, massive KT, occasional layers of wood remains, eg. at 50,15 → 48,85 and 49,30 → 49,25	BK 2-20 48,90 → 48,60 (Drill cuttings)	BK 2-20
	50,90	51,70	bedded, grey, fine-grained sand, plant detritus, massive KT, layers of wood remains. at 51,50 m	51,70 → 51,60 (bag) 51,60 → 50,90 (tube) 50,90 → 50,10 (tube) 50,10 → 49,70 (tube) 49,70 → 49,00 (tube) 49,00 → 48,40 (tube)	
End of Drilling at 51,70					

Core Log Buor Khaya - Core BK2

## C Appendix Drilling Campaign

List of core sections, sample depths, codes and thermally insulated storage box for the terrestrial bore hole (BK2).

core section	depth [m]	sample code	box number
BK 2-1	6,52-6,00	BK 2-1 6,52-6,00	box BK 11
BK 2-2	8,45-8,25	BK 2-2 8,45-8,25	box BK 11
BK 2-2	9,35-8,45	BK 2-2 9,35-8,45	box BK 11
BK 2-3	12,35-12,25	BK 2-3 12,35-12,25	box BK 11
BK 2-3	12,45-12,35	BK 2-3 12,45-12,35	box BK 11
BK 2-3	12,55-12,45	BK 2-3 12,55-12,45	box BK 11
BK 2-3	12,65-12,55	BK 2-3 12,65-12,55	box BK 11
BK 2-3	12,75-12,65	BK 2-3 12,75-12,65	box BK 11
BK 2-3	12,85-12,75	BK 2-3 12,85-12,75	box BK 11
BK 2-3	13,65-12,85	BK 2-3 13,65-12,85	box BK 11
BK 2-3	13,75-12,50	BK 2-3 13,75-12,50	box BK 11
(drill cuttings)			
BK 2-4	13,85-13,80	BK 2-4 13,85-13,80	box BK 11
BK 2-4	13,90-13,85	BK 2-4 13,95-13,91	box BK 11
BK 2-4	13,95-13,90	BK 2-4 13,90-13,85	box BK 11
BK 2-5	14,05-13,95	BK 2-5 14,05-13,95	box BK 22
BK 2-5	14,15-14,05	BK 2-5 14,15-14,05	box BK 22
BK 2-5	14,25-14,15	BK 2-5 14,25-14,15	box BK 22
BK 2-5	14,35-14,25	BK 2-5 14,35-14,25	box BK 22
BK 2-5	14,45-14,35	BK 2-5 14,45-14,35	box BK 22
BK 2-5	14,55-14,45	BK 2-5 14,55-14,45	box BK 22
BK 2-5	14,65-14,55	BK 2-5 14,65-14,55	box BK 22
BK 2-5	14,75-14,65	BK 2-5 14,75-14,65	box BK 22
BK 2-5	14,85-14,75	BK 2-5 14,85-14,75	box BK 22
BK 2-5	14,95-14,85	BK 2-5 14,95-14,85	box BK 22
BK 2-5	15,05-14,95	BK 2-5 15,05-14,95	box BK 22
BK 2-5	15,10-15,05	BK 2-5 15,10-15,05	box BK 22
BK 2-5	15,15-15,10	BK 2-5 15,15-15,10	box BK 22
BK 2-5	15,20-15,15	BK 2-5 15,20-15,15	box BK 22
BK 2-5	15,25-15,20	BK 2-5 15,25-15,20	box BK 22
BK 2-6	15,35-15,25	BK 2-6 15,35-15,25	box BK 22
BK 2-6	15,45-15,35	BK 2-6 15,45-15,35	box BK 22

*continuation on next side*



List of core sections, sample depths, codes and thermally insulated storage box for the terrestrial bore hole (BK2). - continuation

core section	depth [m]	sample code	box number
BK 2-7	15,60-15,45	BK 2-7 15,60-15,45	box BK 22
BK 2-8	above 15,60	BK 2-8 above 15,60 (drill cuttings)	box BK 22
BK 2-8	15,70-15,60	BK 2-8 15,70-15,60	box BK 22
BK 2-8	15,80-15,70	BK 2-8 15,80-15,70	box BK 22
BK 2-8	15,90-15,80	BK 2-8 15,90-15,80	box BK 22
BK 2-8	16,00-15,90	BK 2-8 16,00-15,90	box BK 22
BK 2-9	16,25-16,15	BK 2-9 16,25-16,15	box BK 99
BK 2-9	16,35-16,25	BK 2-9 16,35-16,25	box BK 99
BK 2-9	16,45-16,35	BK 2-9 16,45-16,35	box BK 99
BK 2-9	16,65-16,45	BK 2-9 16,65-16,45	box BK 99
BK 2-9	16,80-16,65	BK 2-9 16,80-16,65	box BK 99
BK 2-9	16,90-16,80	BK 2-9 16,90-16,80	box BK 99
BK 2-9	17,00-16,90	BK 2-9 17,00-16,90	box BK 99
BK 2-9	17,10-17,00	BK 2-9 17,10-17,00	box BK 99
BK 2-9	17,20-17,10	BK 2-9 17,20-17,10	box BK 99
BK 2-9	17,30-17,20	BK 2-9 17,30-17,20	box BK 99
BK 2-9	17,50-17,30	BK 2-9 17,50-17,30	box BK 99
BK 2-9	17,65-17,50	BK 2-9 17,65-17,50	box BK 99
BK 2-9	17,70-17,65	BK 2-9 17,70-17,65	box BK 99
BK 2-9	17,85-17,70	BK 2-9 17,85-17,70	box BK 99
BK 2-9	18,00-17,85	BK 2-9 18,00-17,85	box BK 99
BK 2-9	18,15-18,00	BK 2-9 18,15-18,00	box BK 99
BK 2-9	18,35-18,15	BK 2-9 18,35-18,15	box BK 99
BK 2-9	18,50-18,35	BK 2-9 18,50-18,35	box BK 99
BK 2-9	18,55-18,50	BK 2-9 18,55-18,50	box BK 99
BK 2-9	18,60-18,55	BK 2-9 18,60-18,55	box BK 99
BK 2-9	18,65-18,60	BK 2-9 18,65-18,60	box BK 99
BK 2-9	18,75-18,65	BK 2-9 18,75-18,65	box BK 99
BK 2-10	19,60-19,10	BK 2-10 19,60-19,10	box BK 77
BK 2-10	20,25-19,95	BK 2-10 20,25-19,95	box BK 77
BK 2-10	20,75-20,25	BK 2-10 20,75-20,25	box BK 77
BK 2-10	21,50-20,75	BK 2-10 21,50-20,75	box BK 77
BK 2-10	21,75-21,50	BK 2-10 21,75-21,50	box BK 77
BK 2-10	21,90-21,75	BK 2-10 21,90-21,75	box BK 77
BK 2-10	21,90-21,75	BK 2-10 21,90-21,75	box BK 77
BK 2-10	22,05-21,90	BK 2-10 22,05-21,90	box BK 77
BK 2-10	22,10-22,05	BK 2-10 22,10-22,05	box BK 77
BK 2-11	25,60-25,00	BK 2-11 25,60-25,00	box K 254

*continuation on next side*

List of core sections, sample depths, codes and thermally insulated storage box for the terrestrial bore hole (BK2). - continuation

core section	depth [m]	sample code	box number
BK 2-11	26,25-25,65	BK 2-11 26,25-25,65	box 0342
BK 2-11	23,15-22,10	BK 2-11 23,15-22,10	box K 254
BK 2-11	23,45-23,15	BK 2-11 23,45-23,15	box K 254
BK 2-11	23,75-23,45	BK 2-11 23,75-23,45	box K 254
BK 2-11	24,20-23,75	BK 2-11 24,20-23,75	box K 254
BK 2-11	24,40-24,20	BK 2-11 24,40-24,20	box K 254
BK 2-11	24,70-24,40	BK 2-11 24,70-24,40	box K 254
BK 2-11	25,00-24,70	BK 2-11 25,00-24,70	box K 254
BK 2-11	26,70-26,25	BK 2-11 26,70-26,25	box 0343
BK 2-12	28,75-28,45	BK 2-12 28,75-28,45	box K 254
BK 2-12	29,65-28,75	BK 2-12 29,65-28,75	box K 254
BK 2-12	27,55-27,30	BK 2-12 27,55-27,30	box BK 12
BK 2-12	28,20-27,55	BK 2-12 28,20-27,55	box BK 12
BK 2-12	28,45-28,20	BK 2-12 28,45-28,20	box BK 12
BK 2-13	30,00-29,65	BK 2-13 30,00-29,65	box BK 12
BK 2-13	30,85-30,00	BK 2-13 30,85-30,00	box BK 12
BK 2-13	31,30-30,85	BK 2-13 31,30-30,85	box BK 12
BK 2-13	32,15-31,30	BK 2-13 32,15-31,30	box BK 12
BK 2-14	34,20-33,65	BK 2-14 34,20-33,65	box BK 88
BK 2-15	35,04-34,20	BK 2-15 35,04-34,20	box BK 88
BK 2-15	35,44-35,04	BK 2-15 35,44-35,04	box BK 88
BK 2-15	36,00-35,44	BK 2-15 36,80-36,00	box BK 88
BK 2-15	36,80-36,00	BK 2-15 36,80-36,00	box BK 88
BK 2-16	above 40,55	BK 2-16 above 40,55 (drill cuttings)	box BK 88
BK 2-16	38,74-37,85	BK 2-16 38,74-37,85	box 0345
BK 2-16	39,70-38,74	BK 2-16 39,70-38,74	box 0345
BK 2-16	40,55-39,70	BK 2-16 40,55-39,70	box 0345
BK 2-17	40,65-40,55	BK 2-17 40,65-40,55	box 0345
BK 2-17	40,80-40,65	BK 2-17 40,80-40,65	box 0345
BK 2-17	40,90-40,80	BK 2-17 40,90-40,80	box 0345
BK 2-18	41,50-40,65	BK 2-18 41,50-40,65	box 0188
BK 2-18	42,35-41,50	BK 2-18 42,35-41,50	box 0188
BK 2-18	43,30-42,35	BK 2-18 43,30-42,35	box 0188
BK 2-18	44,10-43,30	BK 2-18 44,10-43,30	box 0188
BK 2-19	45,95-45,10	BK 2-19 45,95-45,10	box BK 33
BK 2-19	47,50-45,95	BK 2-19 46,50-45,95	box BK 33
BK 2-19	48,40-47,50	BK 2-19 47,50-46,50	box BK 33

*continuation on next side*

List of core sections, sample depths, codes and thermally insulated storage box for the terrestrial bore hole (BK2). - continuation

core section	depth [m]	sample code	box number
BK 2-19	48,40-47,50	BK 2-19 48,40-47,50	box BK 33
BK 2-20	48,90-48,60	BK 2-20 48,90-48,60 (drill cuttings)	box BK 44
BK 2-20	49,00-48,40	BK 2-20 49,00-48,40	box BK 44
BK 2-20	49,70-49,00	BK 2-20 49,70-49,00	box BK 44
BK 2-20	50,10-49,70	BK 2-20 50,10-49,70	box BK 44
BK 2-20	50,90-50,10	BK 2-20 50,90-50,10	box BK 44
BK 2-20	51,60-50,90	BK 2-20 51,60-50,90	box BK 44
BK 2-20	51,70-51,60	BK 2-20 51,70-51,60	box BK 44
<i>end of table</i>			

List of core sections, sample depths, codes and thermally insulated storage box for the terrestrial bore hole (BK8).




core section	depth [m]	sample code	box number
BK 8-1	0,85-0	BK 8-1 0,85-0	box 0344
BK 8-2	1,10-0,85	BK 8-2 1,1-0,85	box 0344
BK 8-3	1,30-1,10	BK 8-3 1,30-1,10	box 0344
BK 8-4	1,80-1,30	BK 8-4 1,80-1,30	box 0344
BK 8-5	2,40-1,80	BK 8-5 2,40-1,80	box 0344
BK 8-6	2,85-2,40	BK 8-6 2,85-2,40	box AWI 08
BK 8-7	3,15-2,85	BK 8-7 3,15-2,85	box AWI 08
BK 8-8	3,30-3,15	BK 8-8 3,30-3,15	box AWI 08
BK 8-9	3,40-3,30	BK 8-9 3,40-3,30	box AWI 08
BK 8-10	3,50-3,40	BK 8-10 3,50-3,40	box AWI 08
BK 8-11	3,60-3,50	BK 8-11 3,60-3,50	box AWI 08
BK 8-12	3,65-3,60	BK 8-12 3,65-3,60	box AWI 08
BK 8-13	3,80-3,65	BK 8-13 3,80-3,65	box AWI 08
BK 8-14	3,90-3,80	BK 8-14 above 3,90	box AWI 08
BK 8-15	4,10-3,90	BK 8-15 above 4,10	box AWI 08
BK 8-16	4,35-4,10	BK 8-16 above 4,35	box AWI 08
BK 8-17	4,65-4,35	BK 8-17 above 4,65	box AWI 08
BK 8-18	5,00-4,65	BK 8-18 above 5,00	box AWI 08
BK 8-19	5,35-5,00	BK 8-19 above 5,35	box AWI 08
BK 8-20	5,70-5,35	BK 8-20 above 5,70	box AWI 08
BK 8-21	6,00-5,70	BK 8-21 above 6,00	box AWI 08
BK 8-22	6,30-6,00	BK 8-22 above 6,30	box AWI 08
BK 8-23	6,70-6,30	BK 8-23 above 6,70	box AWI 08
<i>continuation on next side</i>			

List of core sections, sample depths, codes and thermally insulated storage box for the terrestrial bore hole (BK8). - continuation

core section	depth [m]	sample code	box number
BK 8-24	7,05-6,70	BK 8-24 above 7,05	box AWI 08
BK 8-25	7,35-7,05	BK 8-25 above 7,35	box AWI 08
BK 8-26	7,60-7,35	BK 8-26 above 7,60	box AWI 08
BK 8-27	7,95-7,60	BK 8-27 above 7,95	box AWI 08
BK 8-28	8,35-7,95	BK 8-28 above 8,35	box AWI 08
BK 8-29	8,75-8,35	BK 8-29 8,75-8,35	box AWI 08
BK 8-30	9,60-8,75	BK 8-30 9,60-8,75	box AWI 08
BK 8-31	9,95-9,60	BK 8-31 9,95-9,60	box 0274
BK 8-32	10,65-9,95	BK 8-32 10,65-9,95	box 0274
BK 8-33	10,90-10,65	BK 8-33 10,90-10,65	box 0274
BK 8-33	11,70-10,90	BK 8-33 11,70-10,90	box 0274
BK 8-34	12,55-11,70	BK 8-34 10,95-10,65	box 0274
BK 8-35	13,10-12,55	BK 8-35 13,10-12,55	box 0274
BK 8-36	13,50-13,10	BK 8-36 13,50-13,10	box 0274
BK 8-37	14,25-13,50	BK 8-37 14,25-13,50	box 0274
BK 8-38	14,65-14,25	BK 8-38 14,65-14,25	box 0274
BK 8-38	15,35-14,65	BK 8-38 15,35-14,65	box 0274
BK 8-39	15,90-15,35	BK 8-39 15,90-15,35	box 0343
BK 8-40	16,70-15,90	BK 8-40 16,70-15,90	box 0343
BK 8-41	17,70-16,70	BK 8-41 17,70-16,70	box 0343
BK 8-42	18,30-17,70	BK 8-42 18,30-17,70	box 0343
BK 8-43	18,90-18,30	BK 8-43 18,90-18,30	box 0343




*end of table*

List of 3 mL sediment samples from subsea sediment core (BK2). These samples were left in Tiksi for transfer to Vladivostok, where Denis Kosmach will perform methane concentration analyses. They were sampled volumetrically using a stainless steel cutter and stored in glass vials with a septum and a crimped closure.

core section	depth [m]	field description	photograph
BK2-2	9.00	unfrozen, alternative bedding of fine sand, silt (grey), organic (dark), wood fragments (?)	
BK2-3	13.25	unfrozen, medium-grained sand, no bedding, plant remains	
BK2-9	18.00	unfrozen, medium-grained sand, no bedding, plant remains	

*continuation on next page*

List of 3 mL sediment samples from subsea sediment core (BK2) - continuation

core section	depth [m]	field description	photograph
BK2-11	25.60	unfrozen, medium-grained sand, bedded, organic layers	
BK2-14	33.65	frozen, fine-grained sand, silt, plant detritus, light grey, cross bedded with medium-grained sand, micro lens-like cryotexture	
BK2-18	44.00	frozen, fine-grained sand, silt, single plant detritus layers, grey, non-bedded, massive cryotexture	

*end of table*

## Sample lists - water/ice/snow

Nº	site	depth	sample	sample box number
1	BK1	snow (surface)	60 mL	O274
2		0 m	60 mL	O274
3		2 m	60 mL	O274
4		3 m	60 mL	O274
5	BK2	snow (surface)	60 mL	O274
6		0 m	60 mL	O274
7		2 m	60 mL	O274
8		3 m	60 mL	O274
9		4 m	60 mL	O274
10	BK4	0 m	60 mL	O274
11		2 m	60 mL	O274
12		2.35 m (bottom)	60 mL	O274
13	BK5	0 m	60 mL	O274
14		1.9 m (bottom)	60 mL	O274
15	BK 6	0 m	60 mL	O274
16		1.5 m (bottom)	60 mL	O274
17	BK7	0 m	60 mL	O274
18		1 m (bottom)	60 mL	O274

Die "**Berichte zur Polar- und Meeresforschung**" (ISSN 1866-3192) werden beginnend mit dem Heft Nr. 569 (2008) als Open-Access-Publikation herausgegeben. Ein Verzeichnis aller Hefte einschließlich der Druckausgaben (Heft 377-568) sowie der früheren "**Berichte zur Polarforschung**" (Heft 1-376, von 1981 bis 2000) befindet sich im open access institutional repository for publications and presentations (**ePIC**) des AWI unter der URL <http://epic.awi.de>. Durch Auswahl "Reports on Polar- and Marine Research" (via "browse"/"type") wird eine Liste der Publikationen sortiert nach Heftnummer innerhalb der absteigenden chronologischen Reihenfolge der Jahrgänge erzeugt.

*To generate a list of all Reports past issues, use the following URL: <http://epic.awi.de> and select "browse"/"type" to browse "Reports on Polar and Marine Research". A chronological list in declining order, issues chronological, will be produced, and pdf-icons shown for open access download.*

#### **Verzeichnis der zuletzt erschienenen Hefte:**

**Heft-Nr. 653/2012** — "Joint Russian-German Polygon Project East Siberia 2011 - 2014: The expedition Kytalyk 2011", edited by Lutz Schirrmester, Lyudmila Pestryakova, Sebastian Wetterich and Vladimir Tumskoy

**Heft-Nr. 654/2012** — "The Expedition of the Research Vessel 'Polarstern' to the Antarctic in 2012 (ANT-XXVIII/5)", edited by Karl Bumke

**Heft-Nr. 655/2012** — "Expeditions to Permafrost 2012: 'Alaskan North Slope / Itkillik', 'Thermokarst in Central Yakutia' and 'EyeSight-NAAT-Alaska', edited by Jens Strauss, Mathias Ulrich and Marcel Buchhorn

**Heft-Nr. 656/2012** — "The Expedition of the Research Vessel 'Sonne' to the Manihiki Plateau in 2012 (So 224)", edited by Gabriele Uenzelmann-Neben

**Heft-Nr. 657/2012** — "The Expedition of the Research Vessel 'Polarstern' to the Antarctic in 2011 (ANT-XXVIII/1) ", edited by Saad El Naggar

**Heft-Nr. 658/2013** — "The Expedition of the Research Vessel 'Polarstern' to the Arctic in 2012 (ARK-XXVII/2)", edited by Thomas Soltwedel

**Heft-Nr. 659/2013** — "Changing Polar Regions - 25<sup>th</sup> International Congress on Polar Research, March 17-22, 2013, Hamburg, Germany, German Society for Polar Research", edited by Eva-Maria Pfeiffer, Heidemarie Kassens, and Ralf Tiedeman

**Heft-Nr. 660/2013** — "The Expedition of the Research Vessel 'Polarstern' to the Arctic in 2012 (ARK-XXVII/1)", edited by Agnieszka Beszczynska-Möller

**Heft-Nr. 661/2013** — "The Expedition of the Research Vessel 'Polarstern' to the Antarctic in 2012 (ANT-XXVIII/3)", edited by Dieter Wolf-Gladrow

**Heft-Nr. 662/2013** — "Climate Change in the Marine Realm: An international summer school in the framework of the European Campus of Excellence", edited by Angelika Dummermuth and Klaus Grosfeld

**Heft-Nr. 663/2013** — "The Expedition of the Research Vessel 'Polarstern' to the Arctic in 2012 (ARK-XXVII/3)", edited by Antje Boetius

**Heft-Nr. 664/2013** — "Russian-German Cooperation SYSTEM LAPTEV SEA: The Expeditions Laptev Sea - Mamontov Klyk 2011 & Buor Khaya 2012", edited by Frank Günther, Pier Paul Overduin, Aleksandr S. Makarov, and Mikhail N. Grigoriev